

Supporting Information for NJ-ART-11-2015-003251

Influence of steric hindrance on the molecular packing and the anchoring of quinonoid zwitterions on gold surfaces

*Minghui Yuan,¹ Iori Tababe,² Jean-Marie Bernard-Schaaf,¹ Qin-Yin Shi,³ Vicki Schlegel,³
Rachel Schurhammer,⁴ Peter A. Dowben,^{2,*} Bernard Doudin,⁵ Lucie Routaboul^{1,*} and Pierre
Braunstein^{1,*}*

¹ Laboratoire de Chimie de Coordination, Institut de Chimie (UMR 7177 CNRS), Université
de Strasbourg, 4 rue Blaise Pascal, 67081 Strasbourg, France

² Dept. of Physics and Astronomy, Nebraska Center for Materials and Nanoscience,
University of Nebraska-Lincoln, Lincoln NE 68588, USA

³ Dept. of Food Science and Technology, 326 Food Industry Complex
University of Nebraska – Lincoln, Lincoln NE 68583-0919

⁴ Laboratoire de Modélisation et Simulations Moléculaires, Institut de Chimie (UMR 7177
CNRS), Université de Strasbourg, 1 rue Blaise Pascal, 67081 Strasbourg, France

⁵ Institut de Physique et Chimie des Matériaux de Strasbourg (UMR 7504 CNRS), Université
de Strasbourg, 23 rue du Loess B.P. 20, 67034 Strasbourg, France

Content of the Supporting Information

| | |
|--|------|
| Figure S1. Packing of molecules 5 and 14 . | S-3 |
| Figure S2. Spacing observed in the molecular arrangements of 5 and 14 . | S-4 |
| Figure S3. IR spectra of zwitterion 6 . | S-5 |
| Figure S4. IR spectra of zwitterion 7 . | S-6 |
| Figure S5. IR spectra of zwitterion 8 . | S-7 |
| Figure S6. IR spectra of zwitterion 9 . | S-8 |
| Figure S7. IR spectra of zwitterion 10 . | S-9 |
| Figure S8. Comparison of the IR spectra of zwitterion 10 . | S-10 |
| Figure S9. IR spectra of zwitterion 11 . | S-11 |
| Figure S10. Comparison of the IR spectra of zwitterion 11 . | S-12 |
| Figure S11. Relative energies (in kJ.mol ⁻¹) as a function of the ϕ dihedral angle | S-13 |
| Figure S12. Relative energies (in kJ.mol ⁻¹) as a function of the ϕ' dihedral angle (°) for (15) performed with different theoretical methods. | S-14 |
| Table S1. Selected X-ray data | S-15 |
| Table S2. B3LYP/6-31+G** optimized energies (in hartree). | S-16 |
| Synthesis of new zwitterions | S-17 |
| Structural analyses by X-ray diffraction | S-20 |
| References | S-35 |
| NMR spectra of zwitterion 6 | S-36 |
| NMR spectra of zwitterion 7 | S-43 |
| NMR spectra of zwitterion 8 | S-47 |
| NMR spectra of zwitterion 9 | S-54 |
| NMR spectra of zwitterion 10 | S-58 |
| NMR spectra of zwitterion 11 | S-65 |
| NMR spectra of zwitterion 12 | S-75 |
| NMR spectra of zwitterion 13 | S-83 |

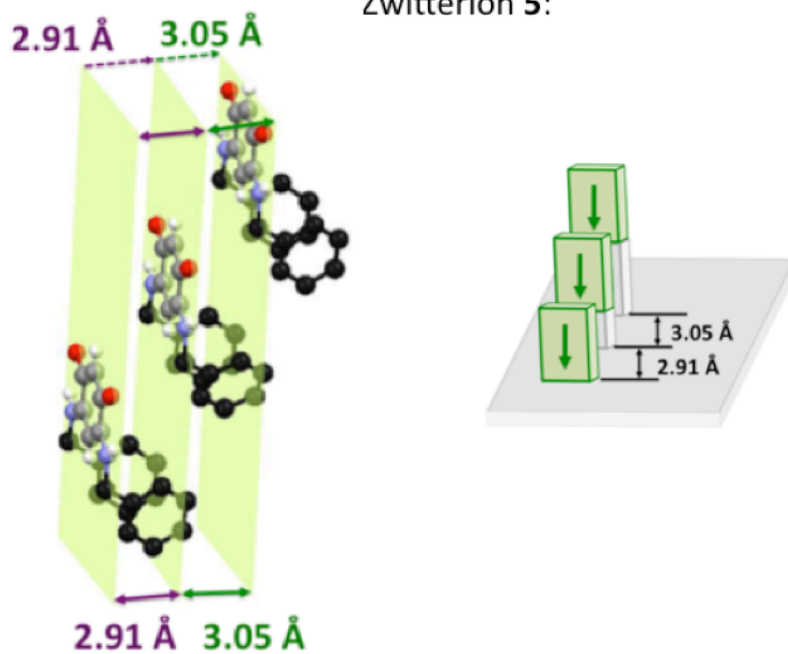
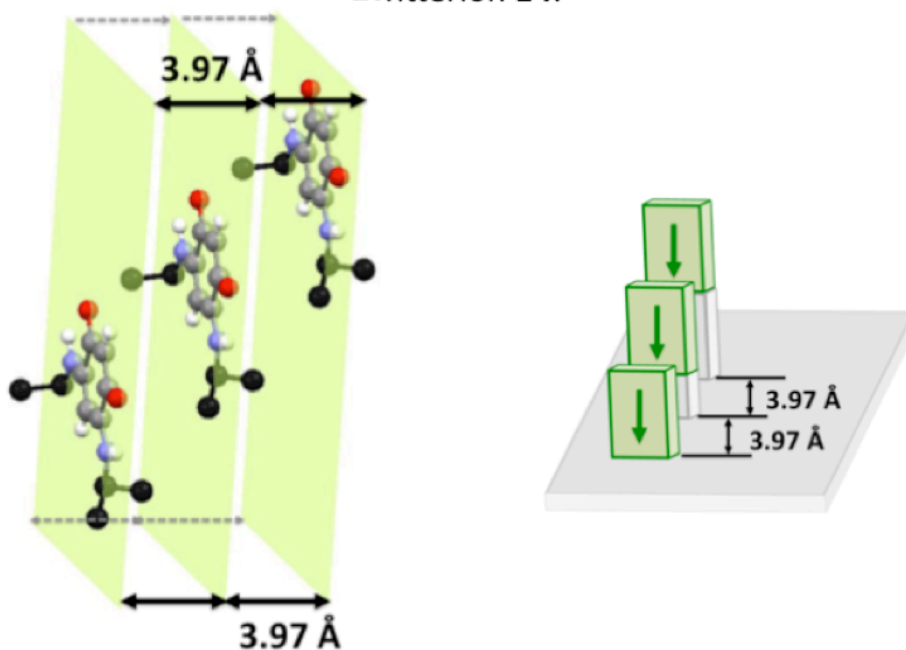
Zwitterion **5**:Zwitterion **14**:

Figure S1. Packing of molecules **5** and **14**. The spacing between the mean planes containing the quinonoid core of **5** are 2.91 and 3.05 Å whereas the separation observed for **14** is 3.97 Å. Left: view showing rows of parallel molecules. Parallelepipeds represent the quinonoid core and the arrows indicate the direction of the dipole.

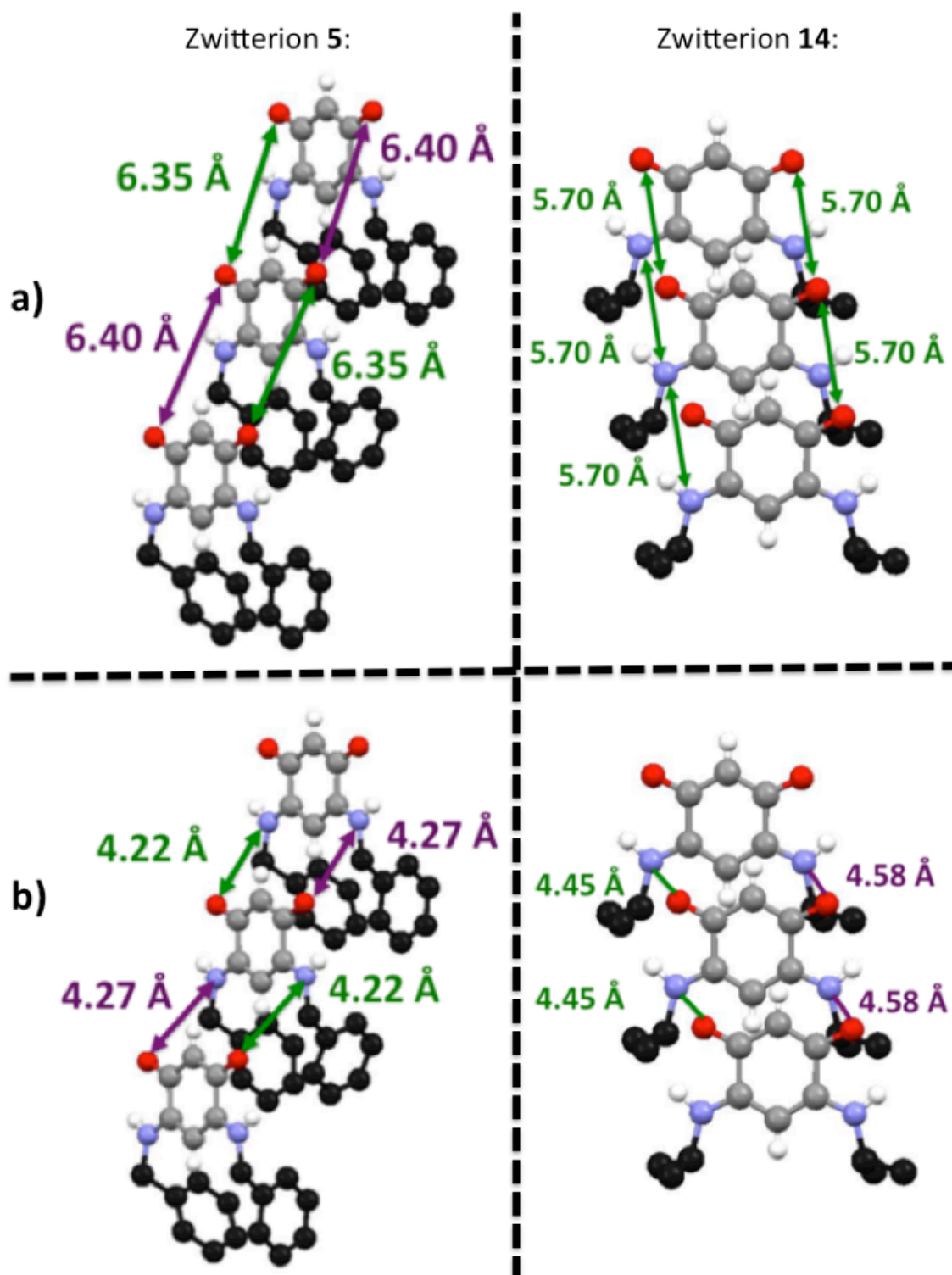


Figure S2. Spacing observed in the molecular arrangements of zwitterions 5 and 14. a) Interatomic spacing between corresponding atoms in two neighboring molecules. b) Spacing between the anionic system and the cationic system of the neighboring molecule.

Zwitterion 6

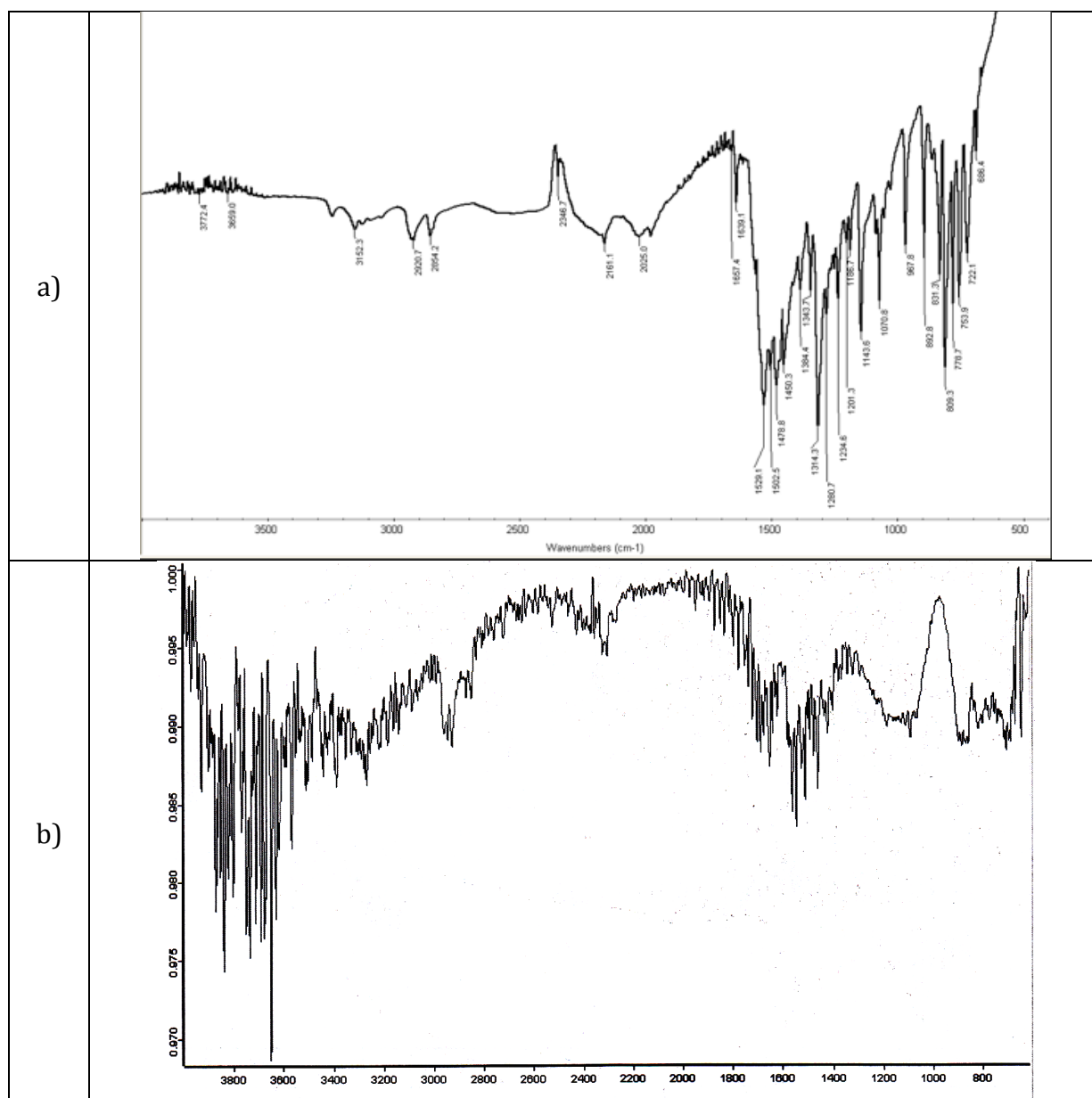
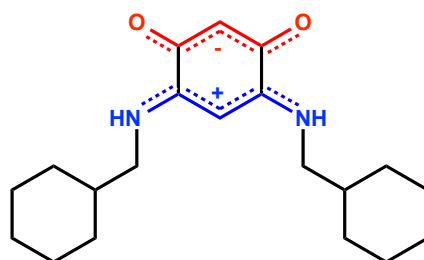


Figure S3. IR spectra of zwitterion 6. a) IR spectrum of 6 in the solid state; b) IR spectrum of the gold surface functionalized by 6.

Zwitterion 7

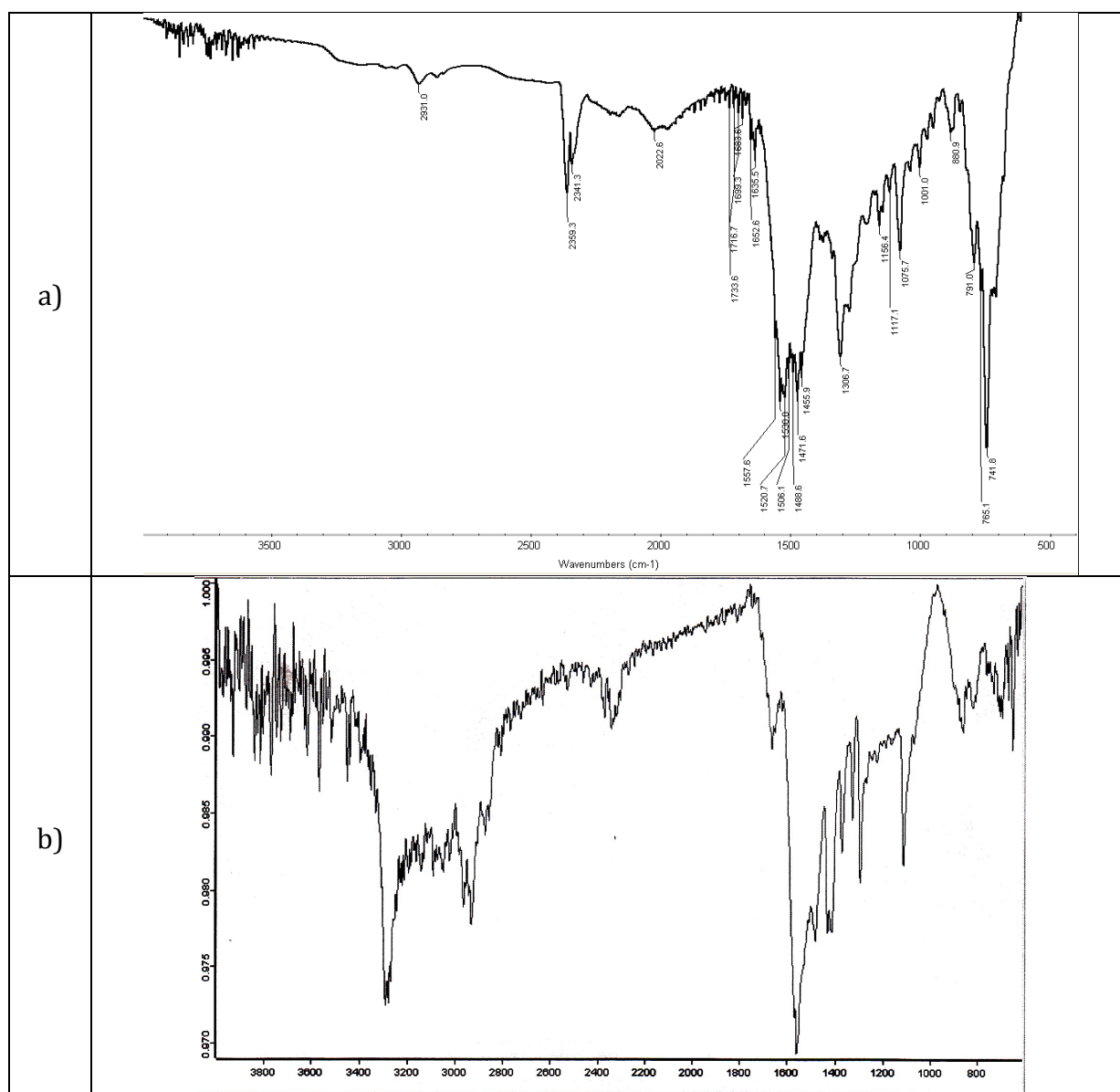
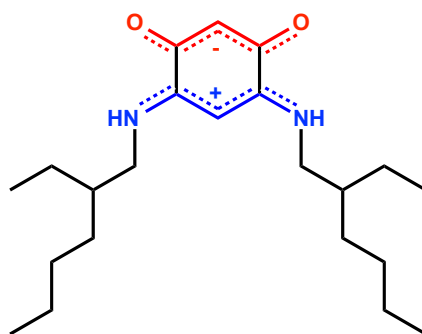


Figure S4. IR spectra of zwitterion 7. a) IR spectrum of 7 in the solid state; b) IR spectrum of the gold surface functionalized by 7.

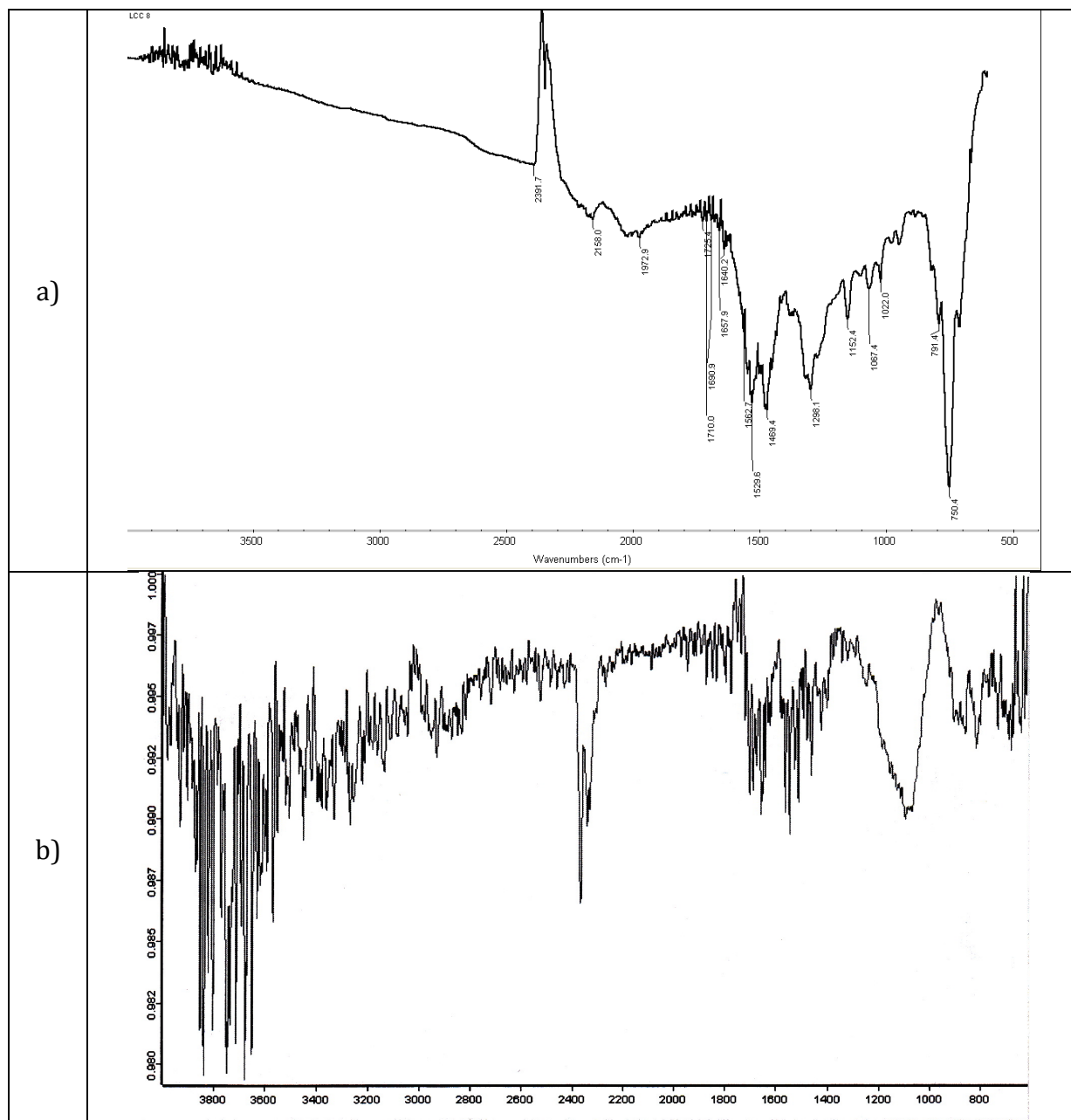
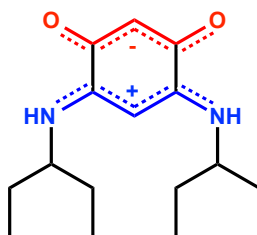
Zwitterion **8**

Figure S5. IR spectra of zwitterion **8**. a) IR spectrum of **8** in the solid state; b) IR spectrum of the gold surface functionalized by **8**.

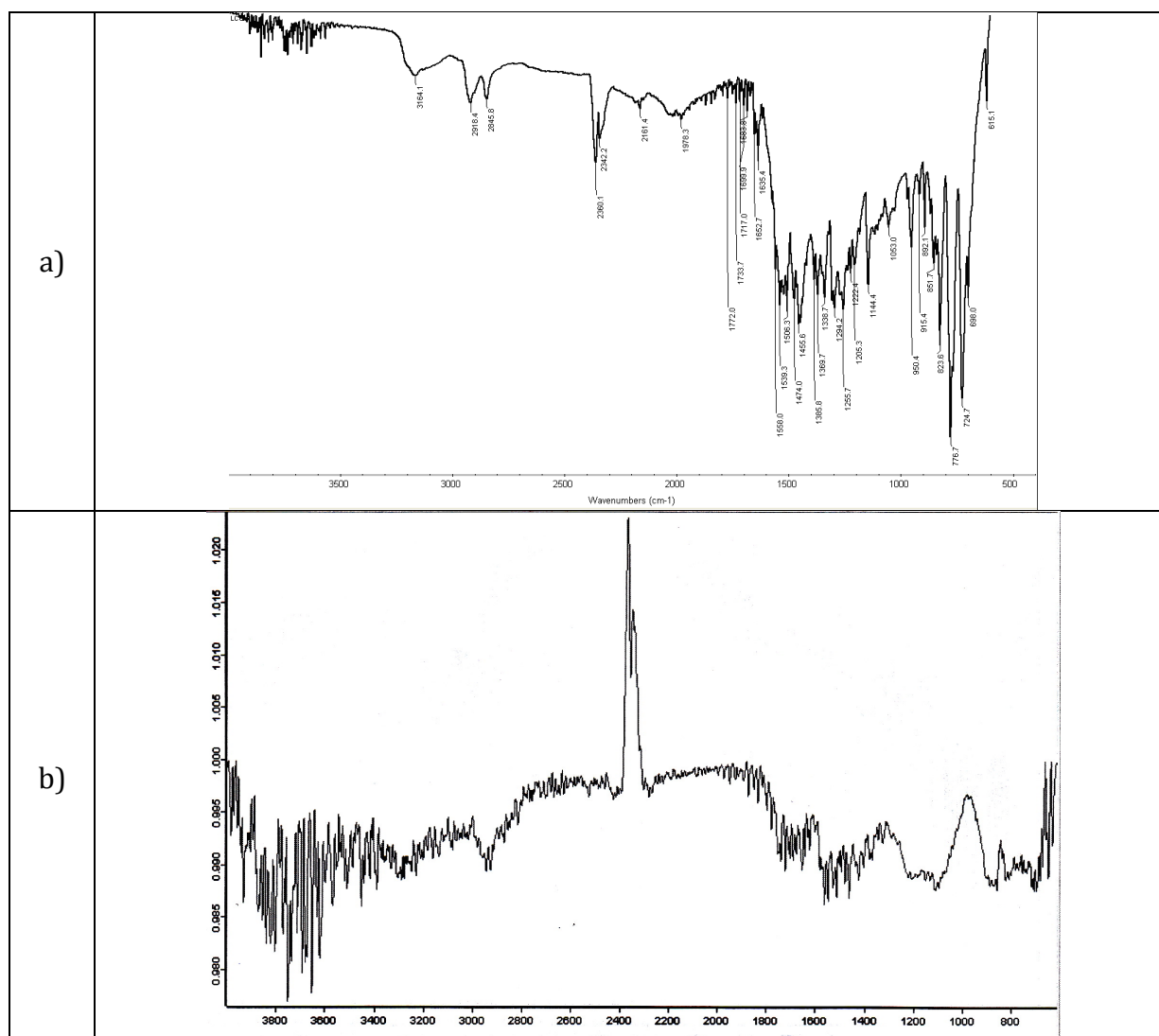
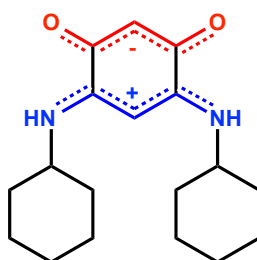
Zwitterion **9**

Figure S6. IR spectra of zwitterion **9**. a) IR spectrum of **9** in the solid state; b) IR spectrum of the gold surface functionalized by **9**.

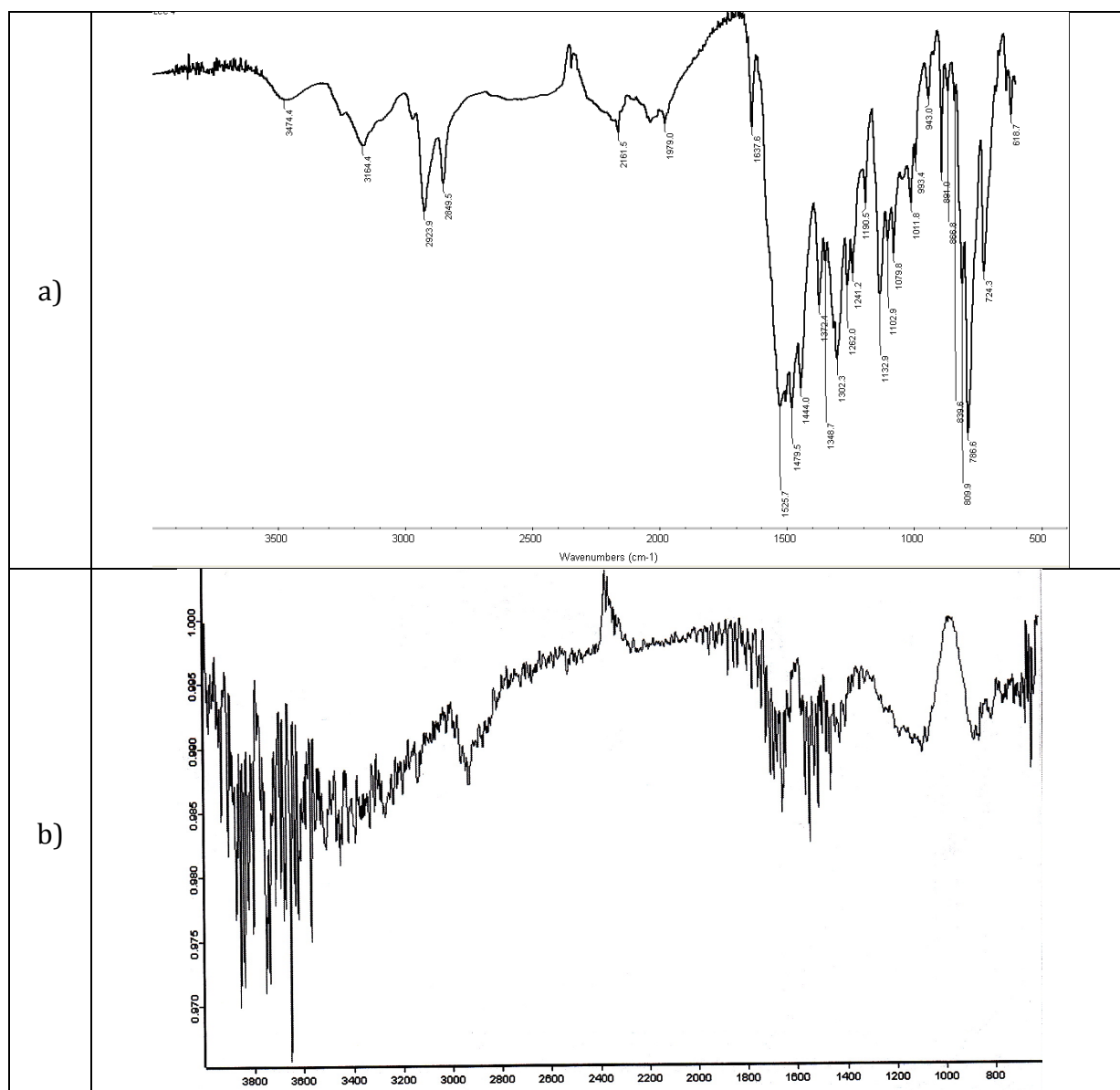
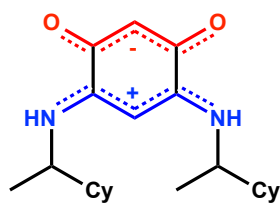
Zwitterion **10**

Figure S7. IR spectra of zwitterion **10**. a) IR spectrum of **10** in the solid state; b) IR spectrum of the gold surface functionalized by **10**.

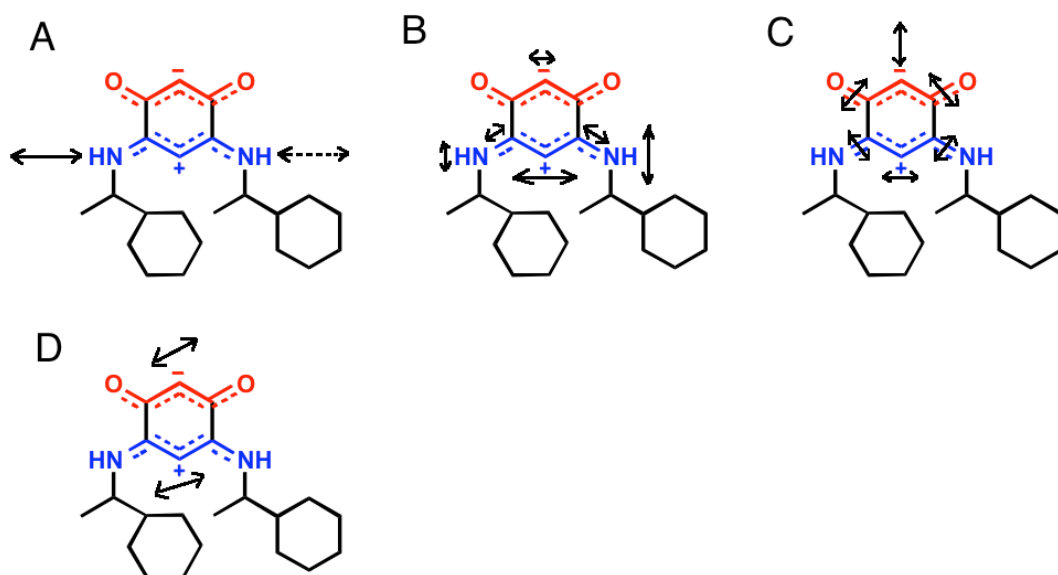
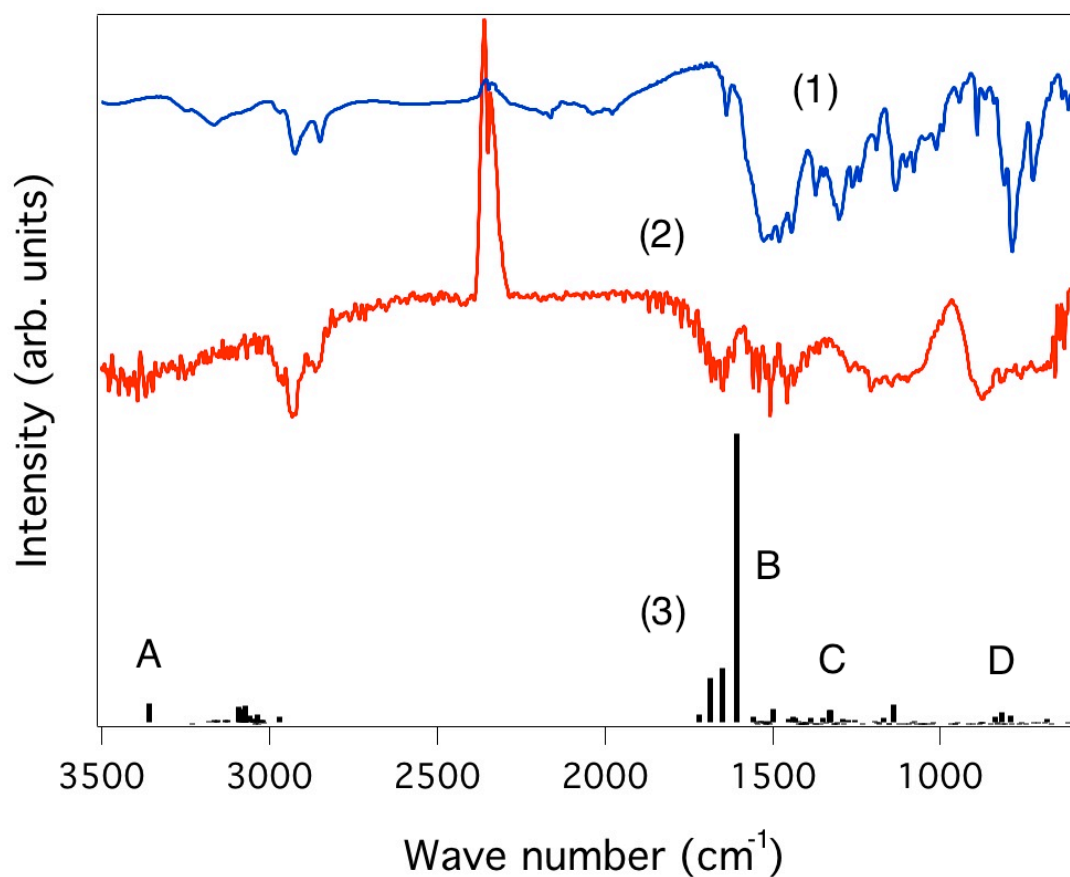


Figure S8. Comparison of the IR spectra of zwitterion **10**. The data in blue (1) correspond to the IR spectrum of the zwitterion in the solid state whereas the IR spectrum of the gold surface functionalized by compound **10** is indicated in red (2). The theoretical spectra, in black, of the compound with the eigenvalues indicated, and the estimated intensities (3).

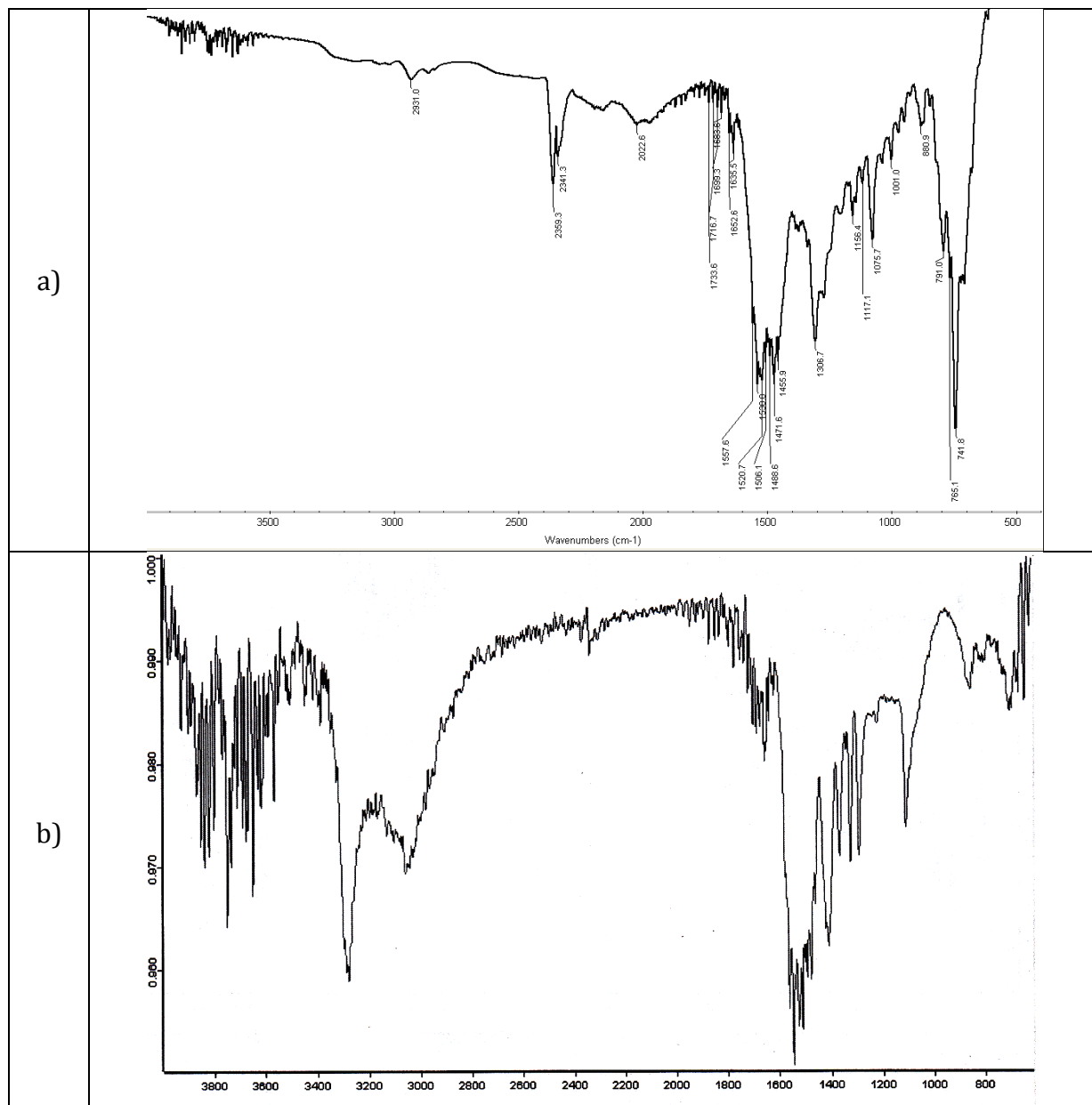
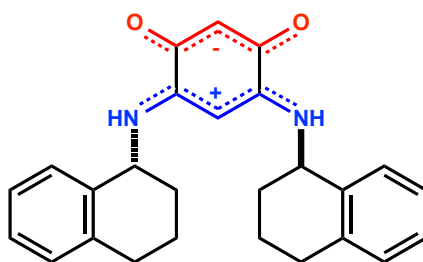
Zwitterion **11**

Figure S9. IR spectra of zwitterion **11**. a) IR spectrum of **11** in the solid state; b) IR spectrum of the gold surface functionalized by **11**.

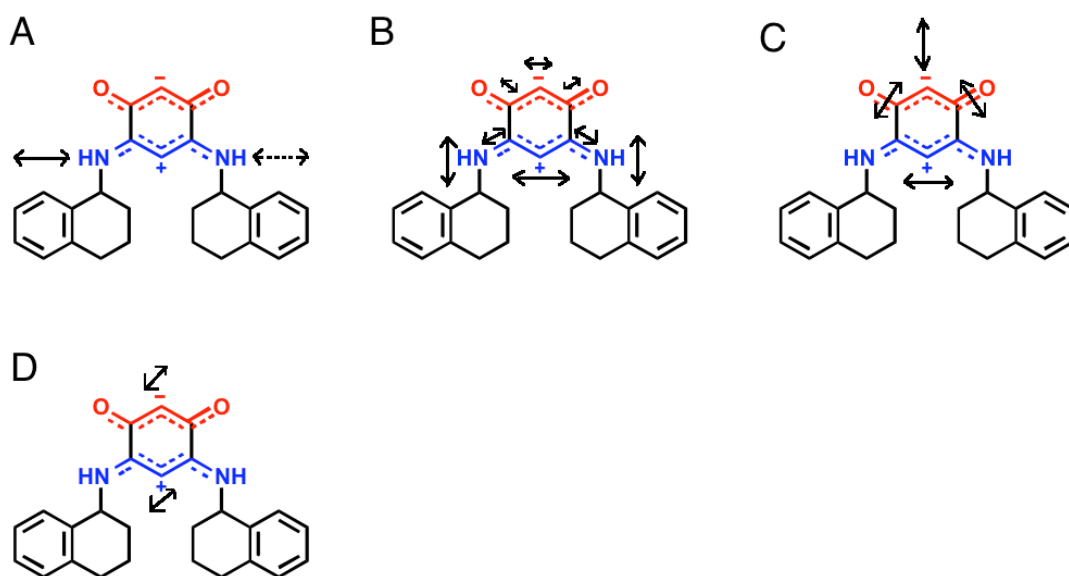
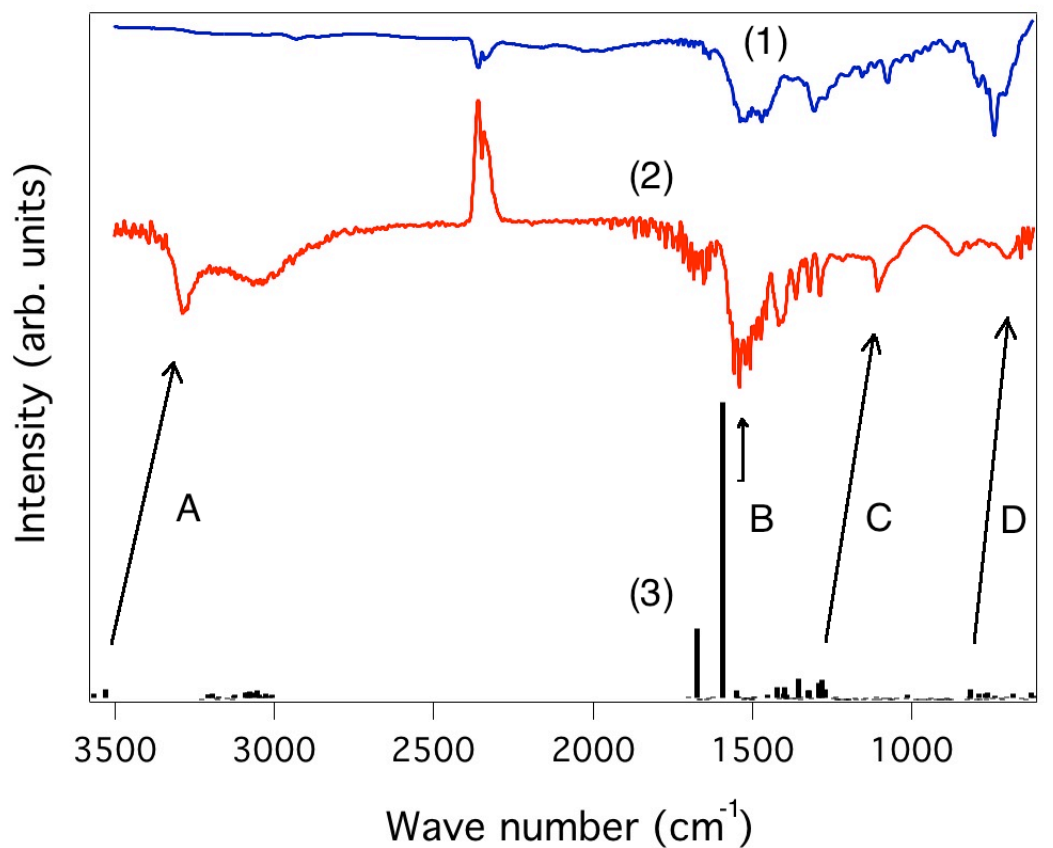


Figure S10. Comparison of the IR spectra of zwitterion **11**. The data in blue (1) correspond to the IR spectrum of the zwitterion in the solid state whereas the IR spectrum of the gold surface functionalized by compound **11** is indicated in red (2). The theoretical spectra, in black, of the compound with the eigenvalues indicated, and the estimated intensities (3).

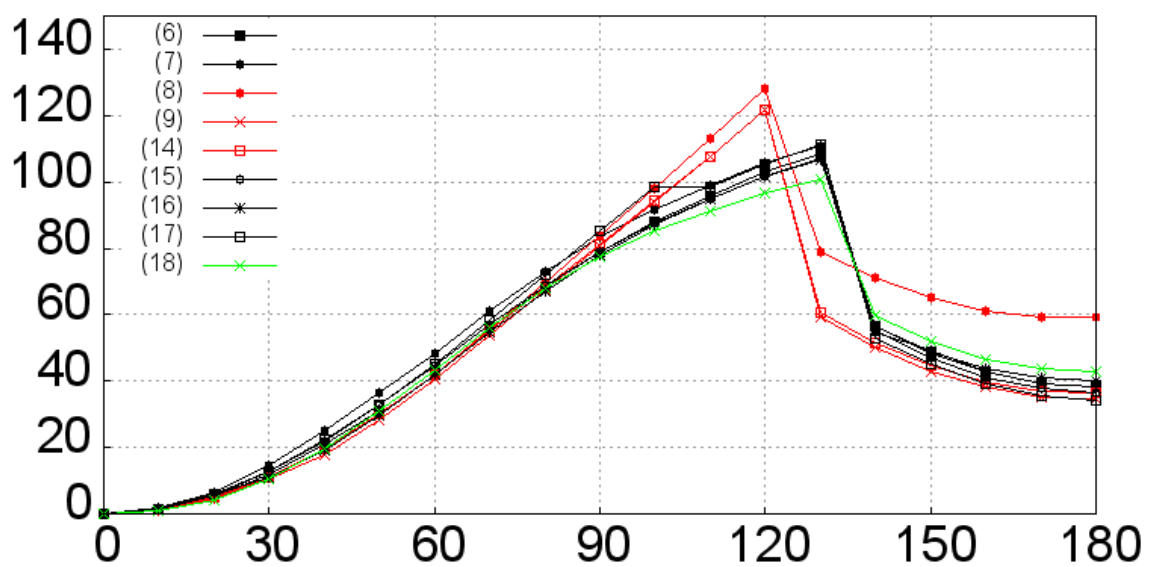
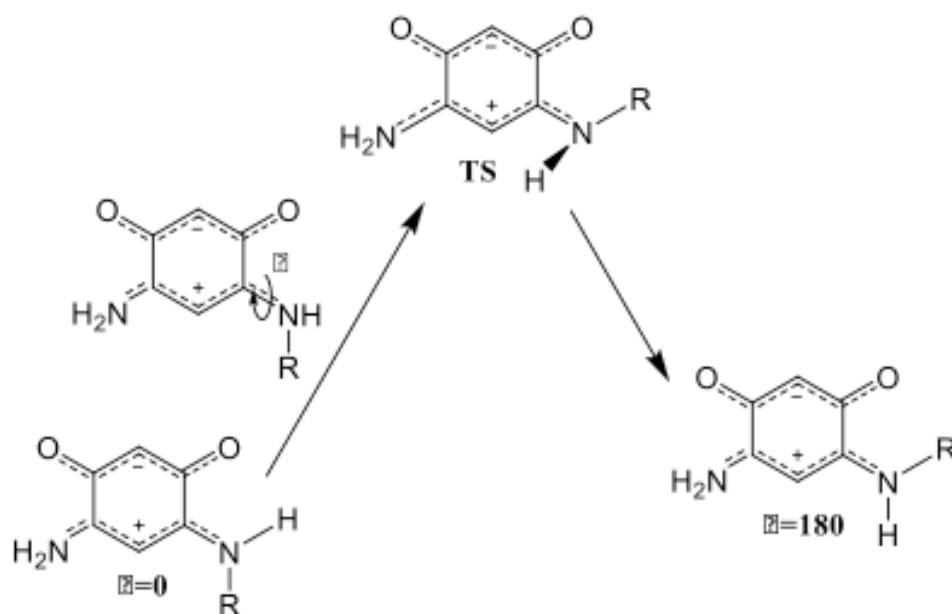


Figure S11. Relative energies (in $\text{kJ}\cdot\text{mol}^{-1}$) as a function of the ϕ dihedral angle ($^{\circ}$) for several zwitterions performed with HF/6-31+G** method.

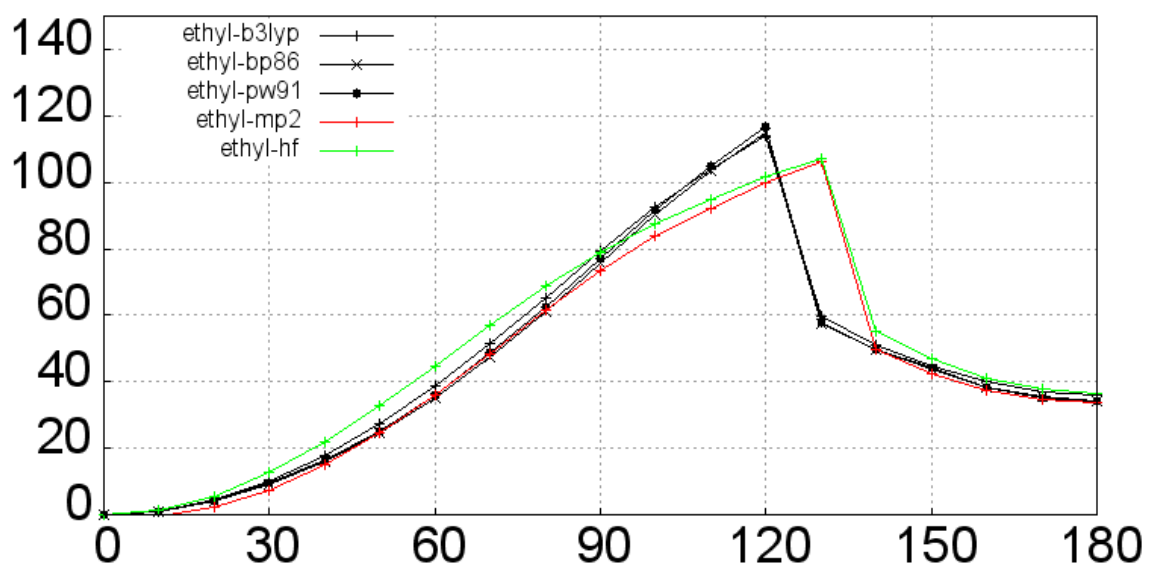
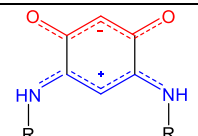
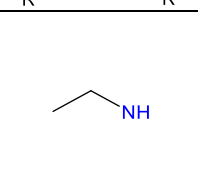
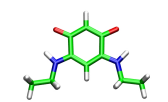
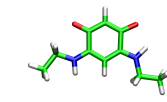
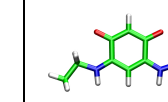
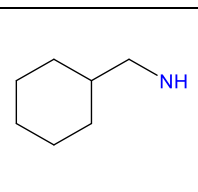
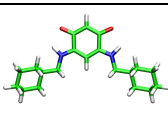
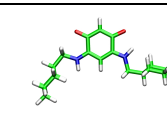
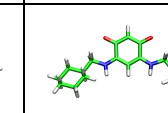
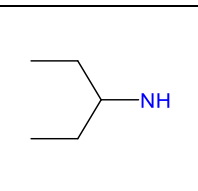
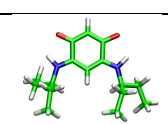
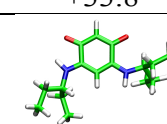
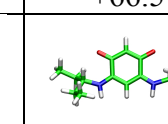
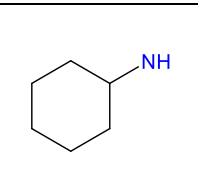
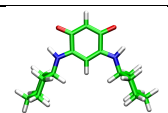
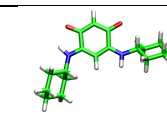
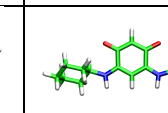
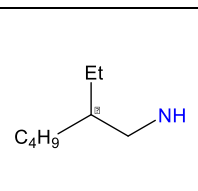
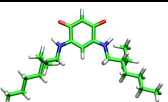
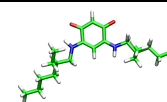
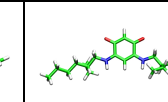


Figure S12. Relative energies (in $\text{kJ}\cdot\text{mol}^{-1}$) as a function of the ϕ' , dihedral angle ($^\circ$) for **(15)** performed with different theoretical methods.

Table S1. Selected X-ray data

| Compound | 9 | 10 | 11 |
|---|---|--|---|
| Chemical formula | C ₁₈ H ₂₆ N ₂ O ₂ | 3(C ₂₂ H ₃₄ N ₂ O ₂), H ₂ O | C ₂₆ H ₂₆ N ₂ O ₂ |
| Formula Mass | 302.41 | 1093.55 | 398.49 |
| Crystal system | Tetragonal | Tetragonal | Orthorhombic |
| <i>a</i> /Å | 11.7927(2) | 11.8773(7) | 8.3180(3) |
| <i>b</i> /Å | 11.7927(2) | 11.8773(7) | 14.3938(5) |
| <i>c</i> /Å | 25.0037(5) | 44.580(3) | 18.1616(6) |
| α /° | 90.00 | 90.00 | 90.00 |
| β /° | 90.00 | 90.00 | 90.00 |
| γ /° | 90.00 | 90.00 | 90.00 |
| Unit cell volume/Å ³ | 3477.21(11) | 6288.9(6) | 2174.45(13) |
| Temperature/K | 193(2) | 173(2) | 173(2) |
| Space group | <i>P</i> 4 ₁ 2 ₁ 2 | <i>P</i> 4 ₃ 2 ₁ 2 | <i>P</i> 2 ₁ 2 ₁ 2 ₁ |
| <i>Z</i> | 8 | 4 | 4 |
| Absorption coefficient, μ /mm ⁻¹ | 0.075 | 0.074 | 0.609 |
| No. of reflections measured | 27890 | 69336 | 11458 |
| No. of independent reflections | 3715 | 4563 | 3631 |
| <i>R</i> _{int} | 0.1091 | 0.0488 | 0.0225 |
| Final <i>R</i> _I values (<i>I</i> > 2σ(<i>I</i>)) | 0.0571 | 0.0527 | 0.0899 |
| Final <i>wR</i> (<i>F</i> ²) values (<i>I</i> > 2σ(<i>I</i>)) | 0.1511 | 0.1145 | 0.2579 |
| Final <i>R</i> _I values (all data) | 0.0829 | 0.0685 | 0.0923 |
| Final <i>wR</i> (<i>F</i> ²) values (all data) | 0.1635 | 0.1228 | 0.2608 |
| Goodness of fit on <i>F</i> ² | 1.120 | 1.074 | 1.072 |

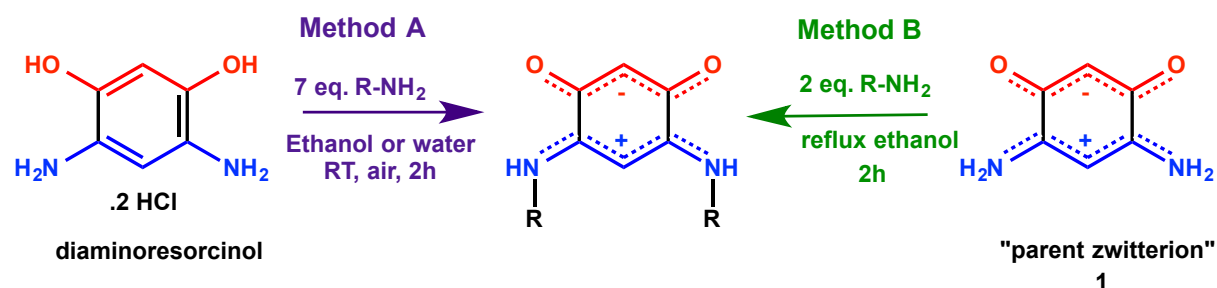
Table S2. B3LYP/6-31+G** optimized energies (in hartree). Relative energies (in $\text{kJ}\cdot\text{mol}^{-1}$) a) $\Delta E_1 = E(0;180) - E(0;0)$ b) $\Delta E_2 = E(180;180) - E(0;0)$

| |  | $E(0;0)$ | $E(0;180)$ ΔE_1^a | $E(180;180)$ ΔE_2^b |
|---|---|------------|---|--|
| 1 |  | -649.4908 | -649.4774 +35.1 | -649.4643 +69.4 |
| |  | |  |  |
| 2 |  | -1040.2487 | -1040.2322 +43.0 | -1040.2210 +72.7 |
| |  | |  |  |
| 3 |  | -885.3918 | -885.3788 +33.8 | -885.3665 +66.5 |
| |  | |  |  |
| 4 |  | -961.6177 | -961.6058 +31.4 | -961.5934 +63.9 |
| |  | |  |  |
| 5 |  | -1121.2894 | -1121.2756 +35.9 | -1121.2621 +71.5 |
| |  | |  |  |

Synthesis of new zwitterions

Quinonoid zwitterions are typically obtained following two different methods (Scheme S1).¹ Following the method A, they are directly obtained by reaction of a primary amine with the diaminoresorcinol (commercial product). This one-pot reaction performed in presence of air yield, in two hours and at room temperature, the desired product. In the method B, the compound is obtained by a trans-amination reaction from the « parent zwitterion » **1**. The latter is easily prepared following the published procedure. This method has the advantage to use only two equivalents of primary amine per « parent zwitterion » **1**.

Scheme S1. General scheme of the two synthetic methods leading to quinonoid zwitterions



We could anticipate that steric hindrance of *N*-substituents would complicate the access to the new zwitterions presented in Scheme 3. Indeed, using method A, the zwitterion **9** was obtained in 14% of yield (Table S3, entry 1) whereas using the same experimental conditions, the butyl zwitterion **2** was obtained quantitatively.

Table S3. Results concerning syntheses of zwitterion **9** under different conditions

| Entry | Method | Experimental conditions | | | | Yield (%) |
|-------|--------|-------------------------|------------|---------|-------------------------|-----------|
| | | Temperature (°C) | Time (min) | solvent | Heating mode | |
| 1 | A | RT | 120 | water | / | 14 |
| 2 | B | 80 | 120 | ethanol | Oil bath ^a | 10 |
| 3 | B | 100 | 120 | water | Oil bath ^a | 55 |
| 4 | B | 80 | 120 | water | Oil bath ^a | 58 |
| 5 | B | 100 | 10 | water | MWI ^b (150W) | 73 |
| 6 | B | 100 | 1 | water | MWI ^b (80W) | 76 |

a) Preheated oil bath, 10 ml of solvent. b) Reaction performed in one close system (sealed CEM 10ml reactor), 2.5ml of water, power up to 150W or 80W, 1 or 10 minutes at 100°C.

Under the typical conditions (ethanol as solvent, 80 °C, 2 h), of method B we could not increase the yield of the reaction (Table S3, entry 2). In contrast, when the reaction was performed in refluxing water, the zwitterion **9** was obtained with a yield of 55% (Table S3, entry 3). This increase is probably due to the use of the water as solvent because when the reaction was carried out at 80 °C (Table S3, entry 4), the product was obtained in 58 % of yield (at this temperature, the yield in ethanol was 10%).

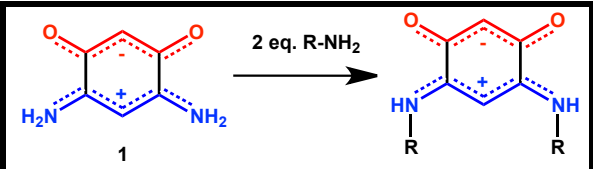
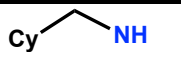
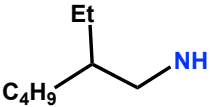
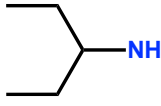
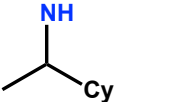
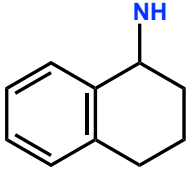
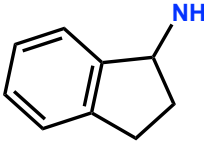
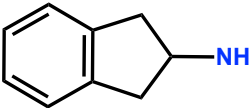
We should emphasize that applying method B in water is unusual because under heating much more decomposition of the “parent zwitterion” **1** is observed in water than in ethanol. To still increase the yield of this reaction, we should reduce the rate of the decomposition of the “parent zwitterion” **1**. One possibility to reach this objective is to use one activating technique allowing performing the reaction at high temperature with short reaction times.² Moreover, scarce examples of trans-amination reaction performed under microwave irradiation are described in the literature.³ Then it was obvious that we should try to synthesize this zwitterion under microwave irradiation. Effectively, compared to the thermal conditions (Table S3, entries 3 and 4), trans-amination under microwave irradiation (Table S3, entry 5) results in a significantly better yield. To perform the reaction under conditions described in the entry 6 of the Table S3 allowed us to obtain the zwitterion **9** with the highest yield. To conclude, to perform the trans-amination reaction under microwave irradiation allows us to obtain the zwitterion **9** in 76% of yield within 1 min.

Then, we have investigate the scope and limitations of the trans-amination reaction under microwave irradiation by the syntheses of all new zwitterions suitable to our study on the anchoring of this family of molecules on gold substrate (Scheme 3). These results are summarized in Table S4.

Performing the trans-amination reaction under microwave irradiation, in water, afforded the best yields (Table S4), except for **10**. The zwitterions **8** and **12** were obtained in much lower yields, probably owing to the solubility of **8** in water (loss of product during work-up), and in the case of **12**, to the lower miscibility of the corresponding amine with water, resulting in a biphasic mixture.

These results show that microwave activation can bring about significant improvements and offers a fast (typical 2 min. reaction time) and efficient access to several sterically-hindered or chiral zwitterions.

Table S4. Results concerning syntheses of zwitterions with steric hindrance. Yields in %.

| | |  | | Method A | | |
|-------|--|--|---------|------------------------|---------|----|
| Entry | R-NH (Zwitterion) | Thermal ^a | | Microwave ^b | | |
| | | water | Ethanol | water | Ethanol | |
| 1 |  (6) | 67 | 66 | 84 | NR | NR |
| 2 |  (7) | 45 | 36 | 68 | 37 | NR |
| 3 |  (8) | ND | ND | 28 | NR | NR |
| 4 |  (10) | 60 | 14 | 29 | NR | 33 |
| 5 |  (11) | 51 | 9 | 61 | NR | NR |
| 6 |  (12) | 13 | NR | 28 | NR | NR |
| 7 |  (13) | 61 | NR | 87 | 23 | NR |

a) Preheated oil bath, 10 ml of solvent, 2 hours at 80 or 100 °C. b) Reaction performed in one close system (sealed CEM 10ml reactor), 2.5ml of water, power up to 80W, 2 minutes at 100°C. NR (Not Realized) and ND (Not Determined)

Structural analyses by X-ray diffraction

Single crystals of zwitterions **9** - **11** were obtained at room temperature by slow diffusion of pentane into their dichloromethane solution. The molecular structures of **9** - **11** (Figure S13) were elucidated by X-ray diffraction. Crystallographic details are given in the Table S1.



Figure S13. Mercury views of the quinonoid zwitterions **9-11**. Thermal ellipsoids are drawn at the 50% probability level. H atoms are not shown for clarity.

1. General structural features of these quinonoid molecules

The bond lengths within the “C₆ core” (Table S5) vary little with substituent and are similar to those observed in related zwitterions.^{1,4} Interestingly, the bond lengths C(3)-C(4) / C(4)-C(5) and C(3)-O(1) / C(5)-O(2), respectively, are almost equal. Likewise C(1)-C(6) / C(1)-C(2) as well as C(2)-N(1) / C(6)-N(2) are respectively similar (Table S5).

The latter bond lengths are intermediate between those for single and double bonds and consistent with extensive electronic delocalization. However, the C(2)-C(3) and C(5)-C(6) bond distances are much longer and consistent with single bonds. On the basis of these values, these zwitterions are well described as two fully delocalized 6 π electrons systems (trimethyne oxonol part: O...C...CH...C...O and the trimethyne cyanine part: N...C...CH...C...N) connected by two C-C single bonds.

Table S5. Interatomic distances (Å) in zwitterions **9-11**

| | Zwitterion 9 | Zwitterion 10 | Zwitterion 11 |
|-----------|---------------------|----------------------|----------------------|
| C(1)-C(2) | 1.394(3) | 1.384(3) | 1.387(7) |
| C(2)-C(3) | 1.529(3) | 1.530(4) | 1.527(7) |
| C(3)-C(4) | 1.397(3) | 1.393(3) | 1.388(7) |
| C(4)-C(5) | 1.389(3) | 1.388(3) | 1.388(8) |
| C(5)-C(6) | 1.532(3) | 1.533(4) | 1.526(8) |
| C(6)-C(1) | 1.388(3) | 1.390(3) | 1.403(7) |
| C(3)-O(1) | 1.254(2) | 1.251(3) | 1.243(6) |
| C(5)-O(2) | 1.251(2) | 1.254(3) | 1.249(7) |
| C(2)-N(1) | 1.316(3) | 1.317(3) | 1.316(7) |
| C(6)-N(2) | 1.315(3) | 1.322(3) | 1.312(8) |

2. Packing in the Solid-State

The steric hindrance of the R substituent in α position, to nitrogen atom, has a considerable influence on the molecular arrangement in the solid state. Molecular arrangements of zwitterions **9-11** are compared to the one of thioether zwitterion **3**.

2.1. Molecular arrangement of zwitterion **3** in the crystalline state

As illustrated by the structure of the N-substituted thioether zwitterion **3**,^{4d} this family of molecules usually forms an infinite 1-D ribbon in which the molecules adopt a head-to-tail arrangement due to hydrogen bonding and dipolar interactions (Figure S14). In this arrangement, adjacent molecules are coplanar. Figure S15a shows that a packed 'row' of molecules is formed in a direction orthogonal to the C₆ core, with a spacing of 3.24 Å.^{4d} Similar packing, hereafter mentioned as 'packing rows', is observed on the gold substrate (Scheme 2a-d). Each row interacts via hydrogen bonds with an adjacent head-to-tail row (Figure S15b).

Zwitterion 3:

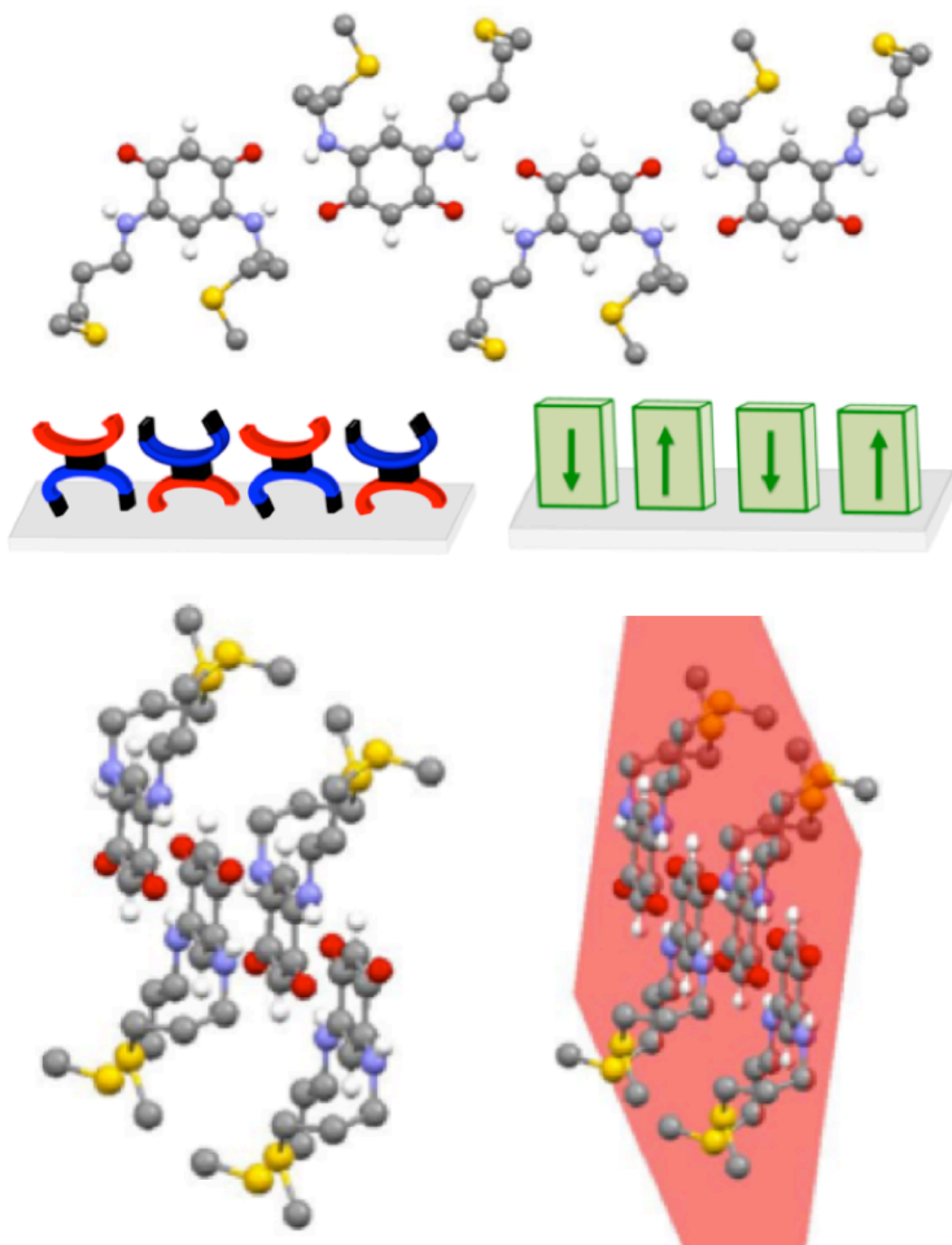


Figure S14. Head-to-tail arrangement of zwitterions **3** in the crystalline state. Parallelepipeds represent the quinonoid core and the arrows indicate the dipoles directions. Anionic and cationic parts of quinonoid zwitterions are represented in red and blue, respectively.

Zwitterion 3:

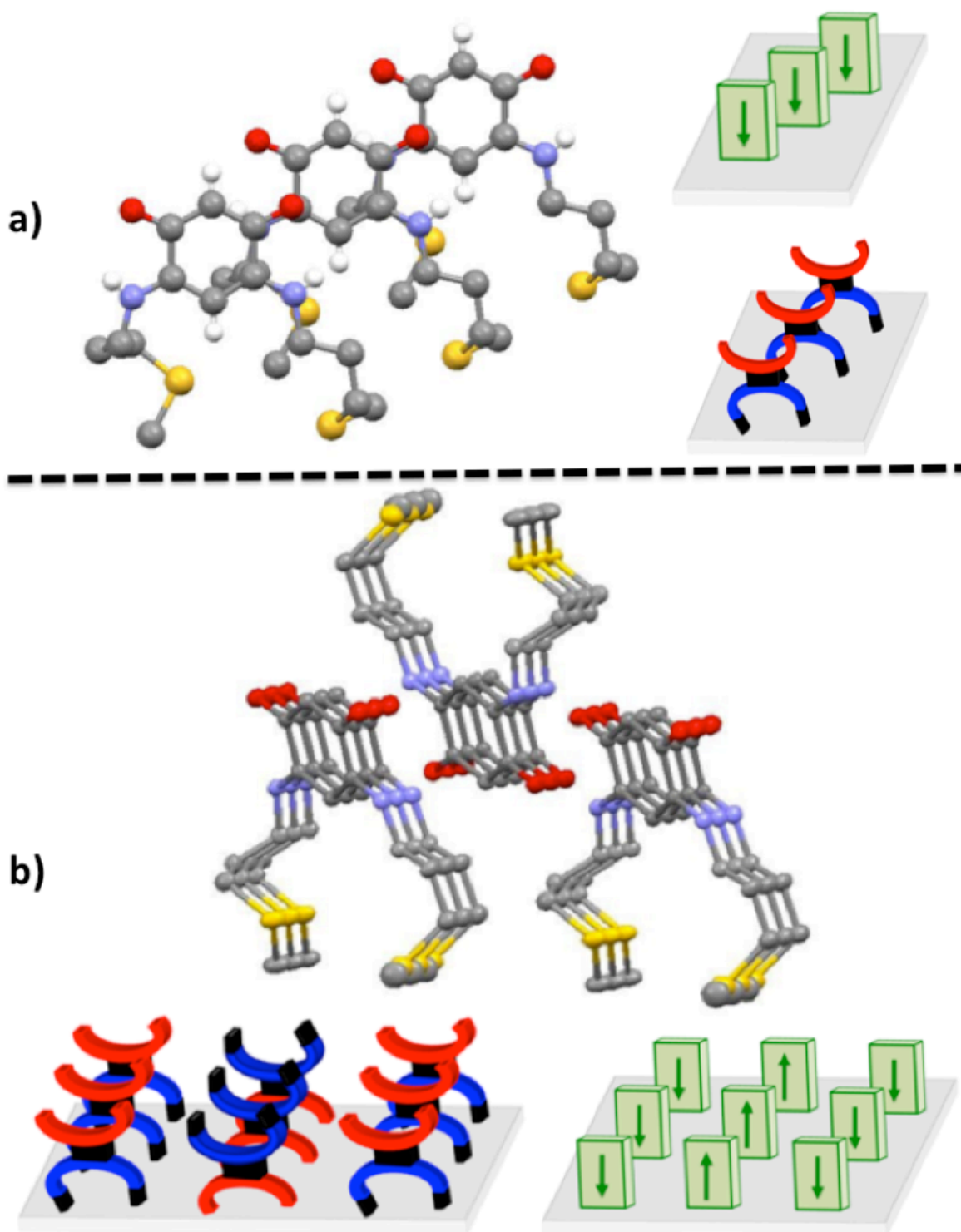


Figure S15. Molecular arrangement of zwitterions 3 in the crystalline state. a) a row of molecules 3. b) a succession of 3 molecular rows. Parallelepipeds represent the quinonoid core and the arrows indicate the dipoles directions. Anionic and cationic parts of quinonoid zwitterions are represented in red and blue, respectively.

2.2.2. Influence of the steric hindrance on the head-to-tail arrangement

The steric hindrance of the molecule substituents is expected to exert an influence on the head-to-tail arrangement. Zwitterion **9-11** are arranged in a head-to-tail manner but the angle formed by the “quinonoid core” ($C_6O_2N_2$) of two adjacent molecules is around 125° for **9** (Figure S16), 135° for **10** (Figure S17) and 150° for **11** (Figure S18). Moreover, in the case of zwitterion **9**, units of two molecules arranged in a head-to-tail manner are isolated (Figure S16).

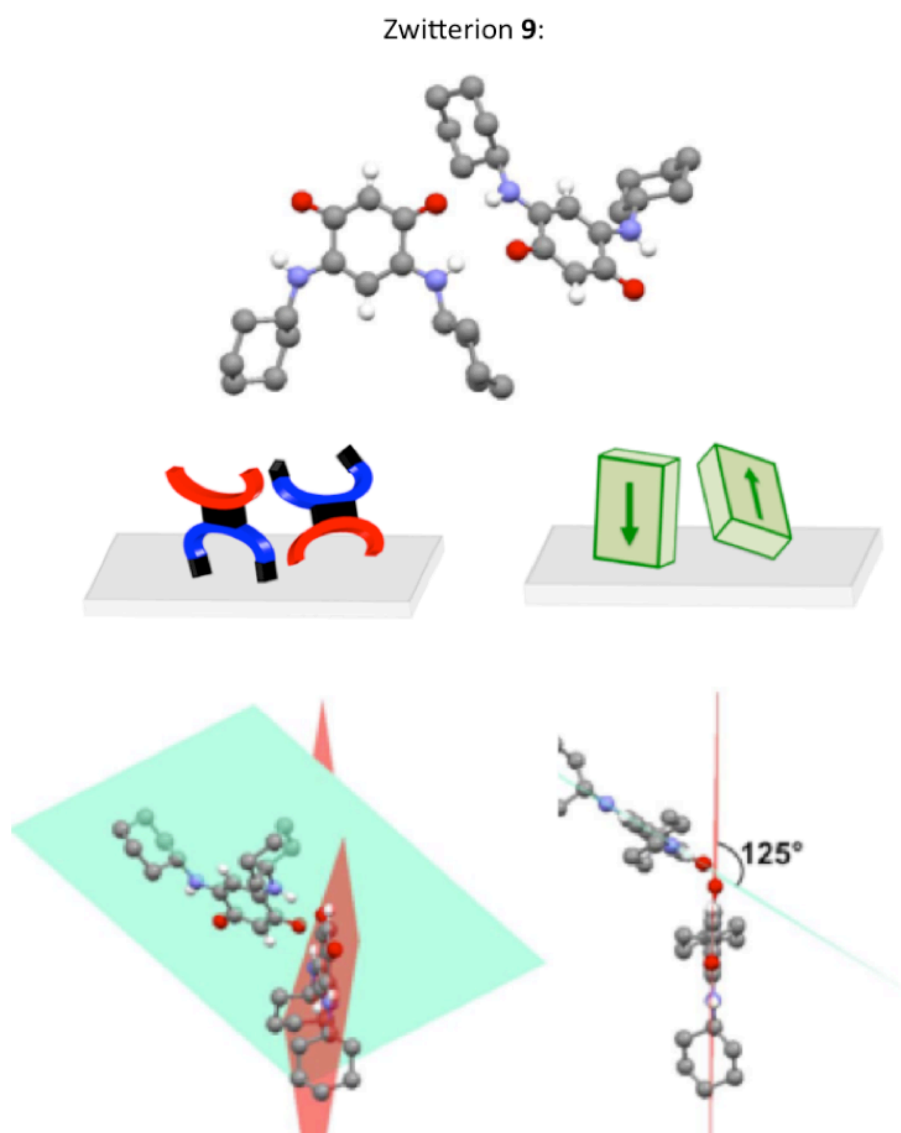


Figure S16. Head-to-tail arrangement of the zwitterion **9** in the crystalline state. In the sketch on the molecular arrangement of **9**, anionic and cationic parts of quinonoid zwitterions are respectively represented in red and blue.

This strongly contrasts with the usual 1-D arrangement observed.⁴ As illustrated for zwitterion **3**, such two units of head-to-tail arrangement interact with each other by hydrogen bonding and dipolar interactions (Figure S14).^{4f} In the case of the zwitterion **10**, an infinite head-to-tail arrangement is obtained. However the compound co-crystallizes with molecules of water. We observe the presence of a molecule of water every three molecules of the head-to-tail arrangement (Figure S17).

Zwitterion **10**:

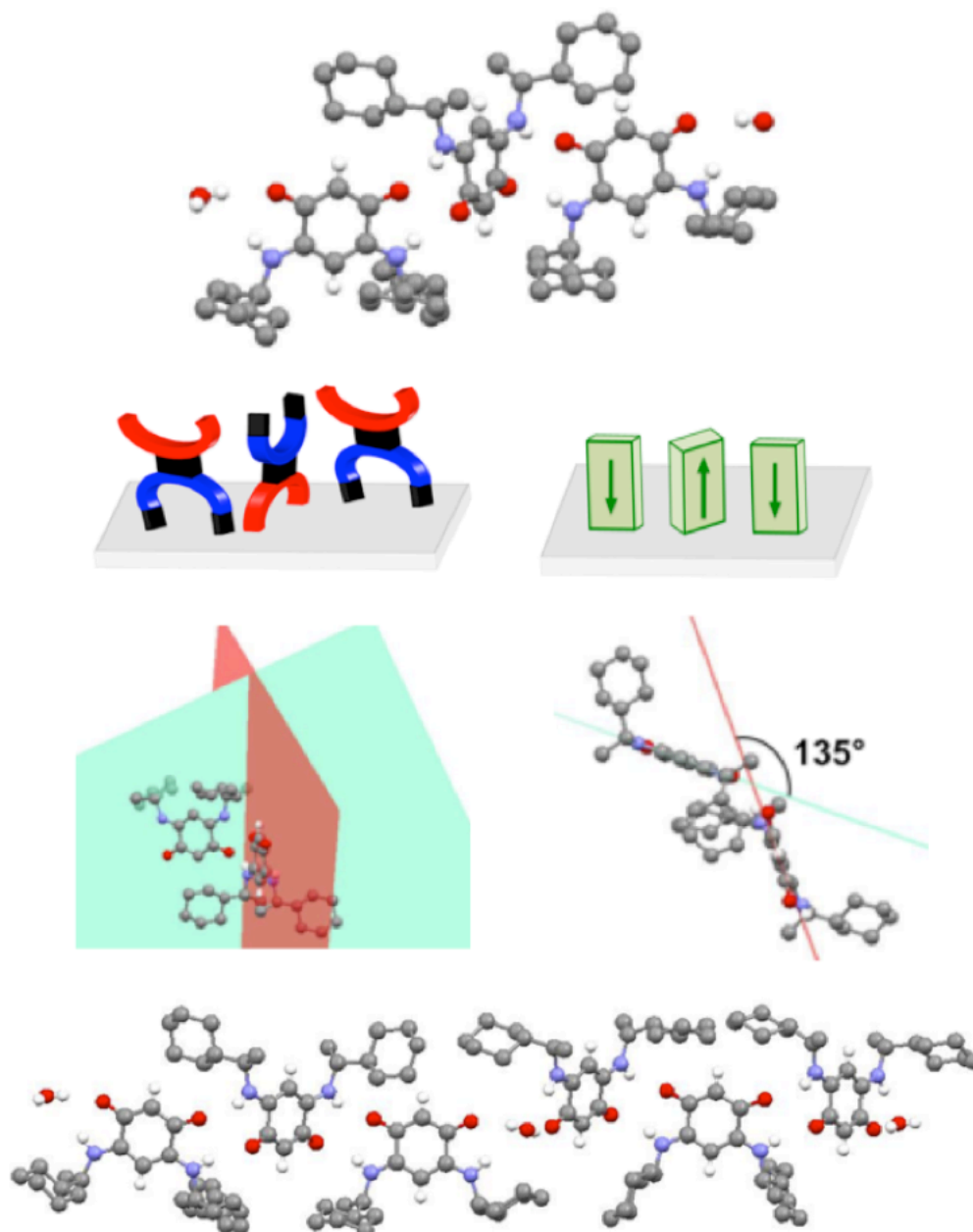


Figure S17. Head-to-tail arrangement of the zwitterion **10** in the crystalline state. In the sketch on the molecular arrangement of **10**, anionic and cationic parts of quinonoid zwitterions are respectively represented in red and blue.

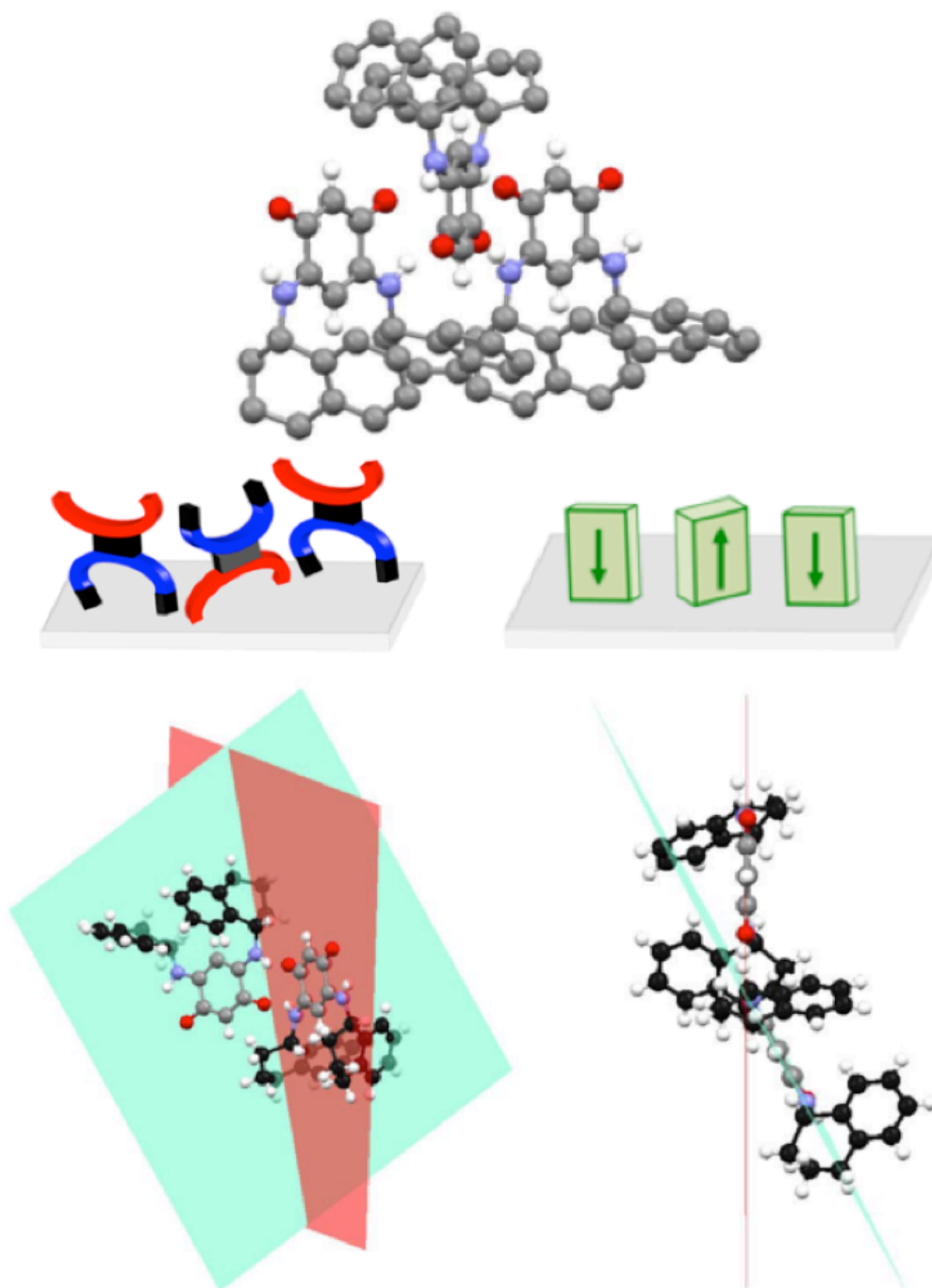
Zwitterion **11**:

Figure S18. Head-to-tail arrangement of the zwitterion **11** in the crystalline state. In the sketch on the molecular arrangement of **11**, anionic and cationic parts of quinonoid zwitterions are respectively represented in red and blue.

We find that in general, molecules with bulky substituents are also arranged in a head-to-tail manner (Figure S19a). In this case, the angle formed by the “quinonoid core” ($C_6O_2N_2$) of two adjacent molecules is around $120-150^\circ$ whereas adjacent

molecules of **3** are coplanar (Figure S14). In the case of **11**, we observe that this difference has an effect on the succession of molecular rows (Figure S19b).

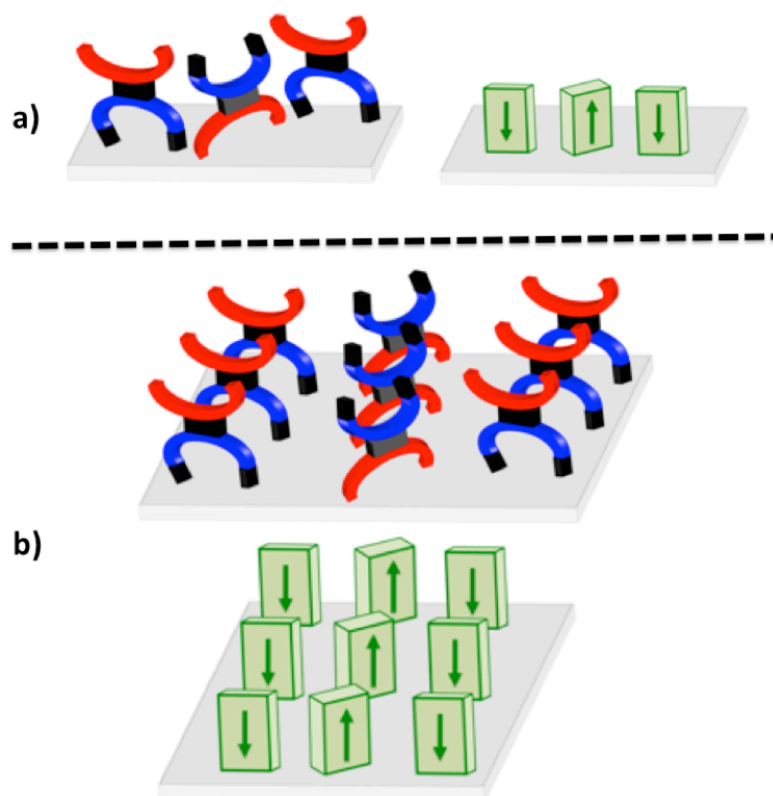


Figure S19. Sketch of the molecular arrangement of zwitterions with a bulky N-substituent. a) head-to-tail arrangement. b) a succession of 3 molecular rows of **11**. Parallelepipeds represent the quinonoid core and the arrows indicate the directions of the dipoles. The anionic and cationic parts of the quinonoid zwitterions are represented in red and blue, respectively.

2.3. Influence of the substituent on the steric hindrance on the molecular rows

Compound **10** co-crystallizes with water molecules which interact via H-bonds with the zwitterions and thereby modify the molecular arrangement (Figure S17).

In the case of **9**, hydrogen bonding is observed between an oxygen atom of the anionic system and the hydrogen of the trimethylene cyanine part (cationic system) and 2 H atoms of the cyclohexyl substituents (Figure S20a). Four hydrogen bonding of this type and one unit of head-to-tail arrangement constitute the motif of the molecular arrangement of **9** (Figure S20b). In other words, each zwitterionic molecule is involved in one unit of head-to-tail arrangement and has hydrogen bonding with two other zwitterions. In the structure of **9**, there are no molecular rows formed.

In the case of the zwitterion **11**, intermolecular hydrogen bonding leads to the arrangement presented in Figure S21a. In contrast to **9**, hydrogen interaction between the tetrahydronaphthyl substituent of **11** and the trimethylene oxonol part of neighboring molecules leads to an arrangement with a molecular row perpendicular to the C6 core (Figure S21b). Figure S21d illustrates the orthogonality of two molecular rows.

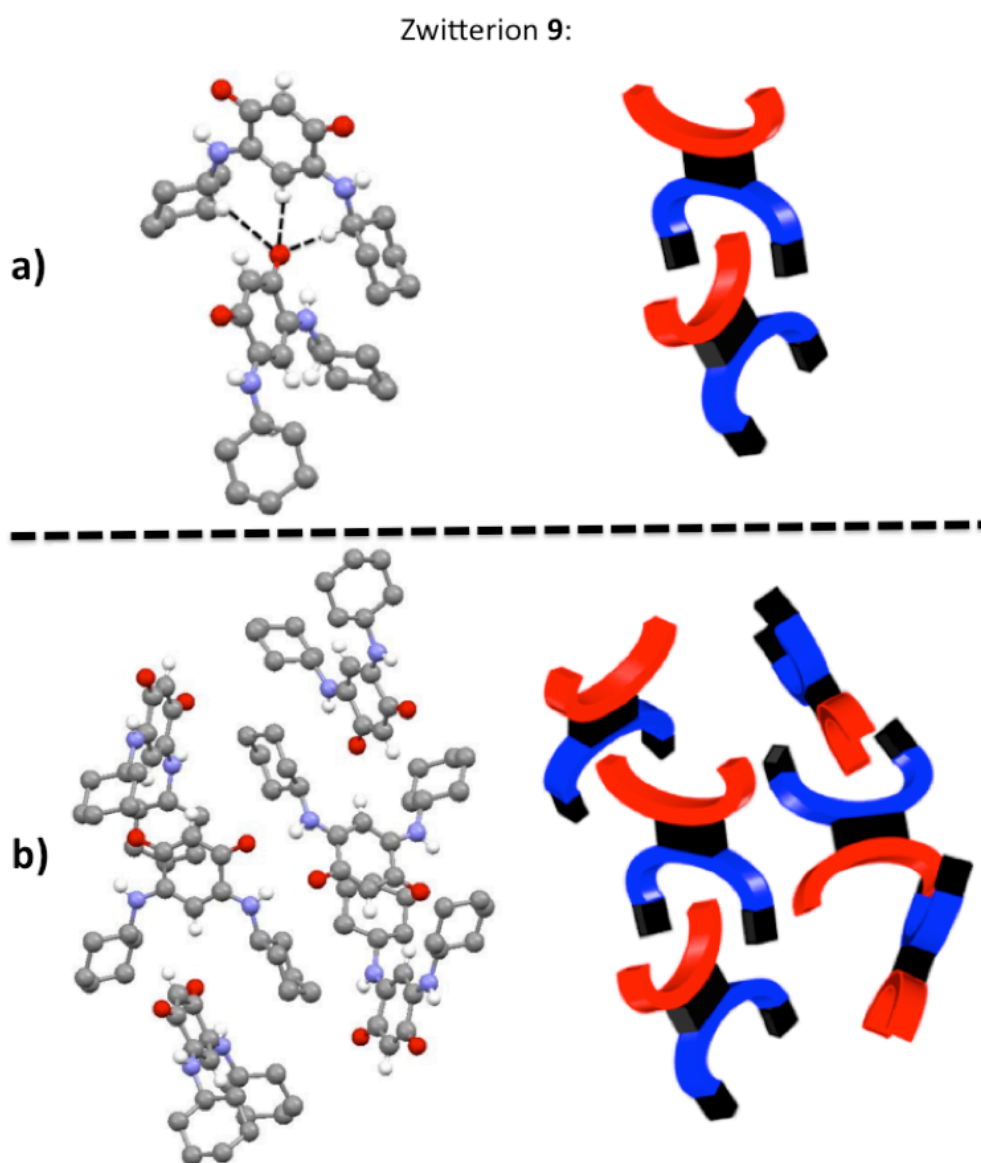


Figure S20. Molecular arrangement of the zwitterion **9** in the crystalline state. a) Hydrogen bonding between two quinonoid zwitterions. b) View of the packing of zwitterion **9**. In the sketch, anionic and cationic parts of quinonoid zwitterions are represented in red and blue, respectively.

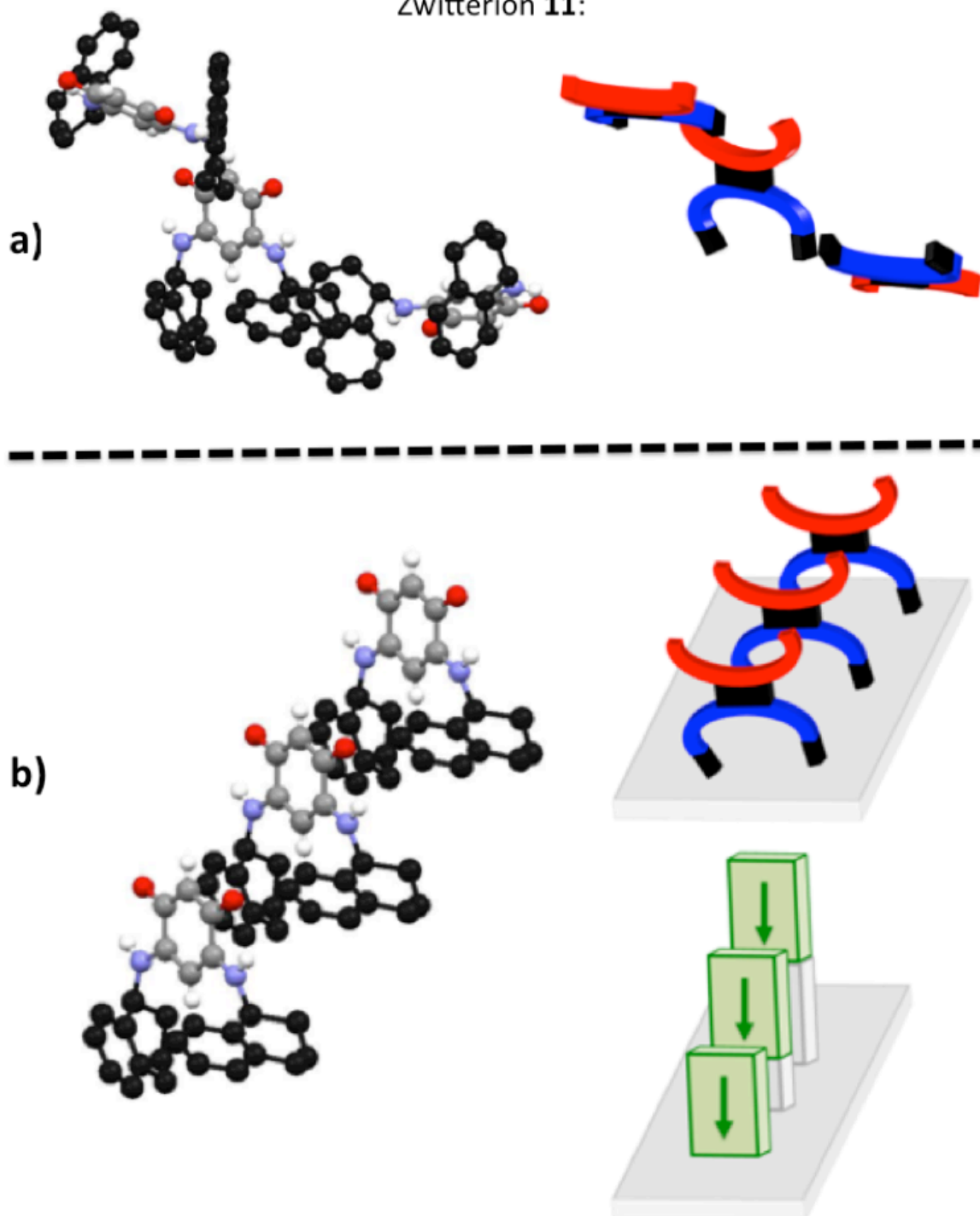
Zwitterion **11**:

Figure S21. a) Hydrogen bonding between two quinonoid zwitterions. b) Pattern of the packing of zwitterion **11**. In the sketch, anionic and cationic parts of quinonoid zwitterions are respectively represented in red and blue.

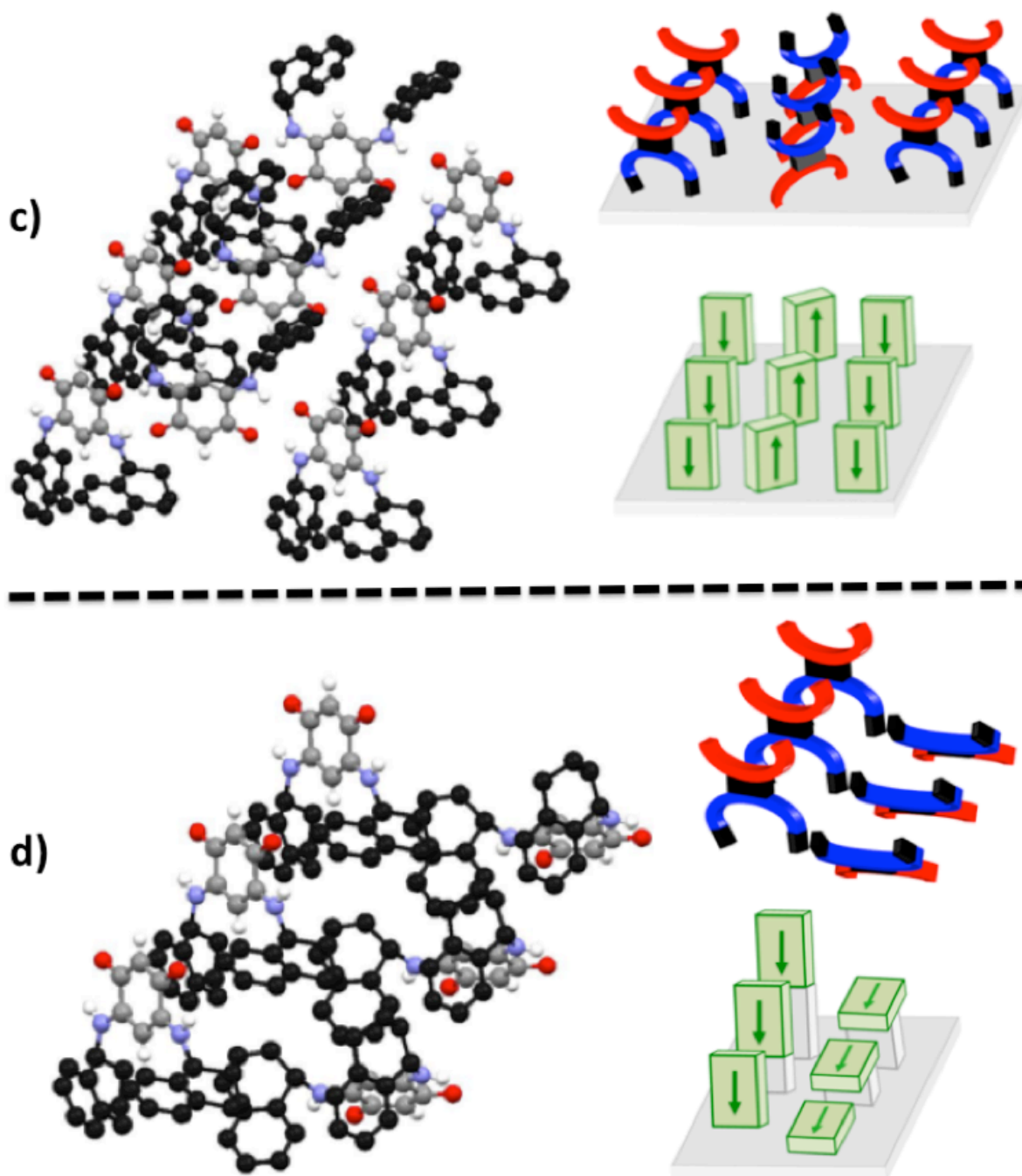
Zwitterion **11**:

Figure S21. c) Pattern that associates the packing of zwitterion **11** and the head-to-tail arrangement. d) Pattern that associates the packing of zwitterion **11** and hydrogen bonding between two quinonoid zwitterions. In the sketch, anionic and cationic parts of quinonoid zwitterions are respectively represented in red and blue.

Interestingly, the molecular arrangement of zwitterion **14** is similar to that observed for zwitterion **11**. The X-ray structure of the isopropyl zwitterion **14** has been briefly described and is detailed below.⁵

Molecules of zwitterion **14** form an infinite 1-D ribbon in which the molecules adopt a head-to-tail arrangement. The angle formed by the “quinonoid core” ($C_6O_2N_2$) of two adjacent molecules is around 130° (Figure S22).

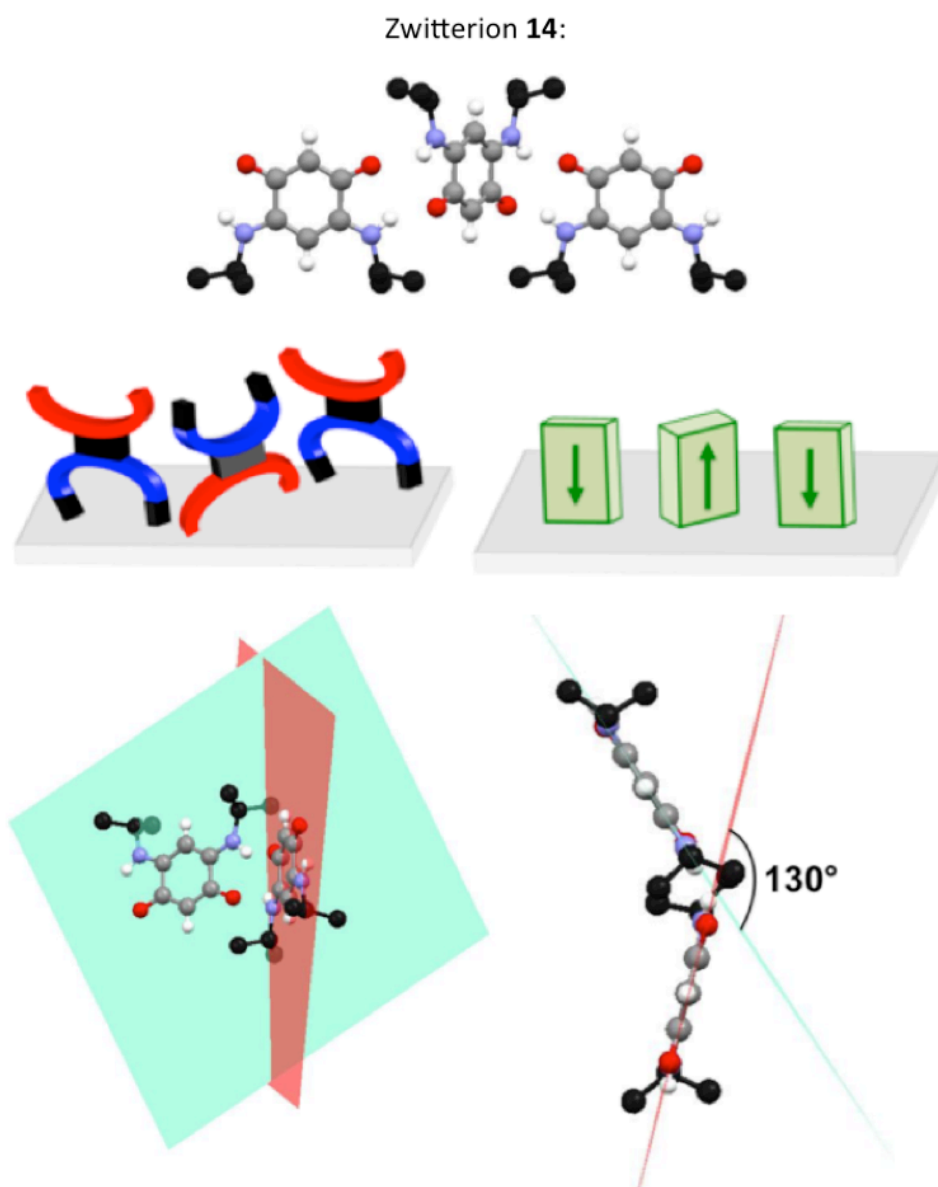


Figure S22. Head-to-tail arrangement of the zwitterion **14** in the crystalline state. In the sketch on the molecular arrangement of **14**, anionic and cationic parts of quinonoid zwitterions are respectively represented in red and blue.

We observed two type of hydrogen interaction between the isopropyl substituent of **14** and the trimethyne oxonol part of neighboring molecules. Hydrogen interaction described in Figure S23a lead to an arrangement in which neighboring zwitterionic cores are alternatively horizontal and vertical (Figure S23b).

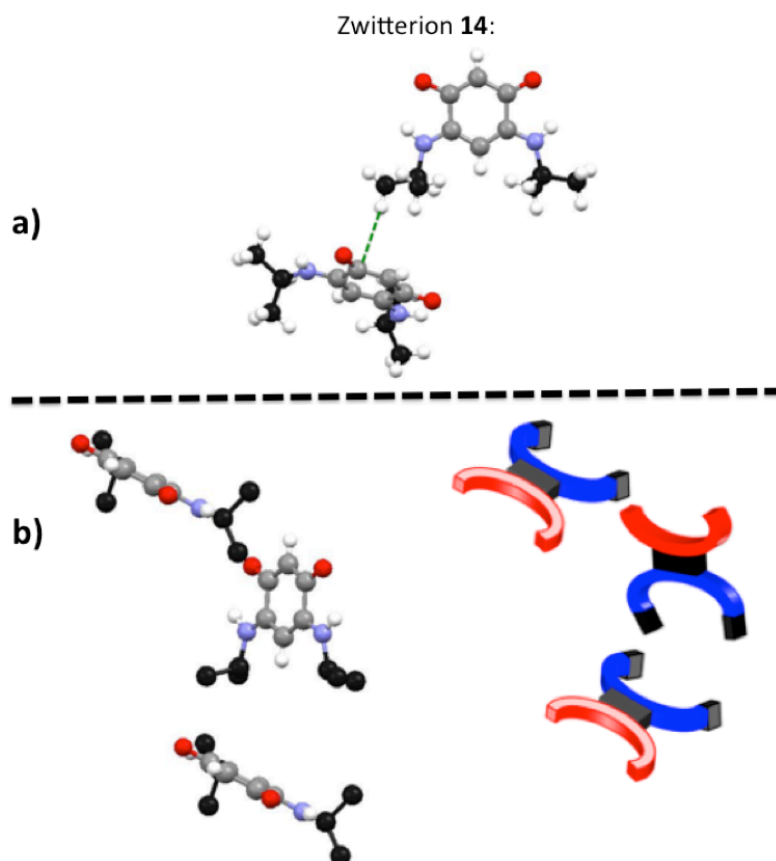


Figure S23. Molecular arrangement of the zwitterion **14** in the crystalline state. a) Interaction between two quinonoid molecules. b) Molecular arrangement of **14**. In the sketch on the molecular arrangement of **14**, anionic and cationic parts of quinonoid zwitterions are respectively represented in red and blue.

Hydrogen interaction described in Figure S24a yield to the formation of a molecular row in an orthogonal direction of the C6 core (Figure S24b).

The Figure S25a indicates a succession of three molecular rows driven by the head-to-tail arrangement. Finally the Figure S25b represents two neighboring molecular rows: one is horizontal and the other one vertical.

The structures of zwitterions **11** and **14** tend to indicate that the absence of a methylene group in α position to the nitrogen atom results in: 1) the formation of a head-to-tail arrangement with a large angle between “quinonoid core” ($C_6O_2N_2$) of two adjacent molecules. 2) to the orthogonality of molecular rows as illustrated in Figures S21d and S25b.

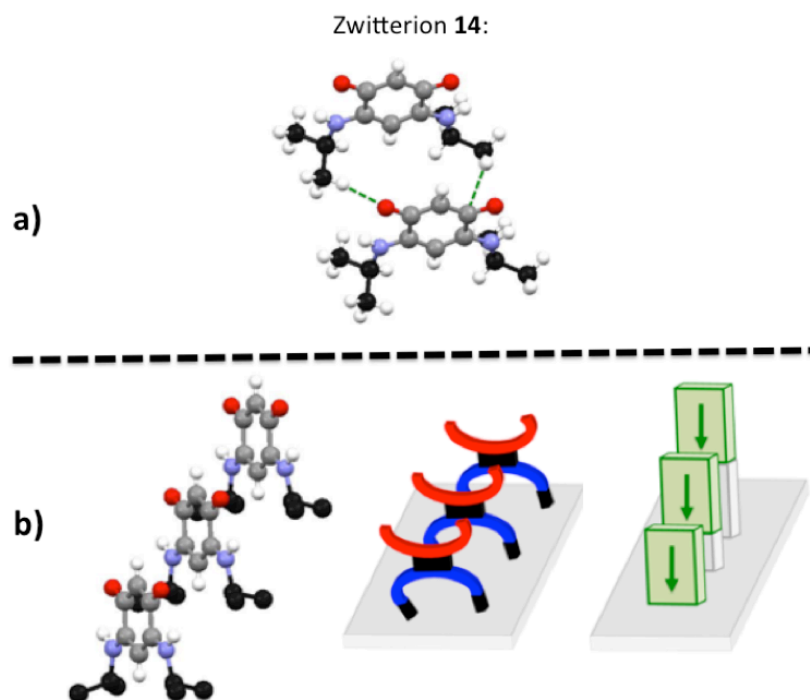


Figure S24. Molecular row of **14** in the crystalline state. a) Hydrogen interaction between two molecules. b) Molecular row of **14**. In the sketch on the molecular arrangement of **14**, anionic and cationic parts of quinonoid zwitterions are respectively represented in red and blue.

The X-ray diffraction analysis establishes that the molecular arrangement of **11** is closer to that of the isopropyl zwitterion **14** than of **9**. Predicting the molecular arrangement in the solid state is very difficult, if not impossible, in view of the complex interplay of interactions.

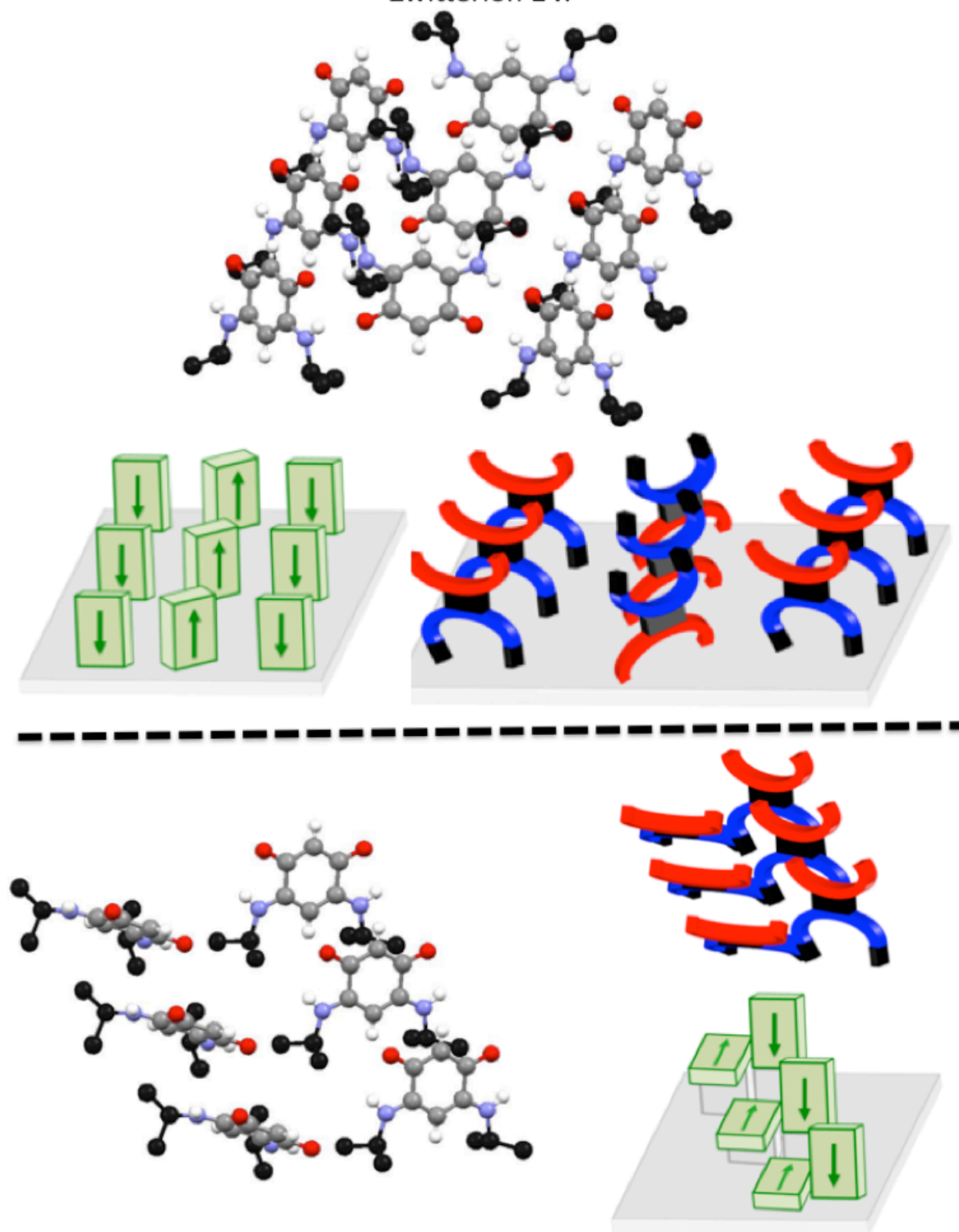
Zwitterion **14**:

Figure S25. Succession of molecular rows of **14**. Parallelepipeds represent the quinonoid core and the arrows indicate the direction of the dipoles. The anionic and cationic parts of the quinonoid zwitterions are represented in red and blue, respectively.

References:

¹ a) P. Braunstein, O. Siri, J.-P. Taquet, M.-M. Rohmer, M. Benard and R. Welter, *J. Am. Chem. Soc.* 2003, **125**, 12246-12256. b) P. Braunstein, O. Siri and J.P. Taquet, WO 2004009534 A1, 2004. c) J.-P. Taquet, O. Siri, P. Braunstein and R. Welter, *Inorg. Chem.* 2004, **43**, 6944-6953. d) Q.-Z. Yang, O. Siri and P. Braunstein, *Chem. Eur. J.* 2005, **11**, 7237-7246. e) P. Braunstein, O. Siri, P. Steffanut, M. Winter and Q.-Z. Yang, *C. R. Chimie* 2006, **9**, 1493-1499. f) Q.-Z. Yang, A. Kermagoret, M. Agostinho, O. Siri, and P. Braunstein, *Organometallics* 2006, **25**, 5518-5527. g) M. Yuan, F. Weisser, B. Sarkar, A. Garci, P. Braunstein, L. Routaboul and B. Therrien, *Organometallics* 2014, **33**, 5043-5045. h) A. Ghisolfi, A. Waldvogel, L. Routaboul and P. Braunstein, *Inorg. Chem.* 2014, **53**, 5515-5526.

² For some recent reviews see for examples: a) Gawande, M. B.; Bonifacio, V. D. B.; Luque, R.; Branco, P. S.; Varma, R. S. *Chem. Soc. Rev.* **2013**, *42*, 5522-5551. b) Gupta, A. K.; Singh, N.; Singh, K. N. *Curr. Org. Chem.* **2013**, *17*, 474-490. c) Majumder, A.; Gupta, R.; Jain, A. *Green Chem. Lett. Rev.* **2013**, *6*, 151-182. d) Bukhariya, V.; Shukla, A.; Mehta, J.; Charde, R. *Int. J. Pharm. Chem.* **2011**, *1*, 21-38. e) Baig, R. B. N.; Varma, R. S. *Chem. Soc. Rev.* **2012**, *41*, 1559-1584. f) Garella, D.; Borretto, E.; Di Stilo, A.; Martina, K.; Cravotto, G.; Cintas, P. *Med. Chem. Commun.* **2013**, *4*, 1323-1343. g) Chandak, S.; Sharma, D.; Sharma, V.; Dubey, A. *Int. J. Pharm. Sci. Rev. Res.* **2012**, *15*, 15-22. h) Messina, F.; Rosati, O. *Curr. Org. Chem.* **2013**, *17*, 1158-1178.

³ a) Gediz Erturk, A.; Bekdemir, Y. *Phosphorus, Sulfur Silicon Relat. Elem.* **2014**, *189*, 285-292. b) Dahmani, Z.; Rahmouni, M.; Brugidou, R.; Bazureau, J. P.; Hamelin, J. *Tetrahedron Lett.* **1998**, *39*, 8453-8456. c) Lefever, M.; Kosmeder, J. W., II; Farrell, M.; Bieniarz, C. *Bioconjugate Chem.* **2010**, *21*, 1773-1778. d) Rashinkar, G.; Kamble, S.; Kumbhar, A.; Salunkhe, R. *Transition Met. Chem.* **2010**, *35*, 185-190.

⁴ a) J. Xiao, Z. Zhang, D. Wu, L. Routaboul, P. Braunstein, B. Doudin, Y. B. Losovyj, O. Kizilkaya, L. G. Rosa, C. N. Borca, A. Gruverman and P. A. Dowben, *Phys. Chem. Chem. Phys.* 2010, **12**, 10329-10340. b) Z. Zhang, J. Alvira, X. Barbosa, L. G. Rosa, L. Routaboul, P. Braunstein, B. Doudin and P. A. Dowben, *J. Phys. Chem. C* 2011, **115**, 2812-2818. c) L. G. Rosa, J. Velez, Z. Zhang, J. Alvira, O. Vega, G. Diaz, L. Routaboul, P. Braunstein, B. Doudin, Y. B. Losovyj and P. A. Dowben, *Phys Status Solidi B* 2012, **249**, 1571-1576. d) L. Routaboul, P. Braunstein, J. Xiao, Z. Zhang, P. A. Dowben, G. Dalmas, V. Da Costa, O. Felix, G. Decher, L. G. Rosa and B. Doudin, *J. Am. Chem. Soc.* 2012, **134**, 8494-8506. e) P. A. Dowben, D. A. Kunkel, A. Enders, L. G. Rosa, L. Routaboul, B. Doudin and P. Braunstein, *Top. Catal.* 2013, **56**, 1096-1103.

⁵ Braunstein, P.; Bubrin, D.; Sarkar, B. *Inorg. Chem.* **2009**, *48*, 2534-2540.

Figure S26. ^1H NMR spectrum of zwitterion **6** (CDCl_3 ; 500 MHz)

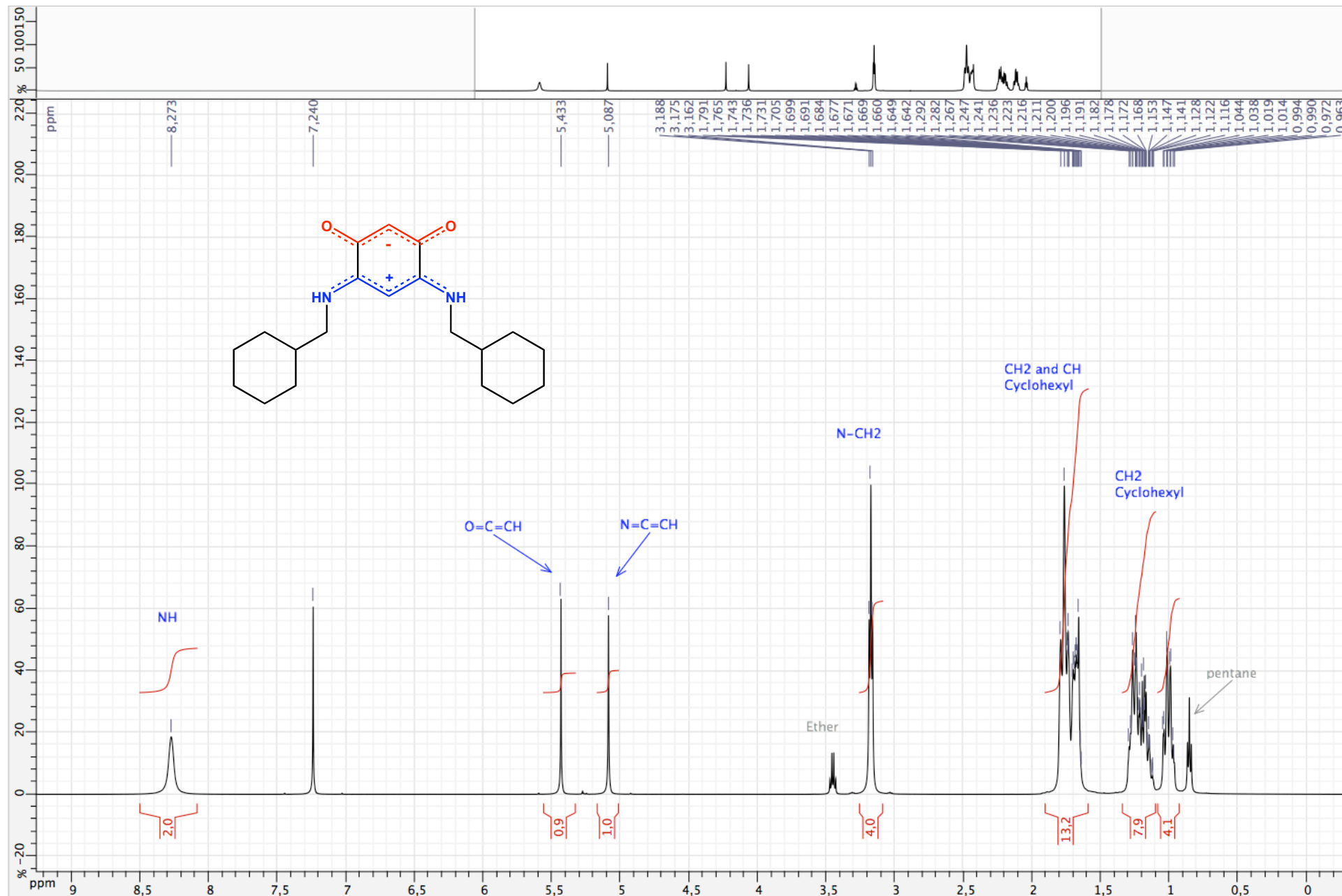


Figure S27. ¹H NMR spectrum of zwitterion **6** (CDCl₃ ; 500 MHz)

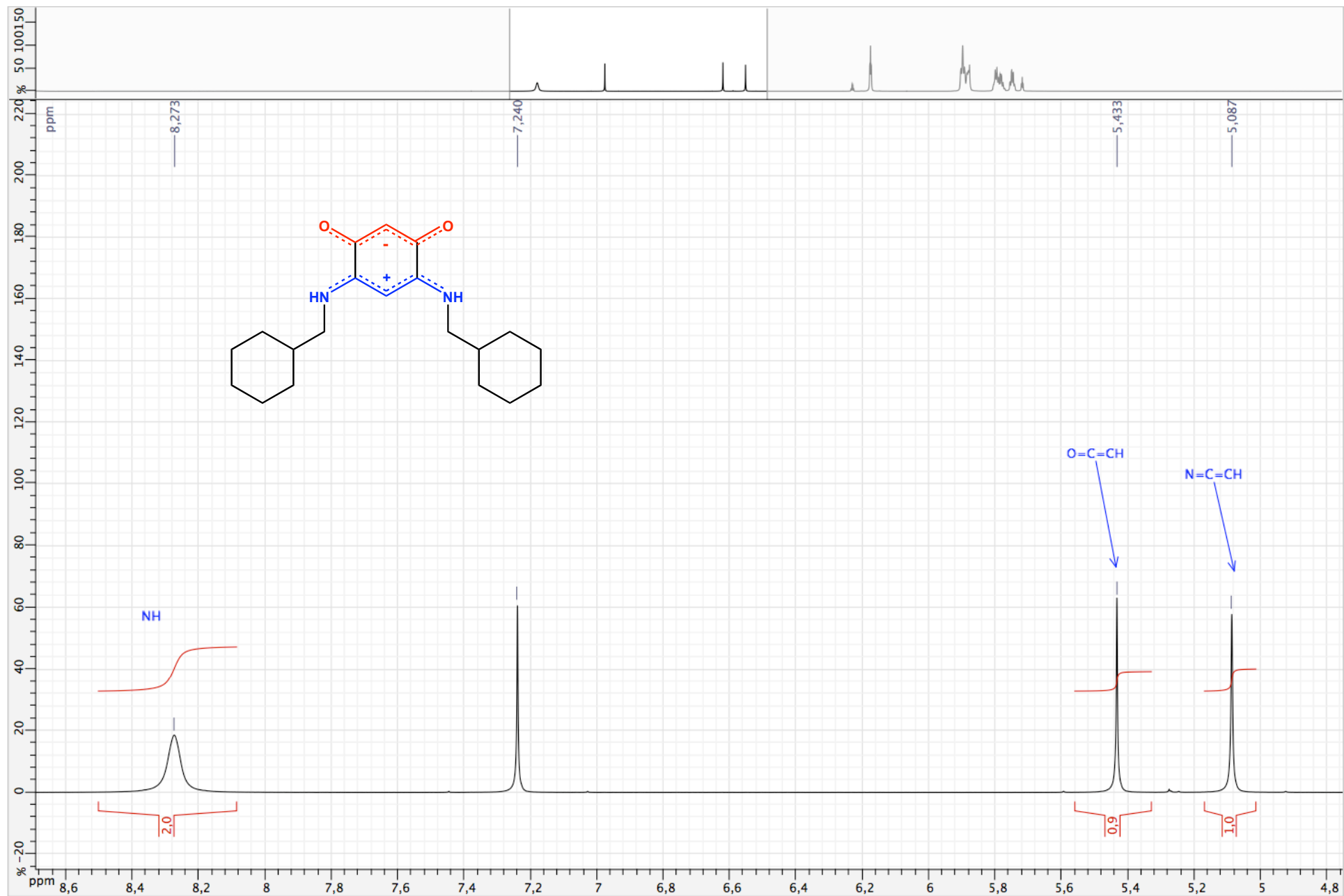


Figure S28. ¹H NMR spectrum of zwitterion **6** (CDCl₃ ; 500 MHz)

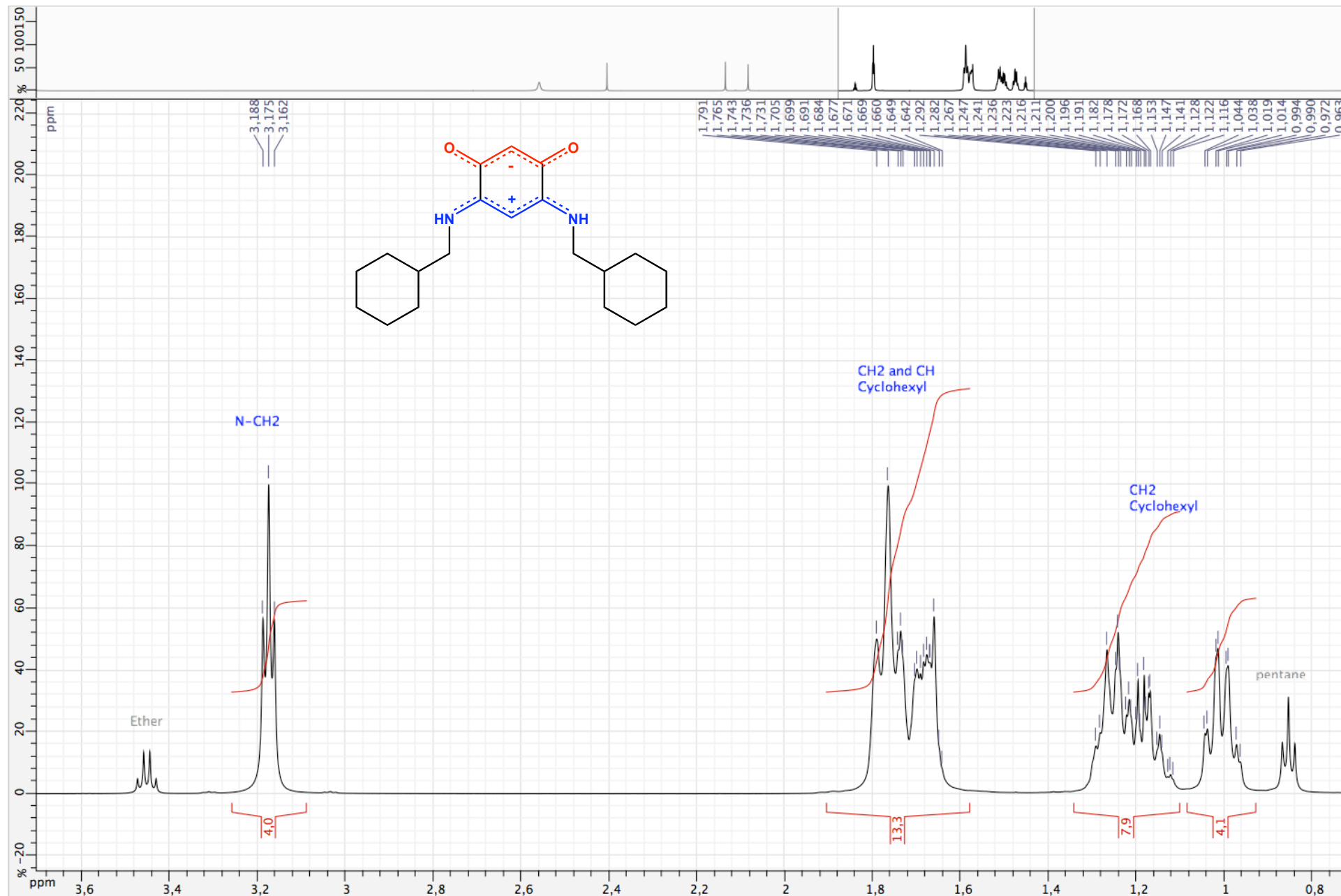


Figure S29. ^{13}C NMR spectrum of zwitterion **6** (CDCl_3 ; 500 MHz)

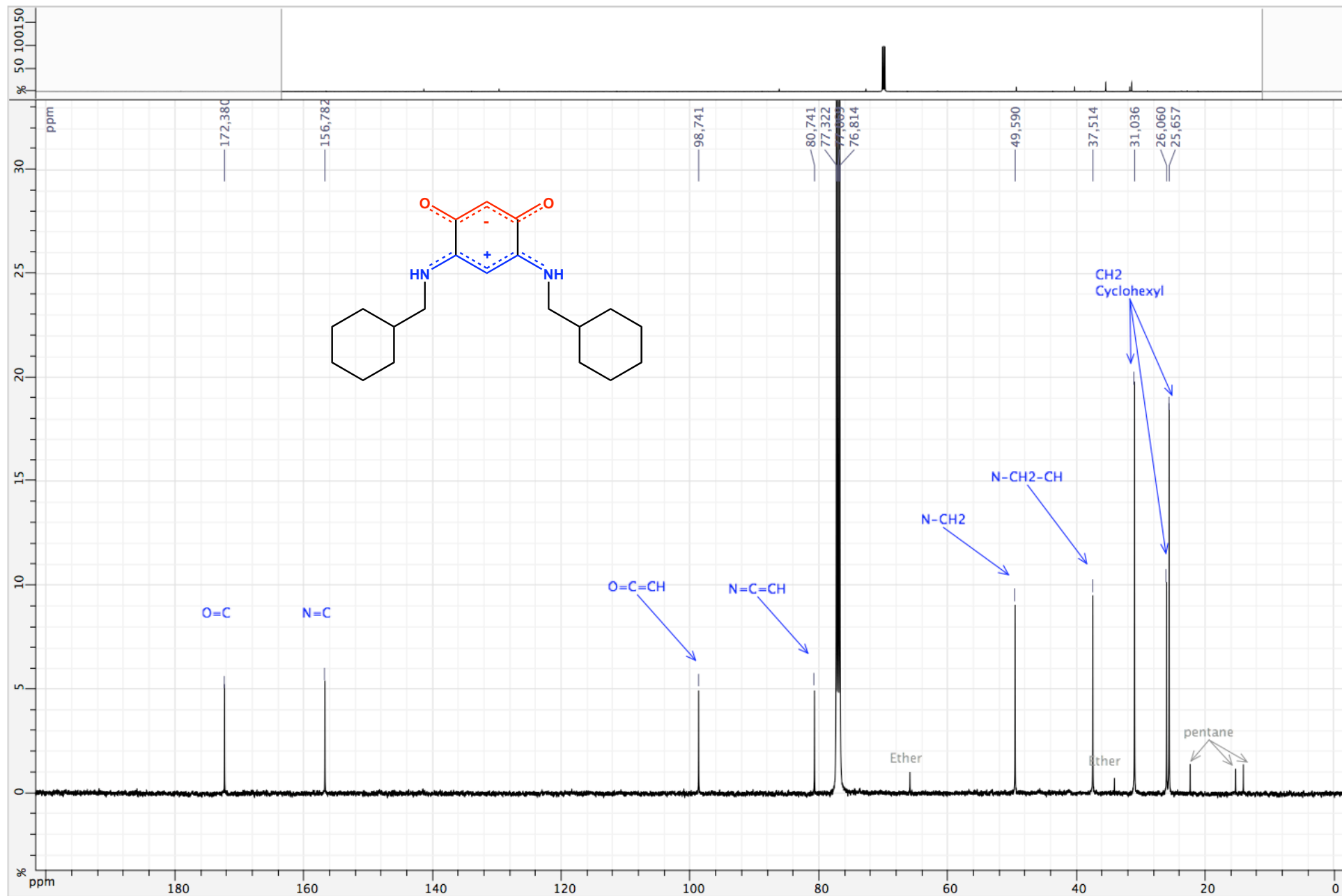


Figure S30. ^{13}C NMR spectrum of zwitterion **6** (CDCl_3 ; 500 MHz)

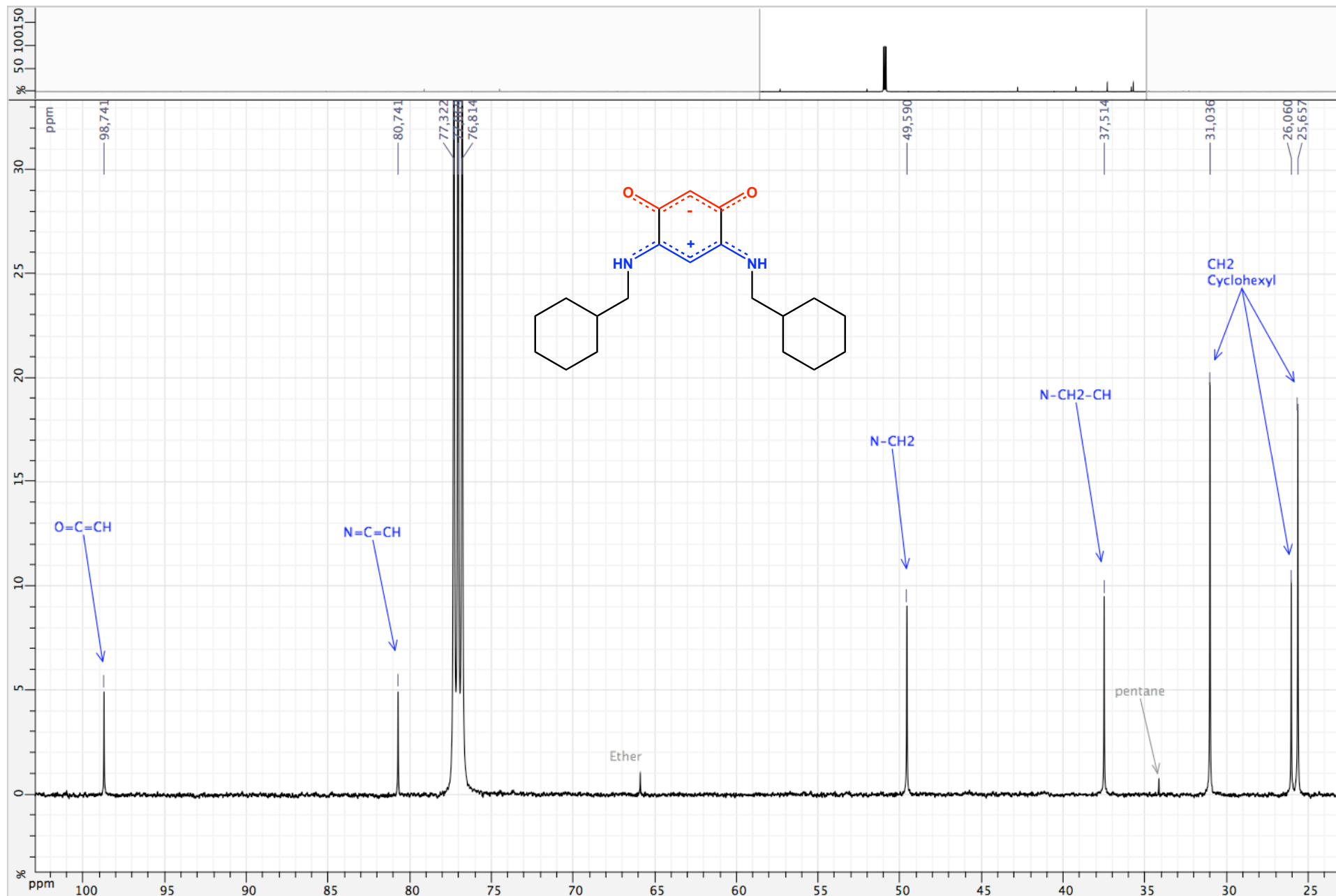


Figure S31. HSQC (^1H / ^{13}C) spectrum of zwitterion **6** (CDCl_3 ; 500 MHz)

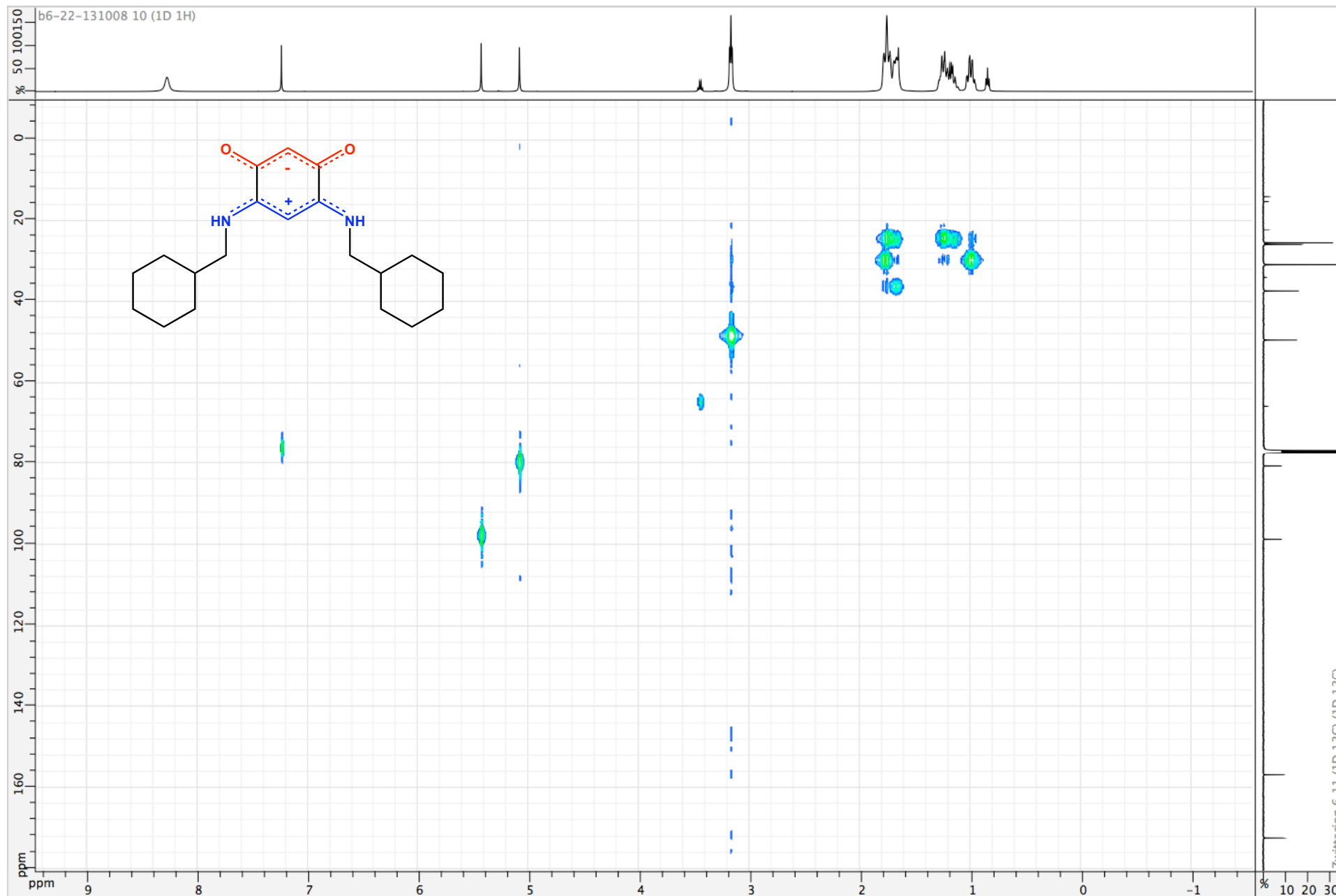


Figure S32. HSQC (^1H / ^{13}C) spectrum of zwitterion **6** (CDCl_3 ; 500 MHz)

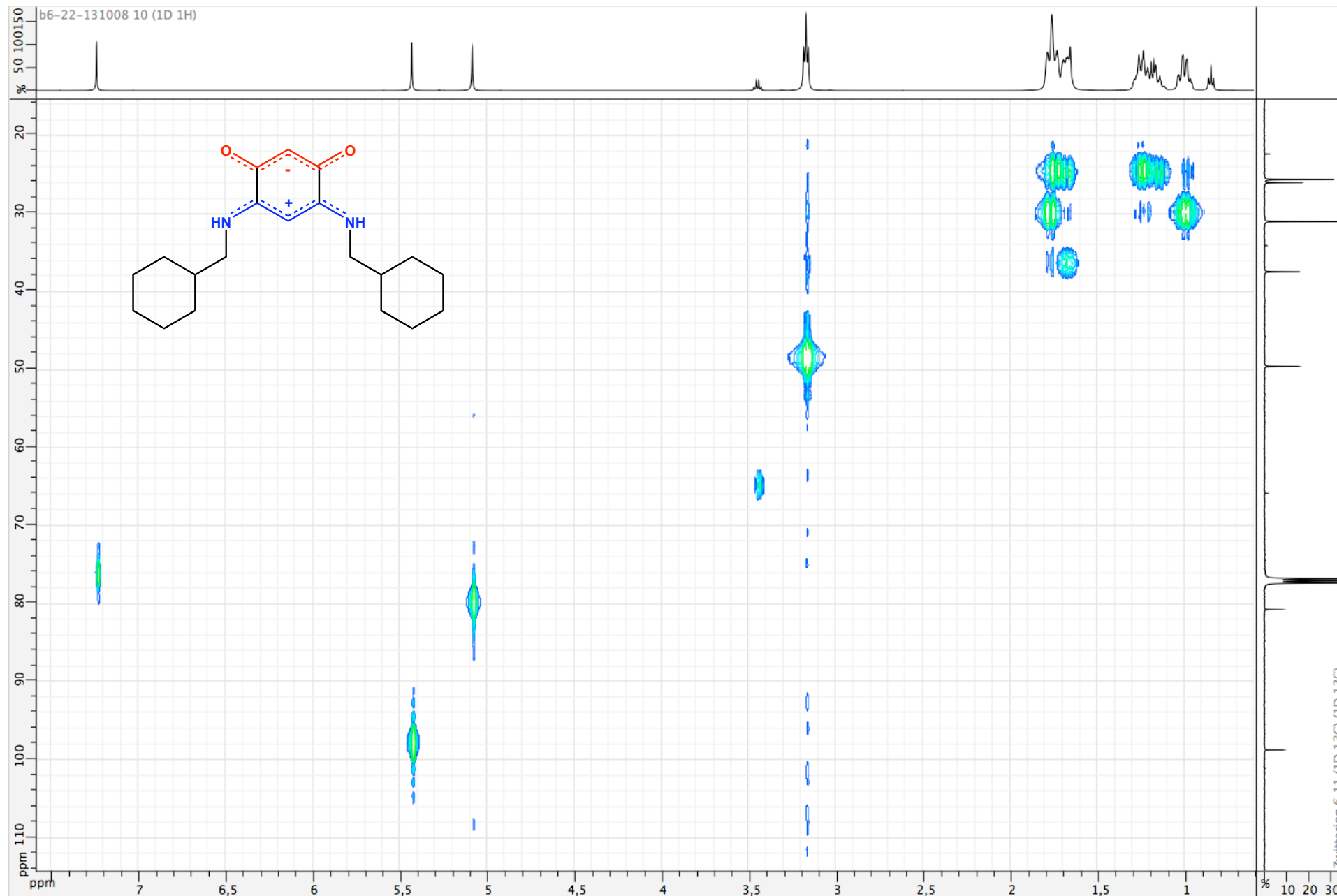


Figure S33. ¹H NMR spectrum of zwitterion 7 (CDCl₃ ; 500 MHz)

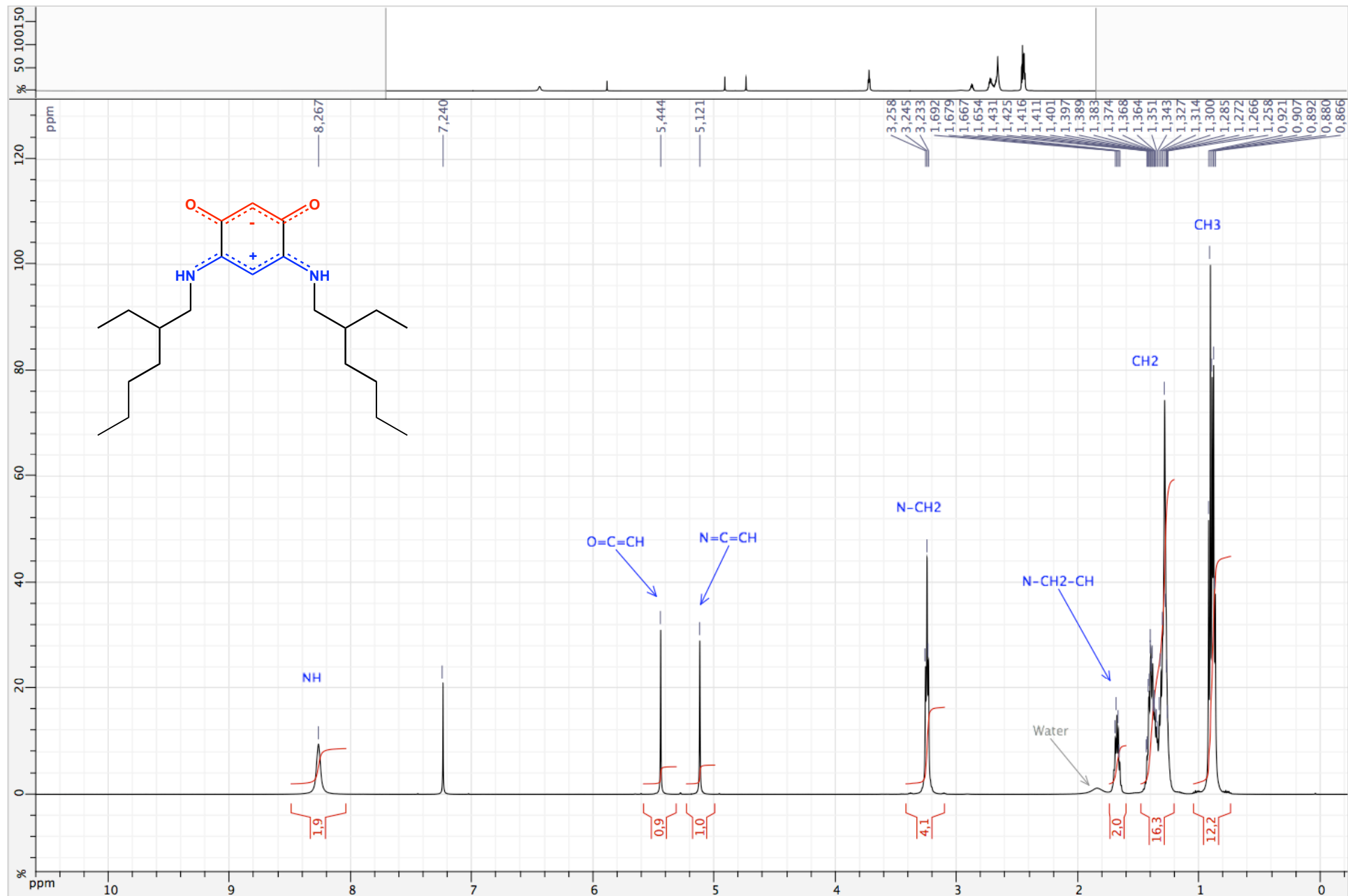


Figure S34. ^1H NMR spectrum of zwitterion **7** (CDCl_3 ; 500 MHz)

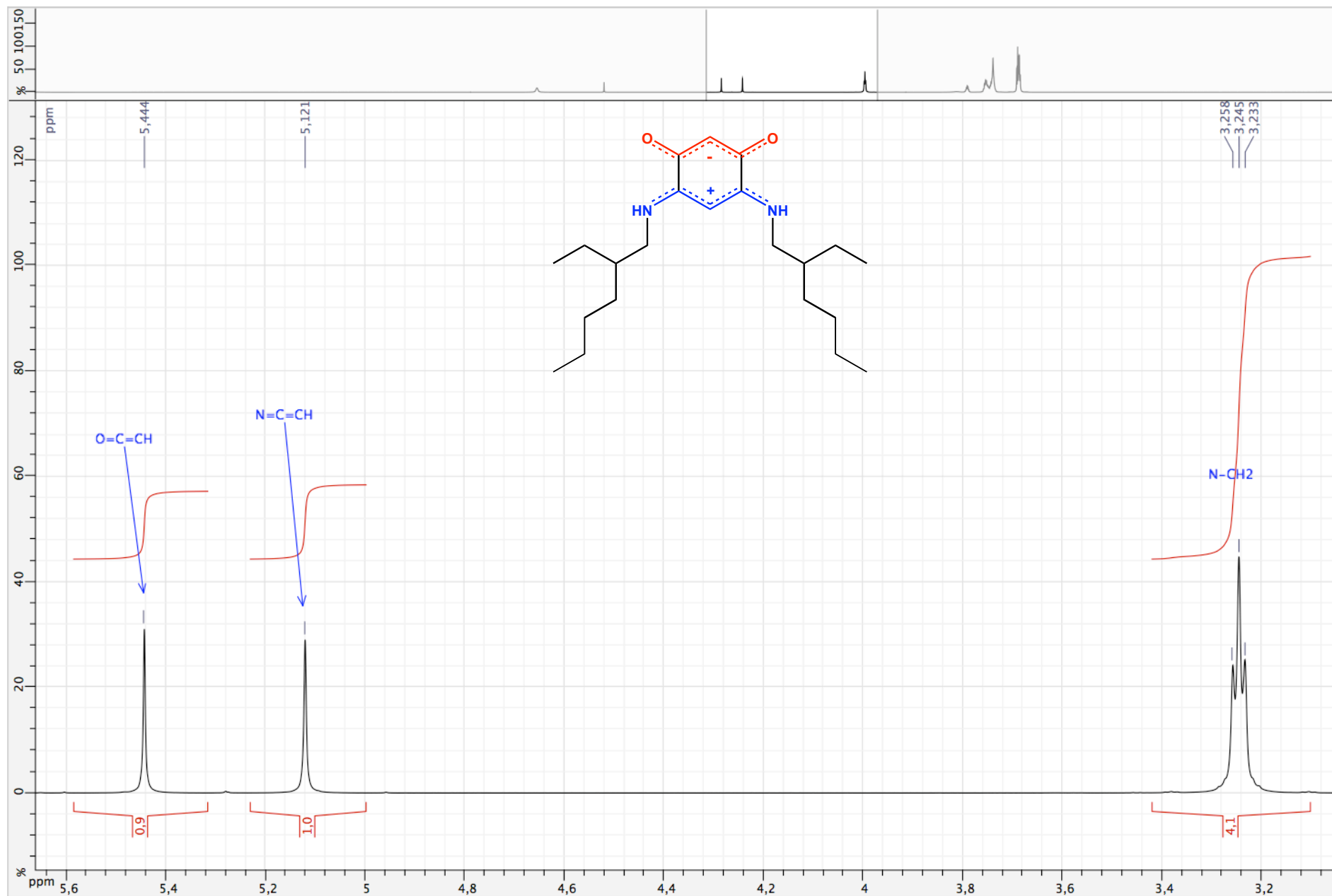


Figure S35. ^1H NMR spectrum of zwitterion **7** (CDCl_3 ; 500 MHz)

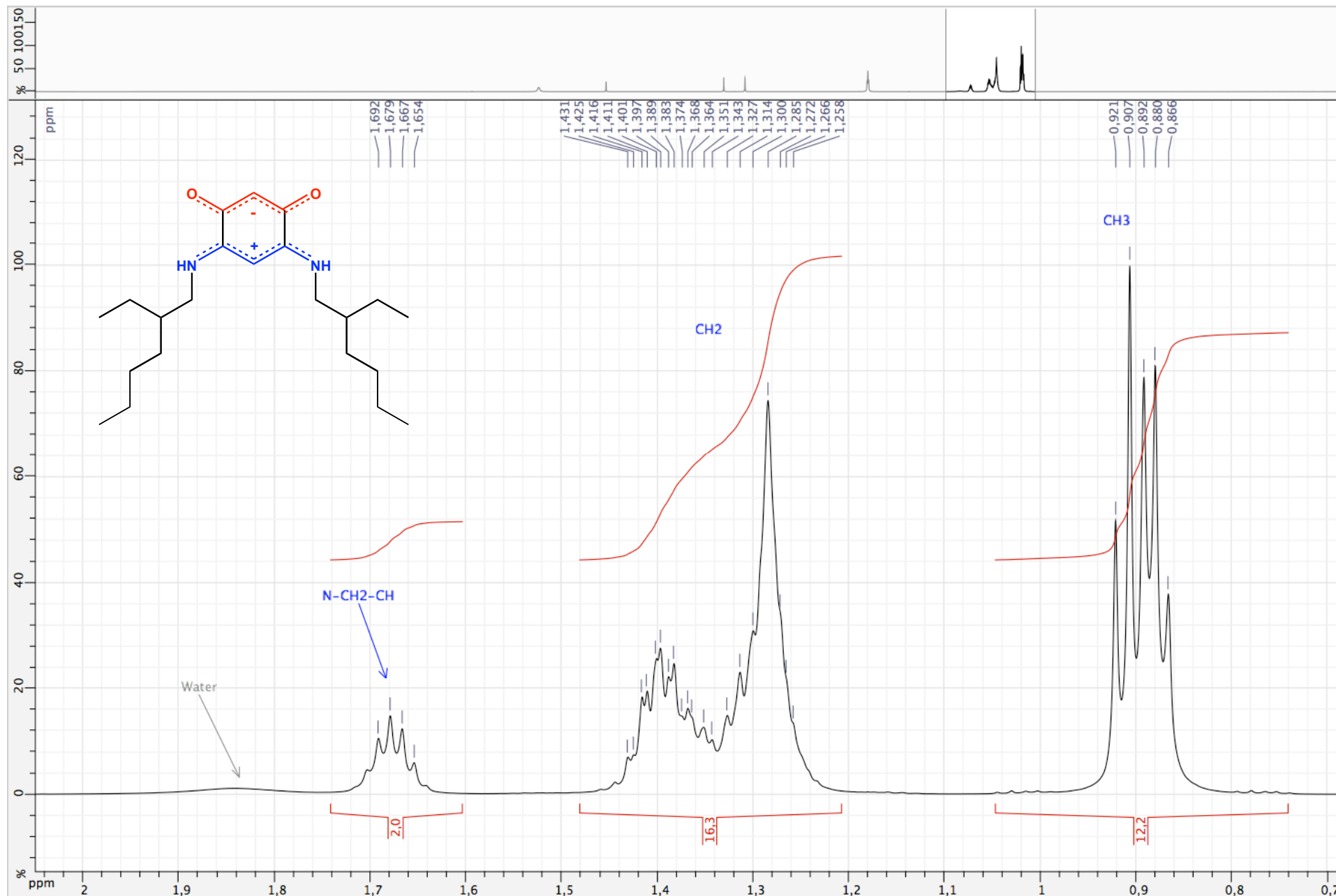


Figure S36. ^{13}C NMR spectrum of zwitterion **7** (CDCl_3 ; 500 MHz)

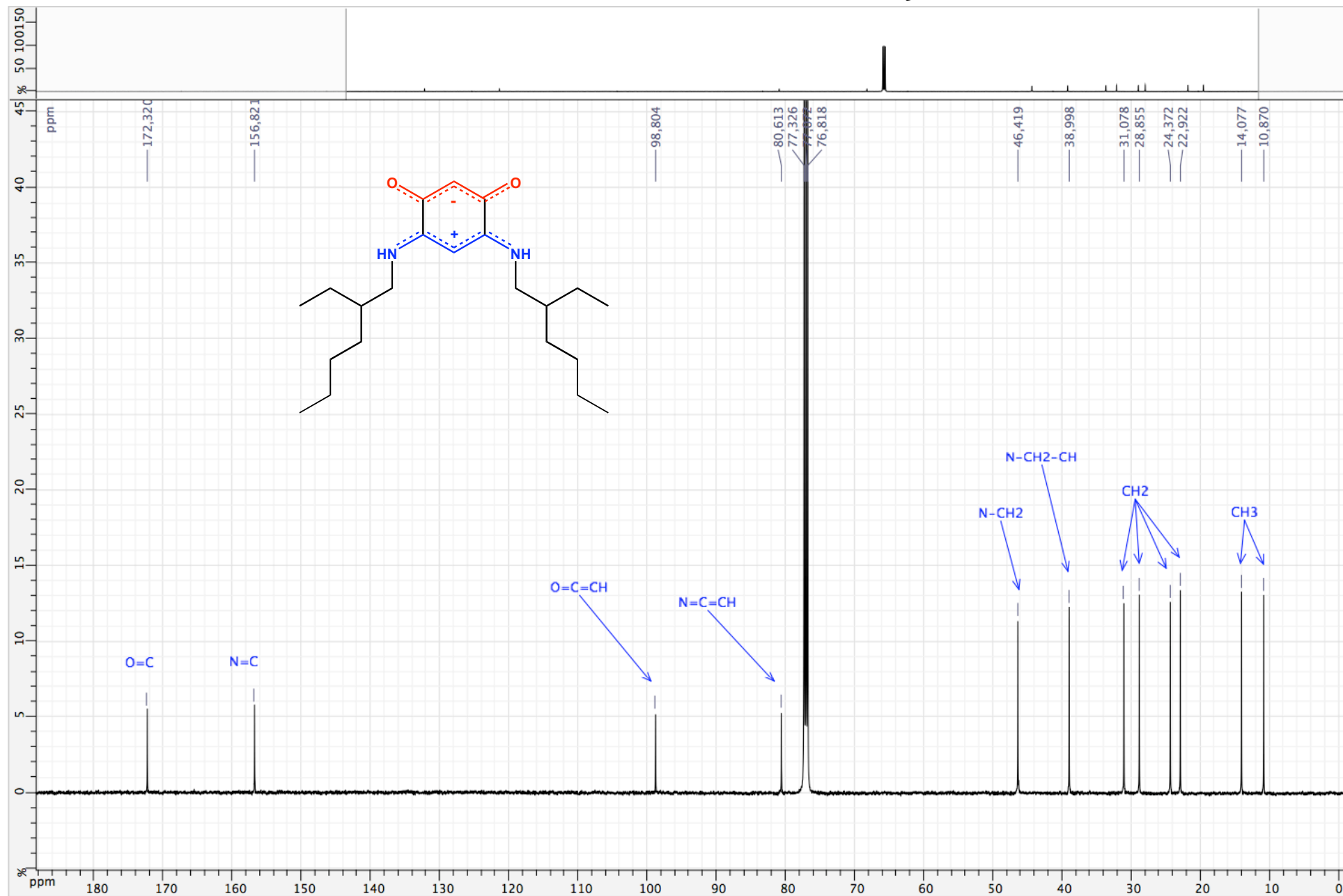


Figure S37. ¹H NMR spectrum of zwitterion **8** (CDCl₃ ; 500 MHz)

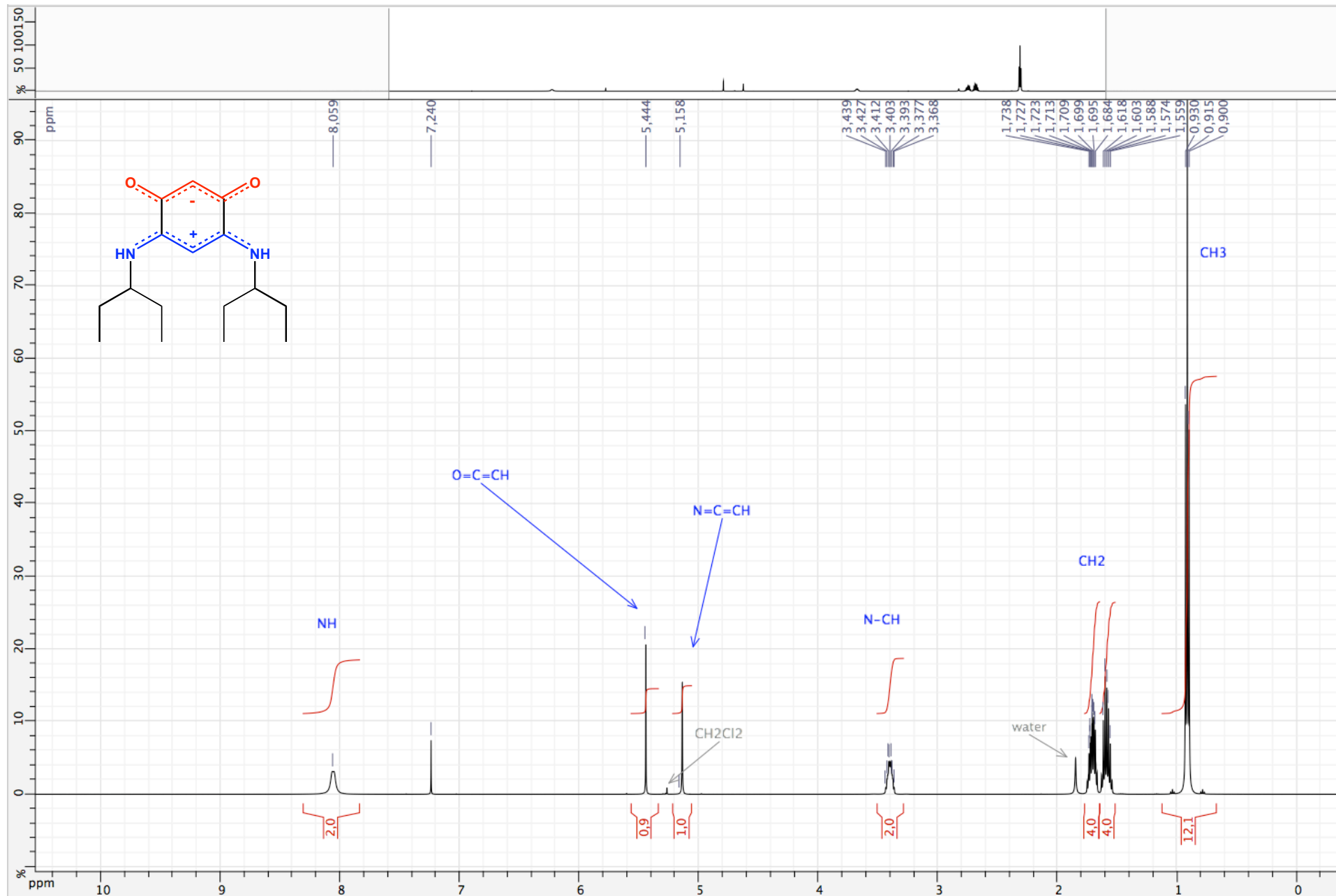


Figure S38. ^1H NMR spectrum of zwitterion **8** (CDCl_3 ; 500 MHz)

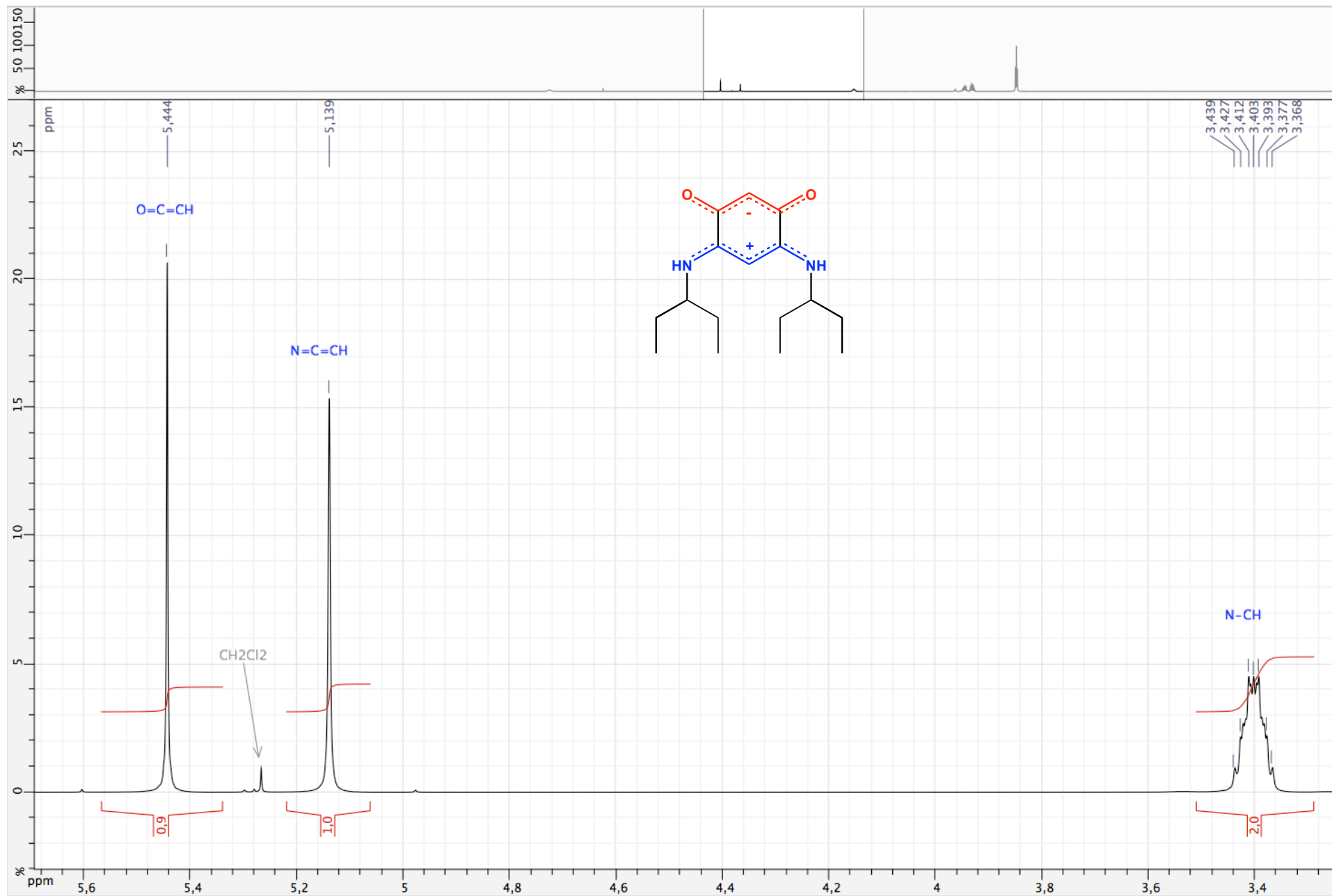


Figure S39. ¹H NMR spectrum of zwitterion **8** (CDCl₃ ; 500 MHz)

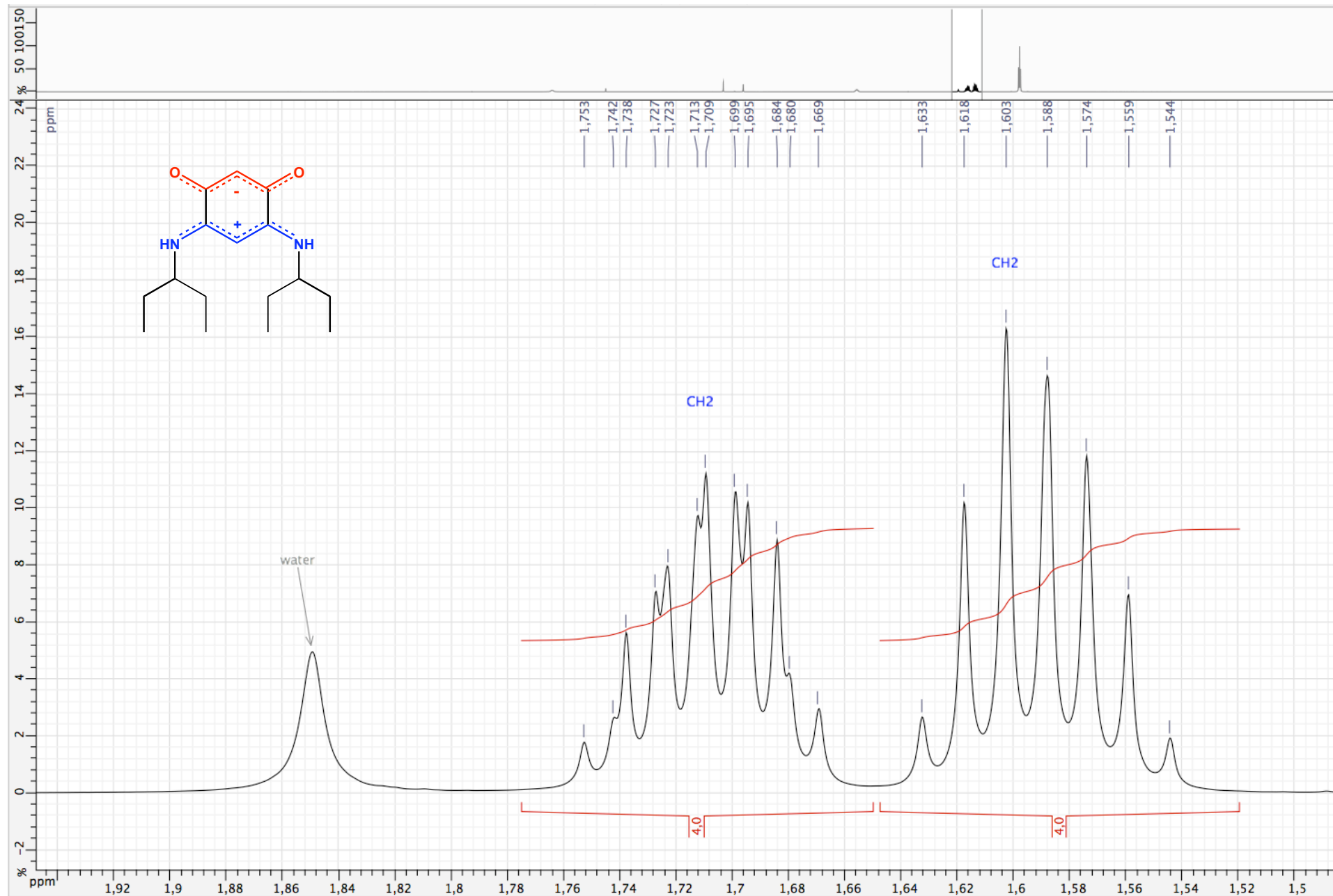


Figure S40. ^1H NMR spectrum of zwitterion **8** (CDCl_3 ; 500 MHz)

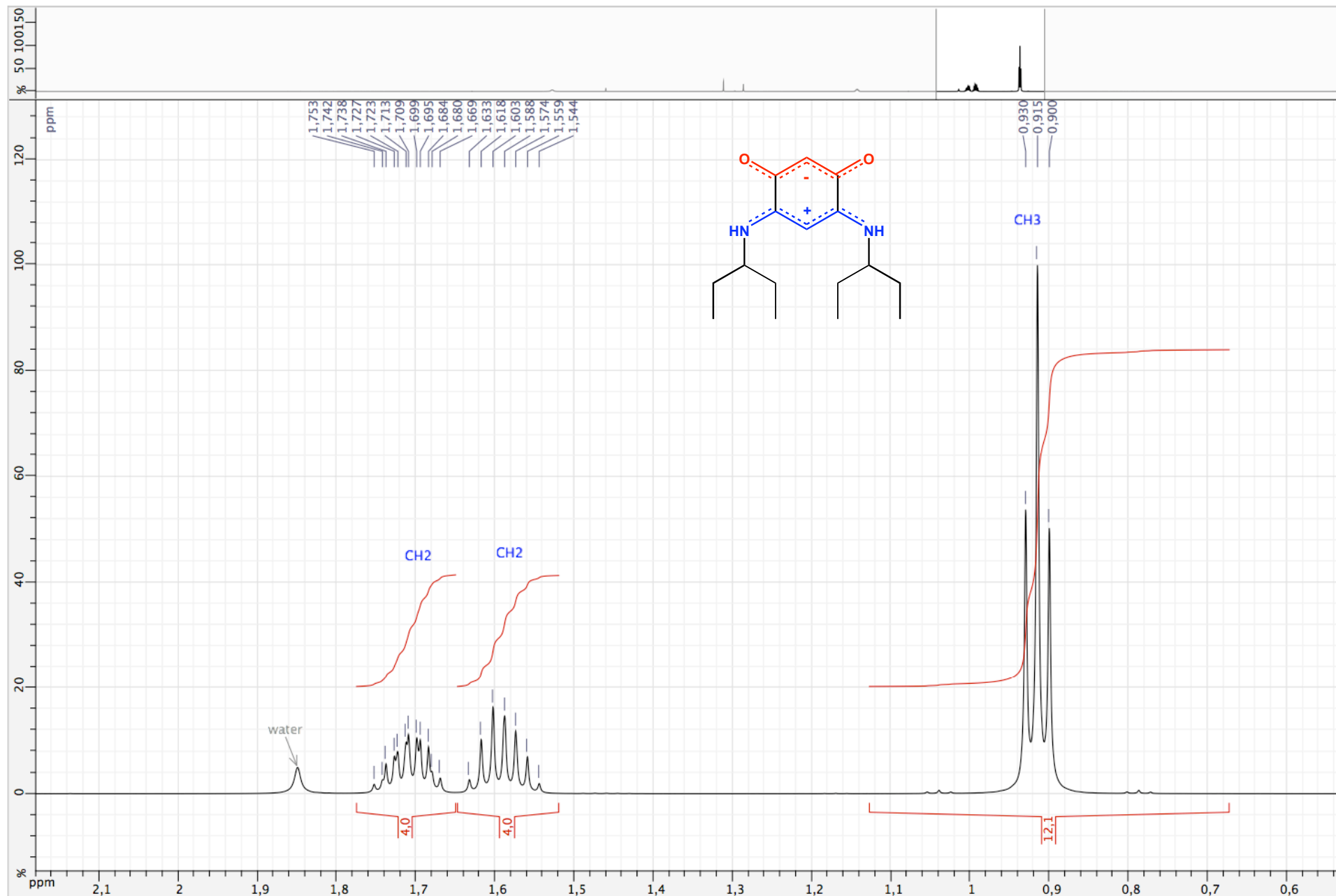


Figure S41. ^1H NMR spectrum of zwitterion **8** (CDCl_3 ; 500 MHz)

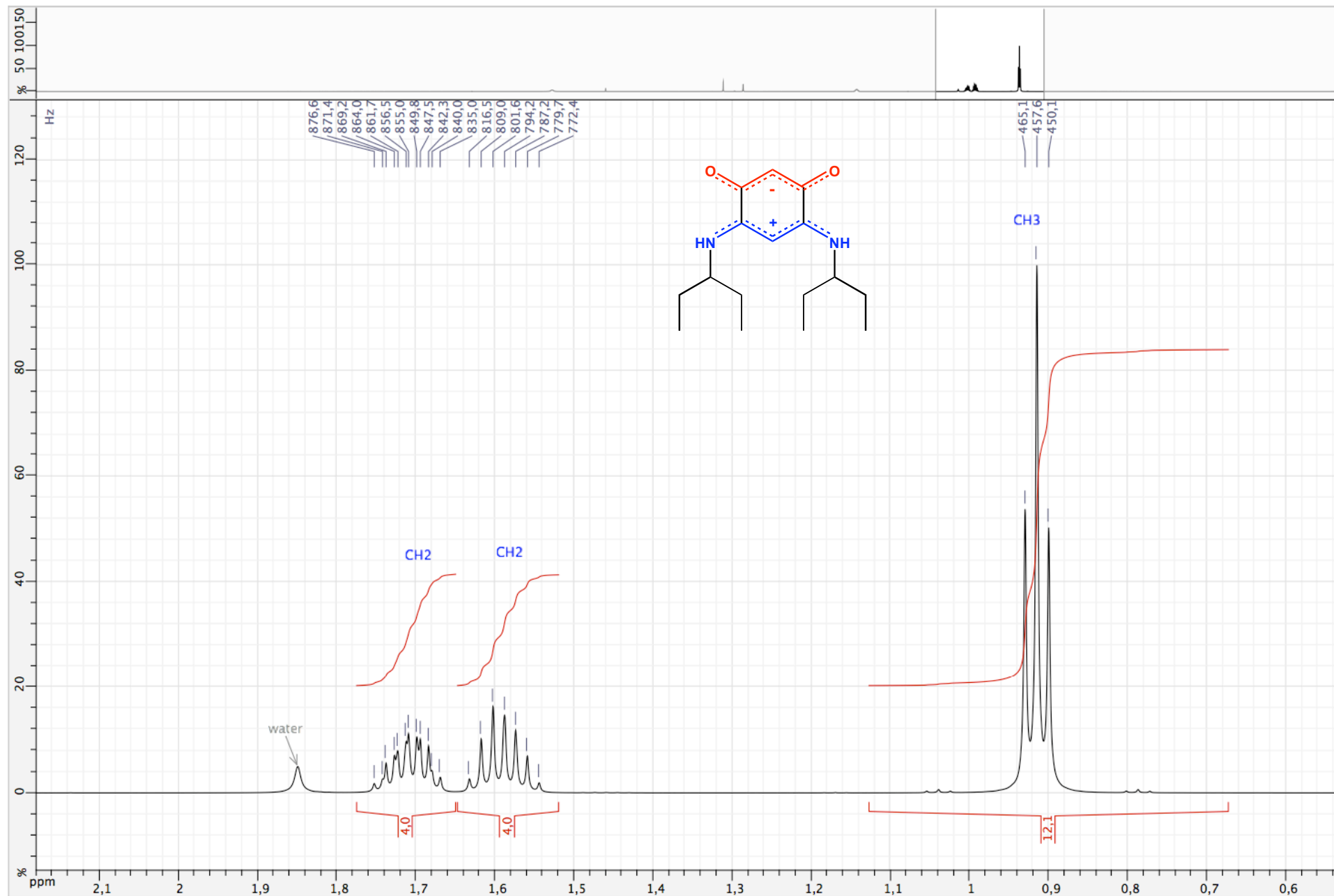


Figure S42. ^{13}C NMR spectrum of zwitterion **8** (CDCl_3 ; 500 MHz)

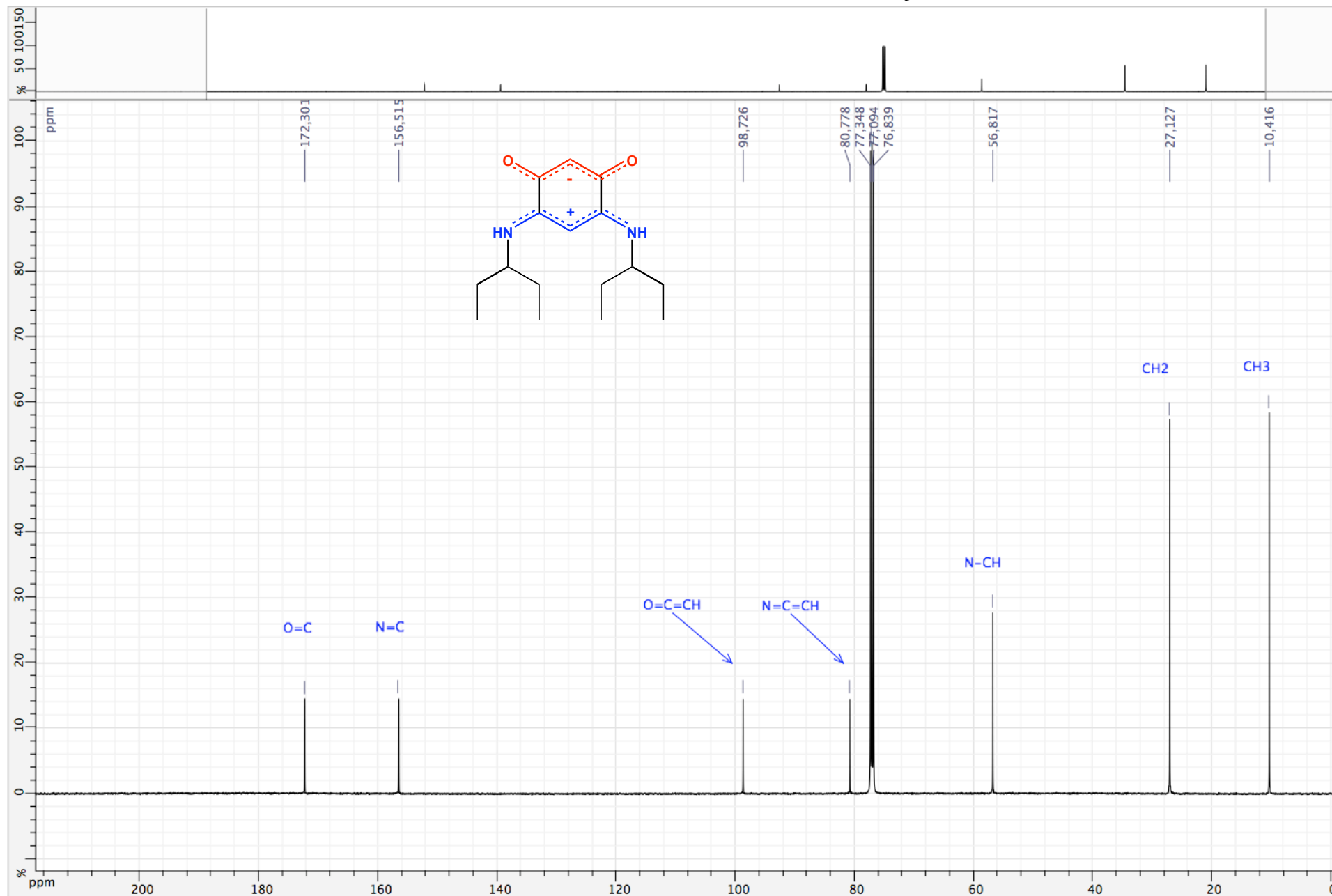


Figure S43. HSQC (^1H / ^{13}C) spectrum of zwitterion **8** (CDCl_3 ; 500 MHz)

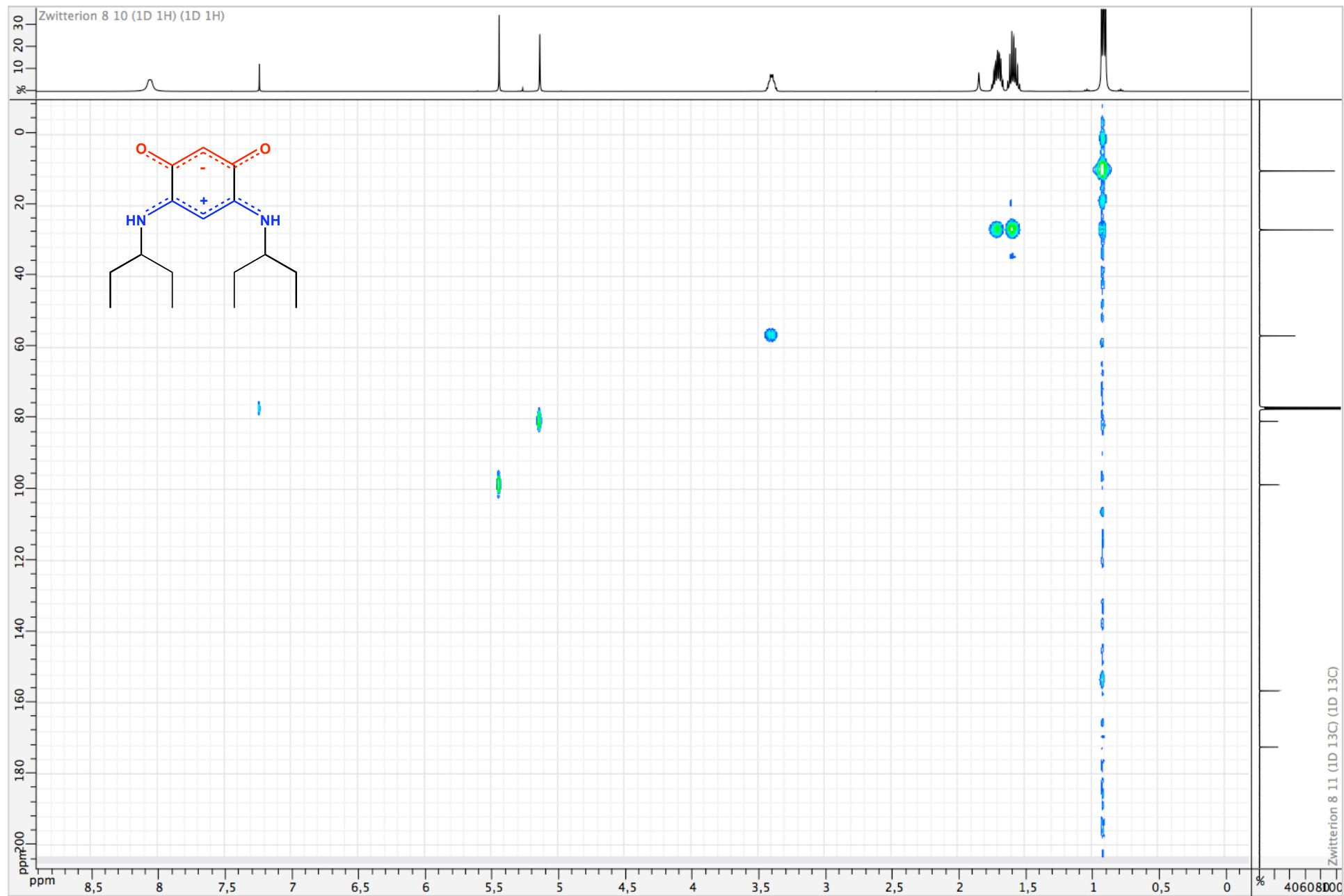


Figure S44. ^1H NMR spectrum of zwitterion **9** (CDCl_3 ; 500 MHz)

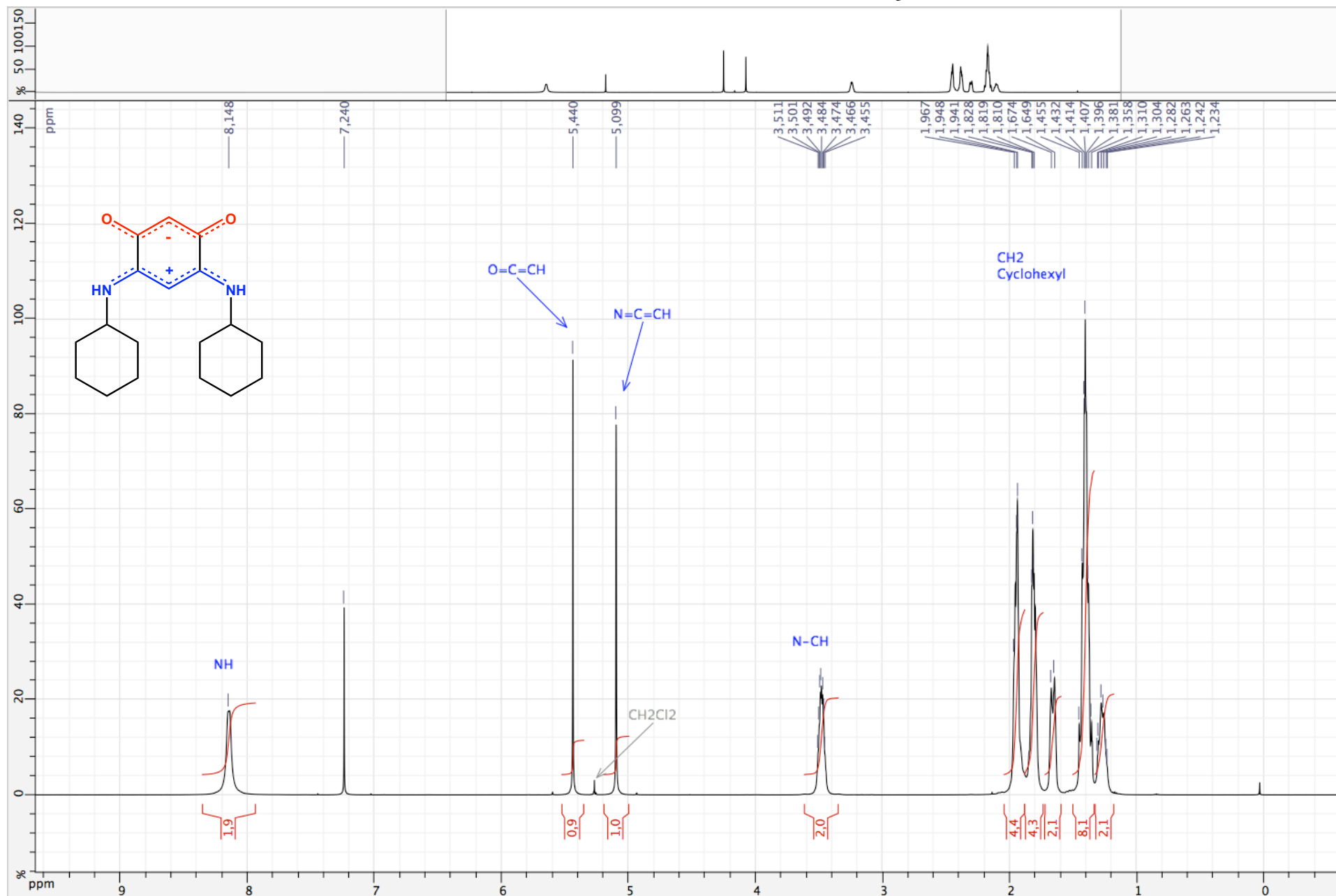


Figure S45. ^1H NMR spectrum of zwitterion **9** (CDCl_3 ; 500 MHz)

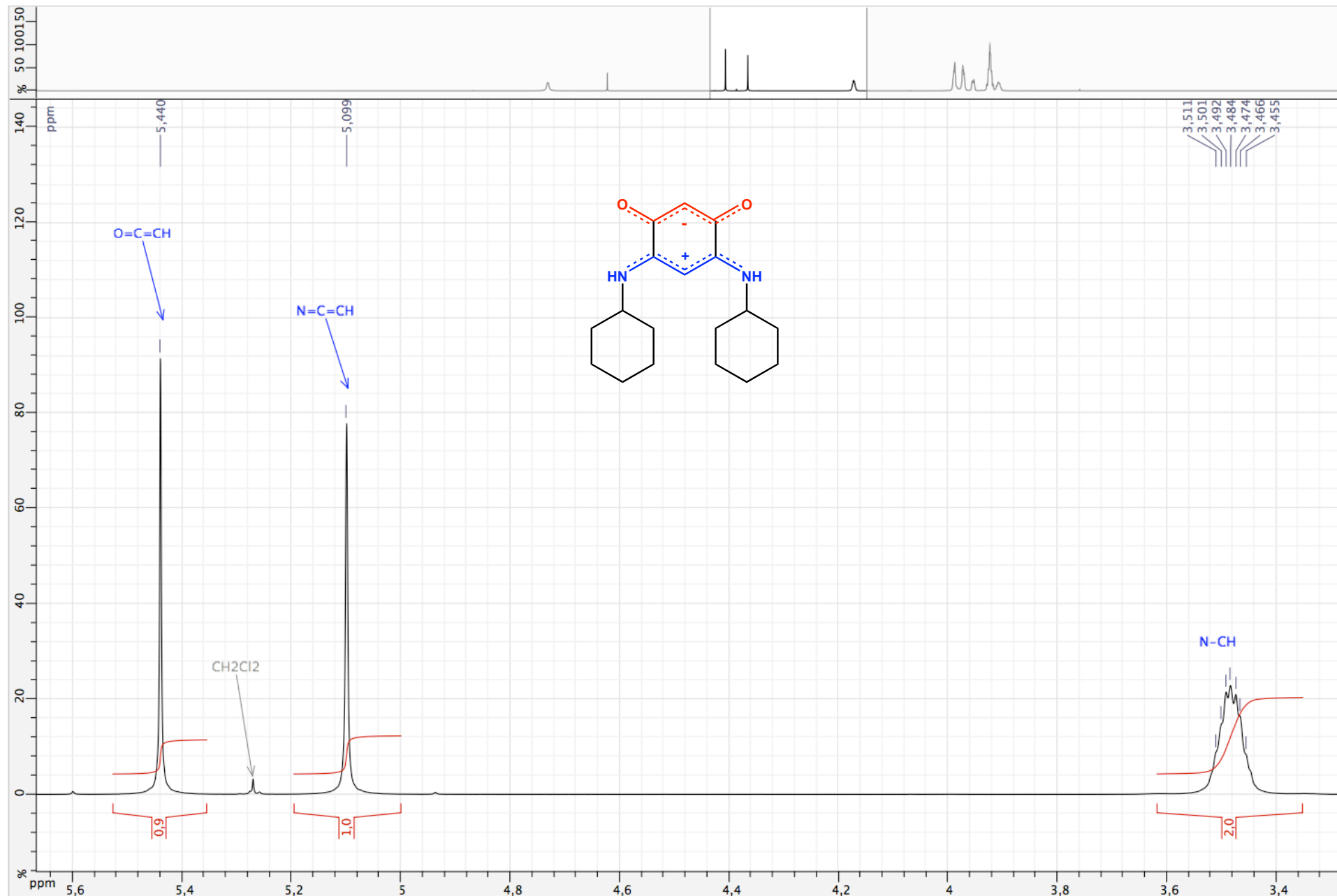


Figure S46. ¹H NMR spectrum of zwitterion **9** (CDCl₃ ; 500 MHz)

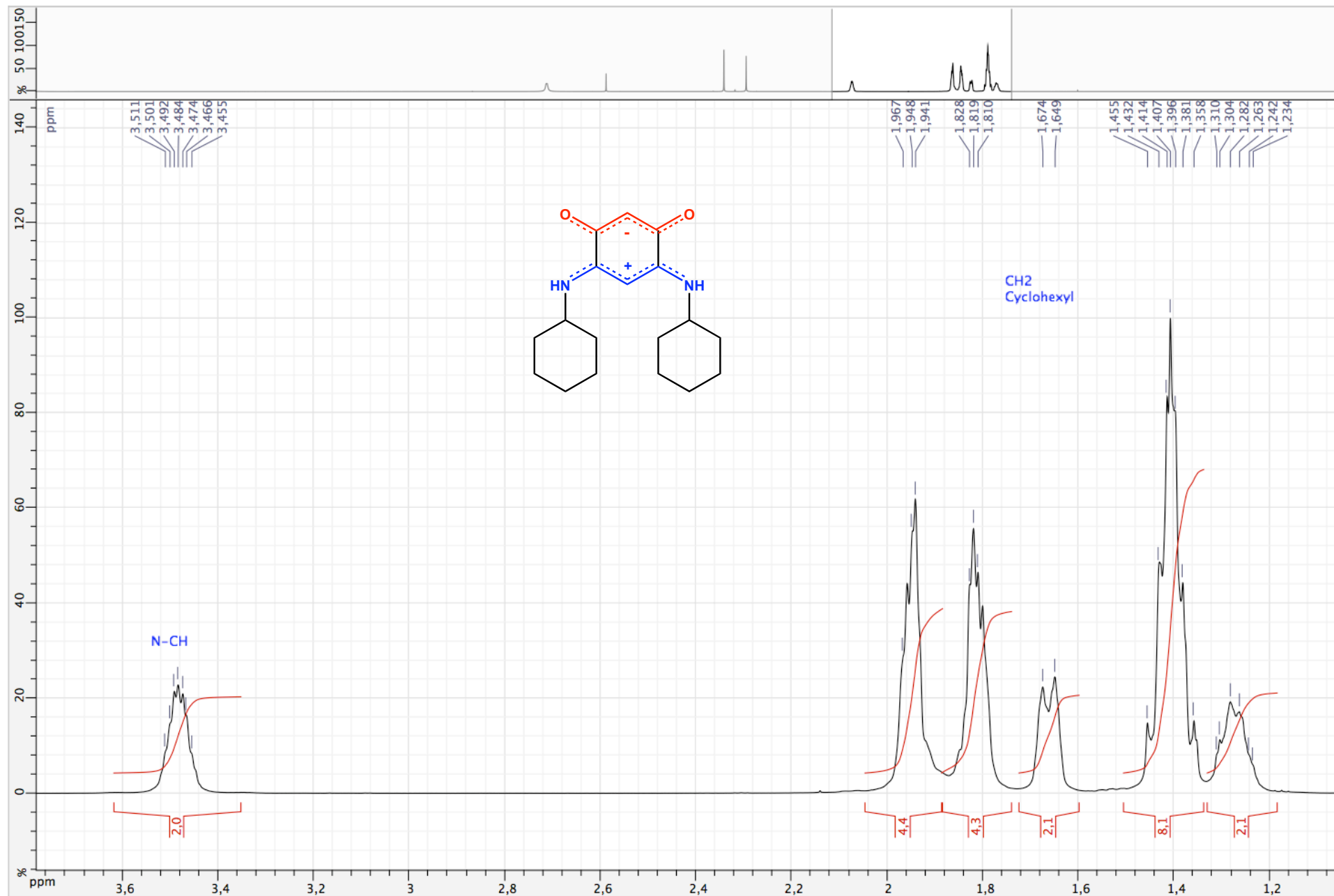


Figure S47. ^{13}C NMR spectrum of zwitterion **9** (CDCl_3 ; 500 MHz)

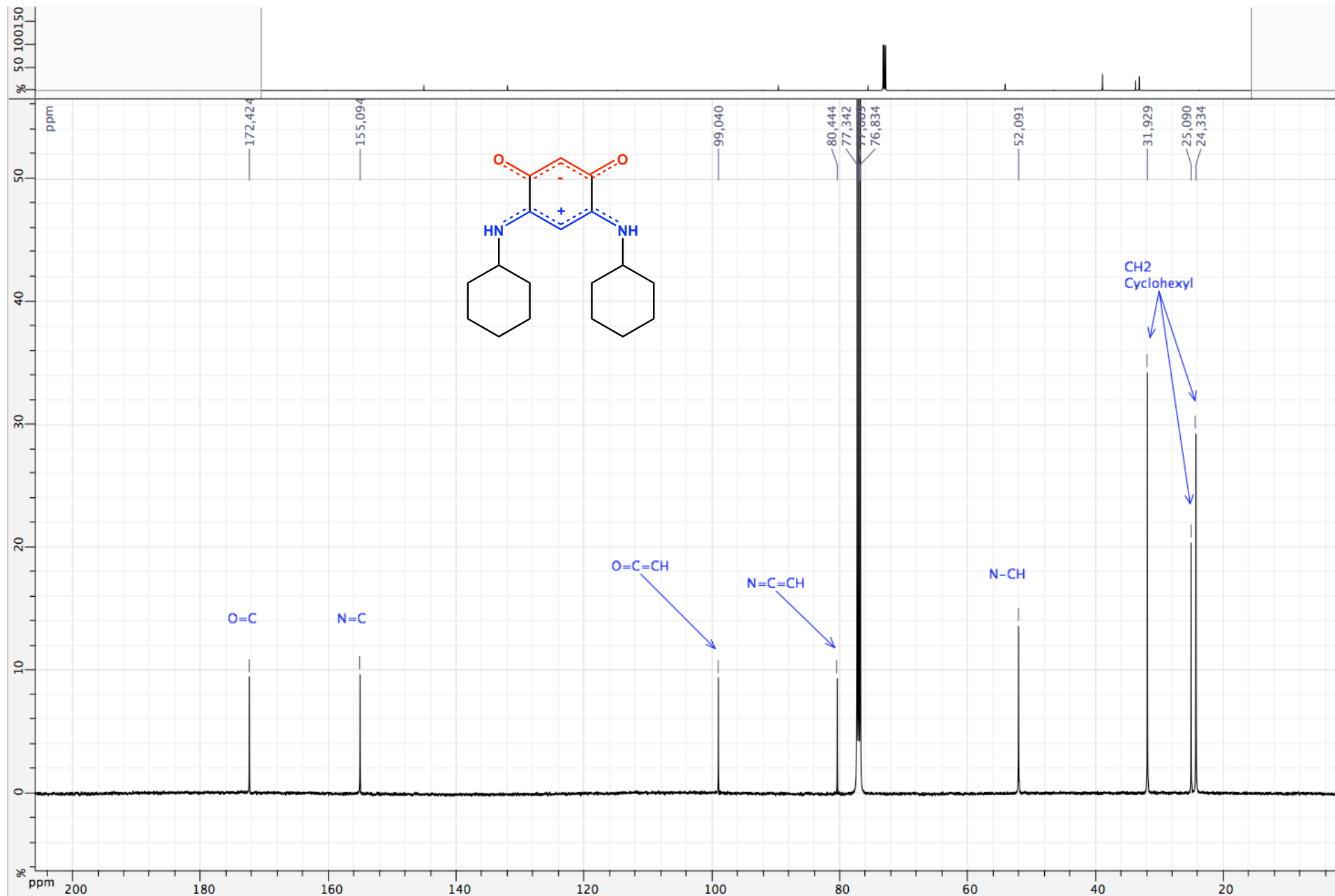


Figure S48. ¹H NMR spectrum of zwitterion 10 (CDCl₃ ; 500 MHz)

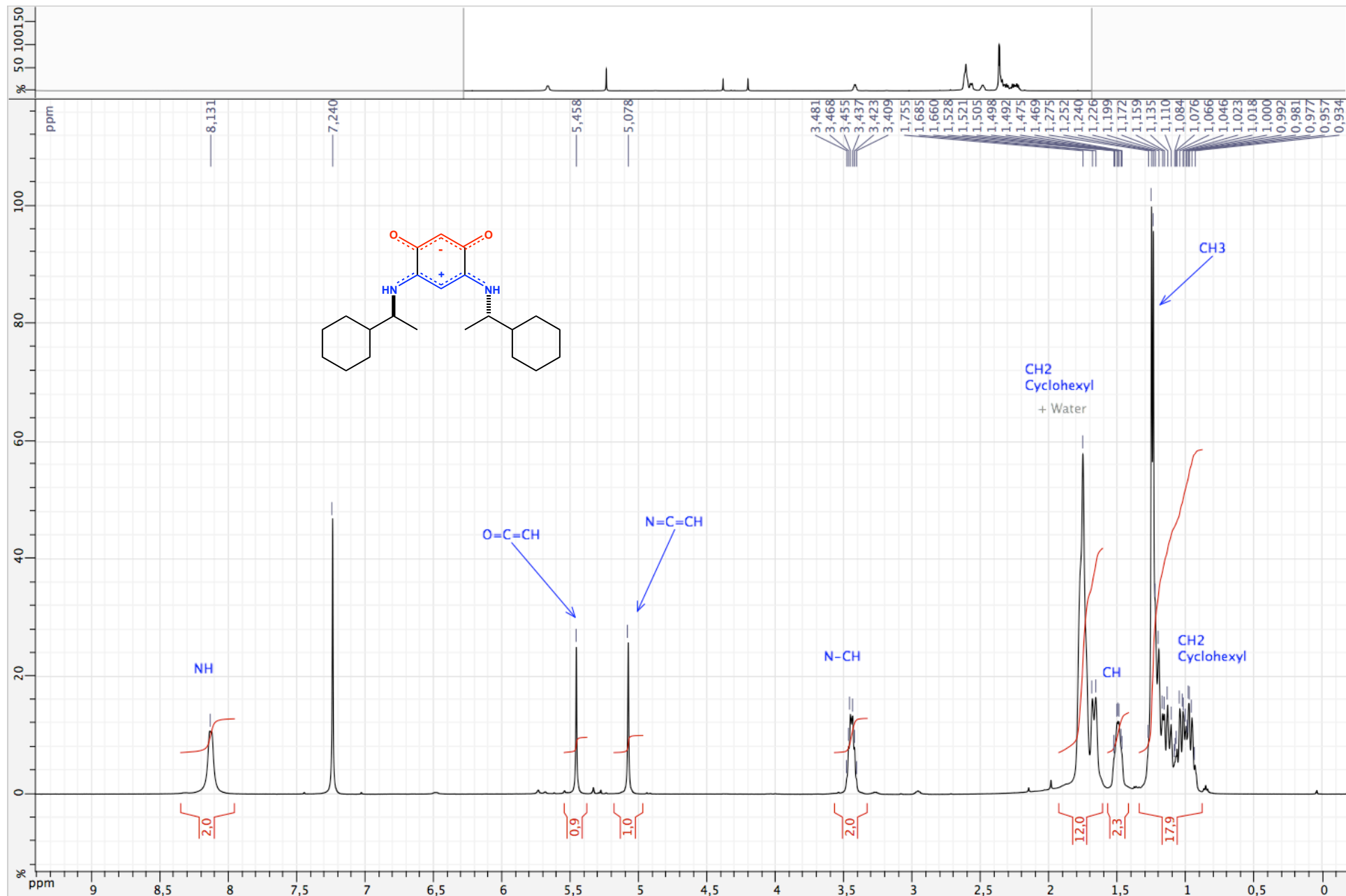


Figure S49. ^1H NMR spectrum of zwitterion **10** (CDCl_3 ; 500 MHz)

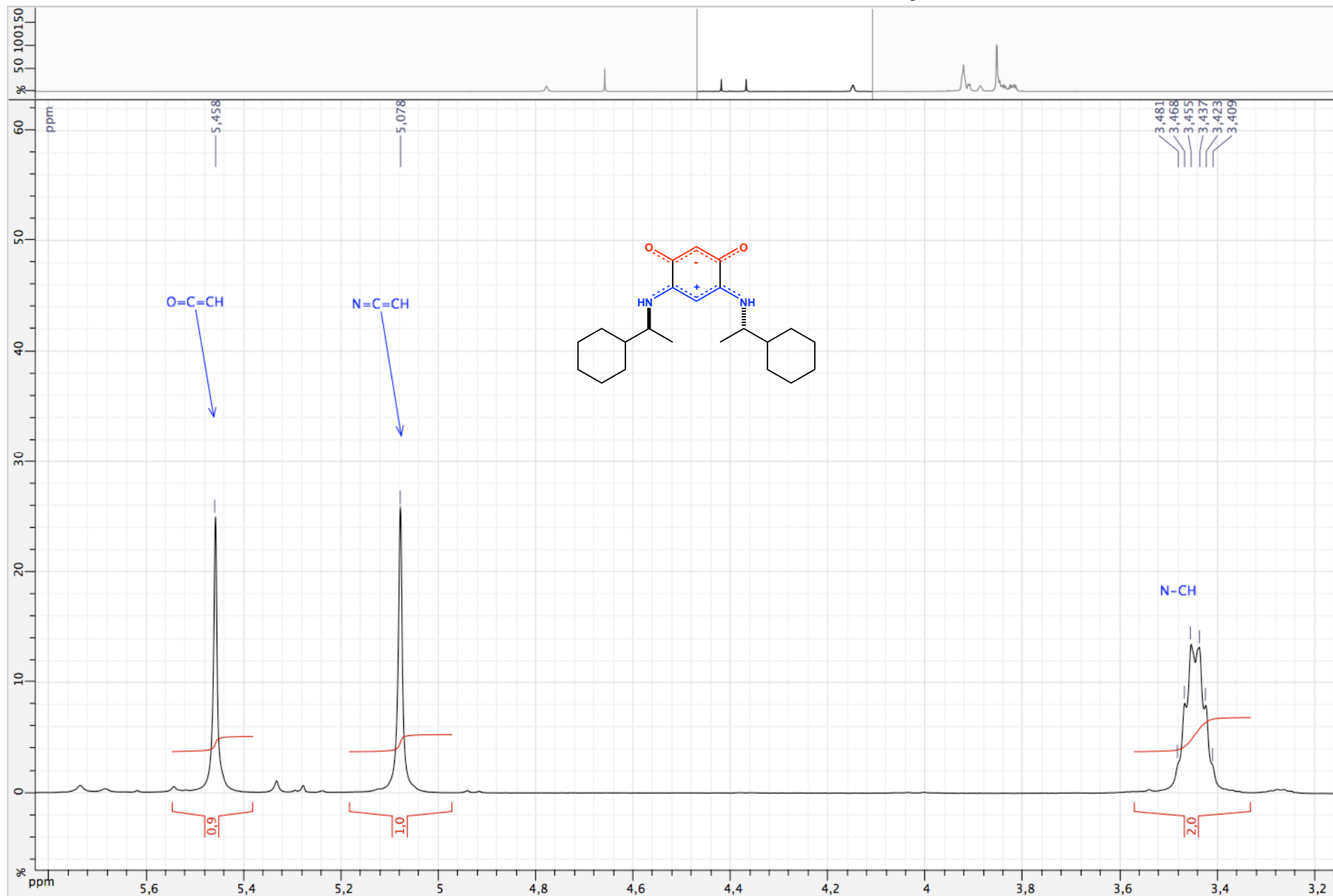


Figure S50. ¹H NMR spectrum of zwitterion **10** (CDCl₃ ; 500 MHz)

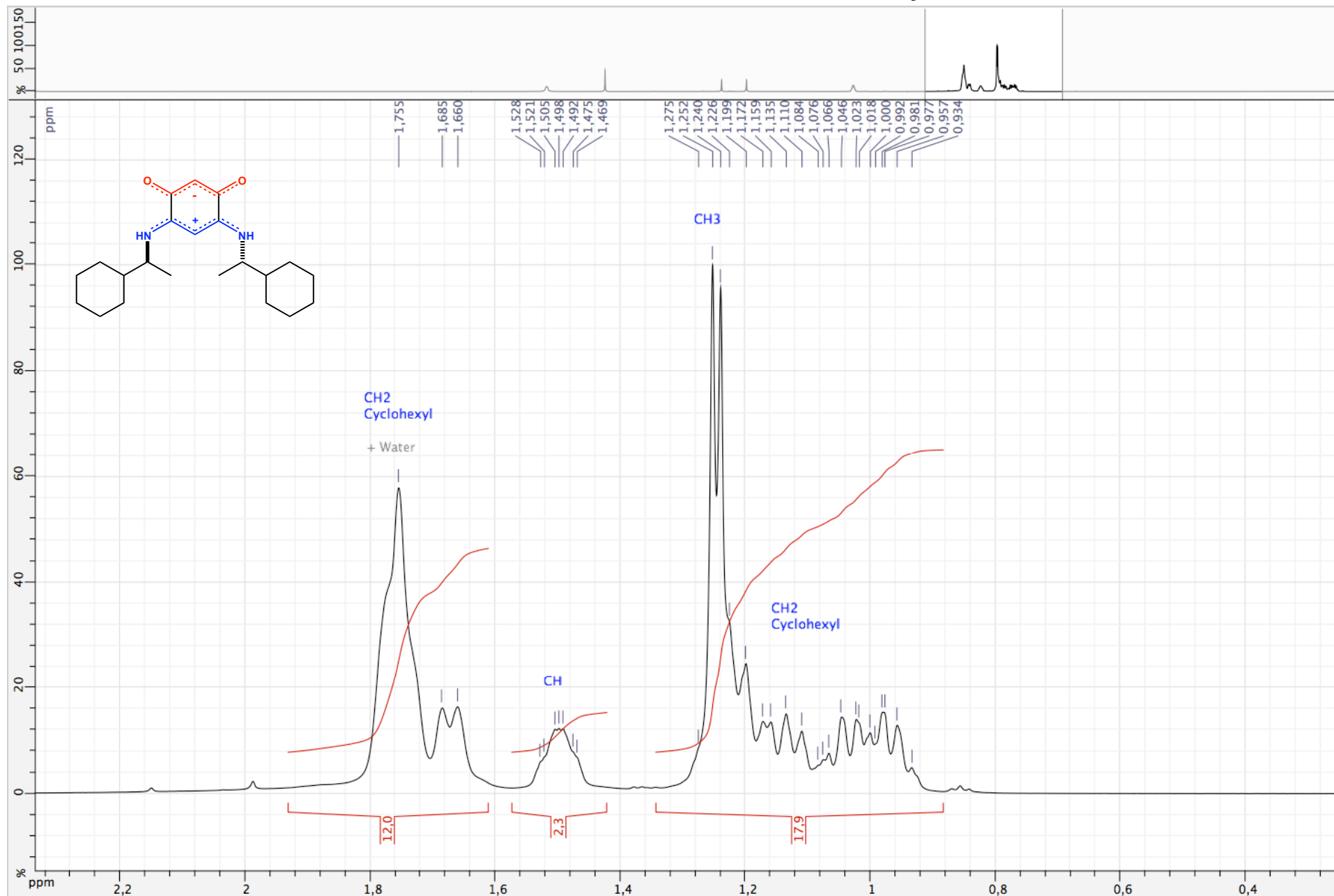


Figure S51. ^{13}C NMR spectrum of zwitterion **10** (CDCl_3 ; 500 MHz)

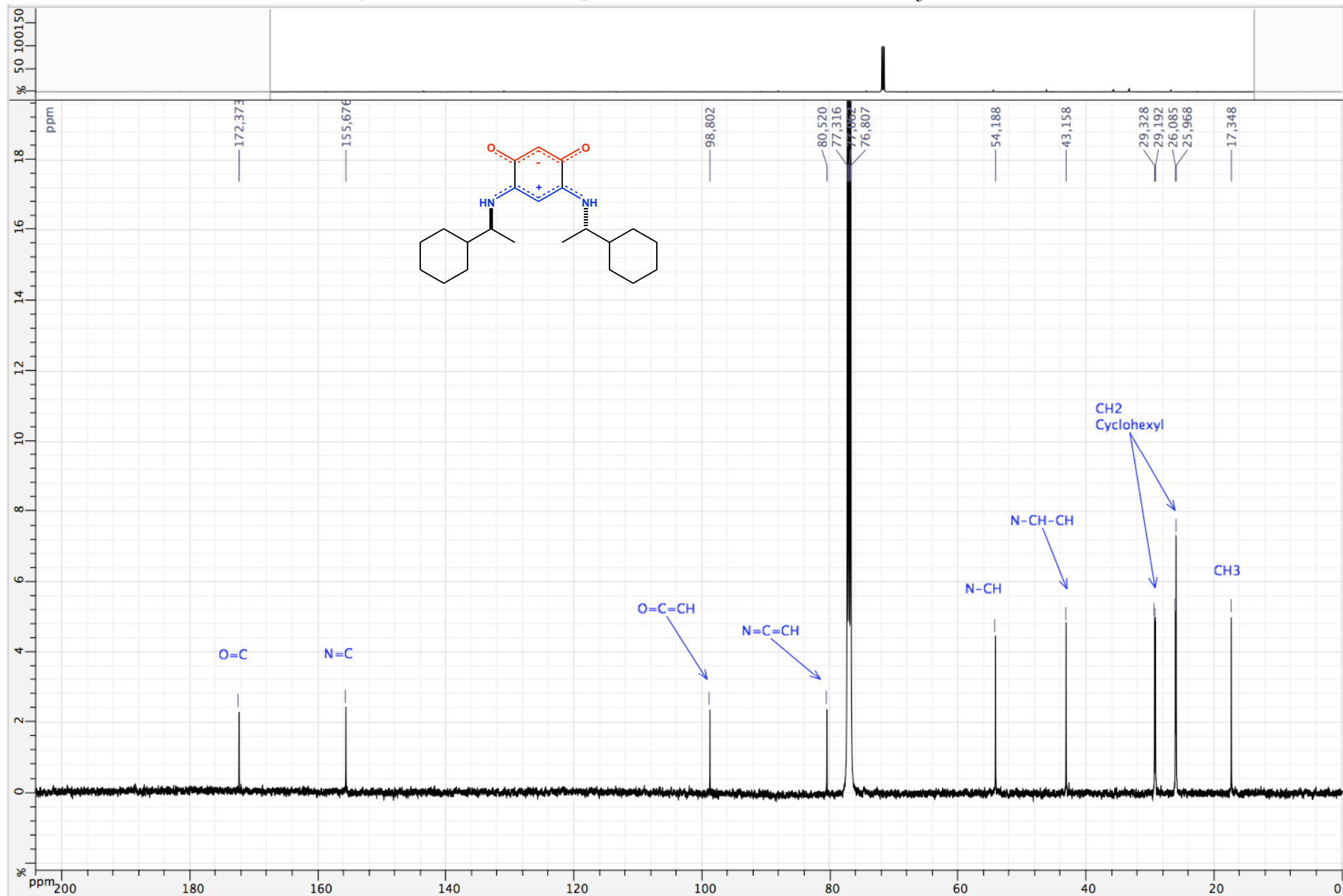


Figure S52. ^{13}C NMR spectrum of zwitterion **10** (CDCl_3 ; 500 MHz)

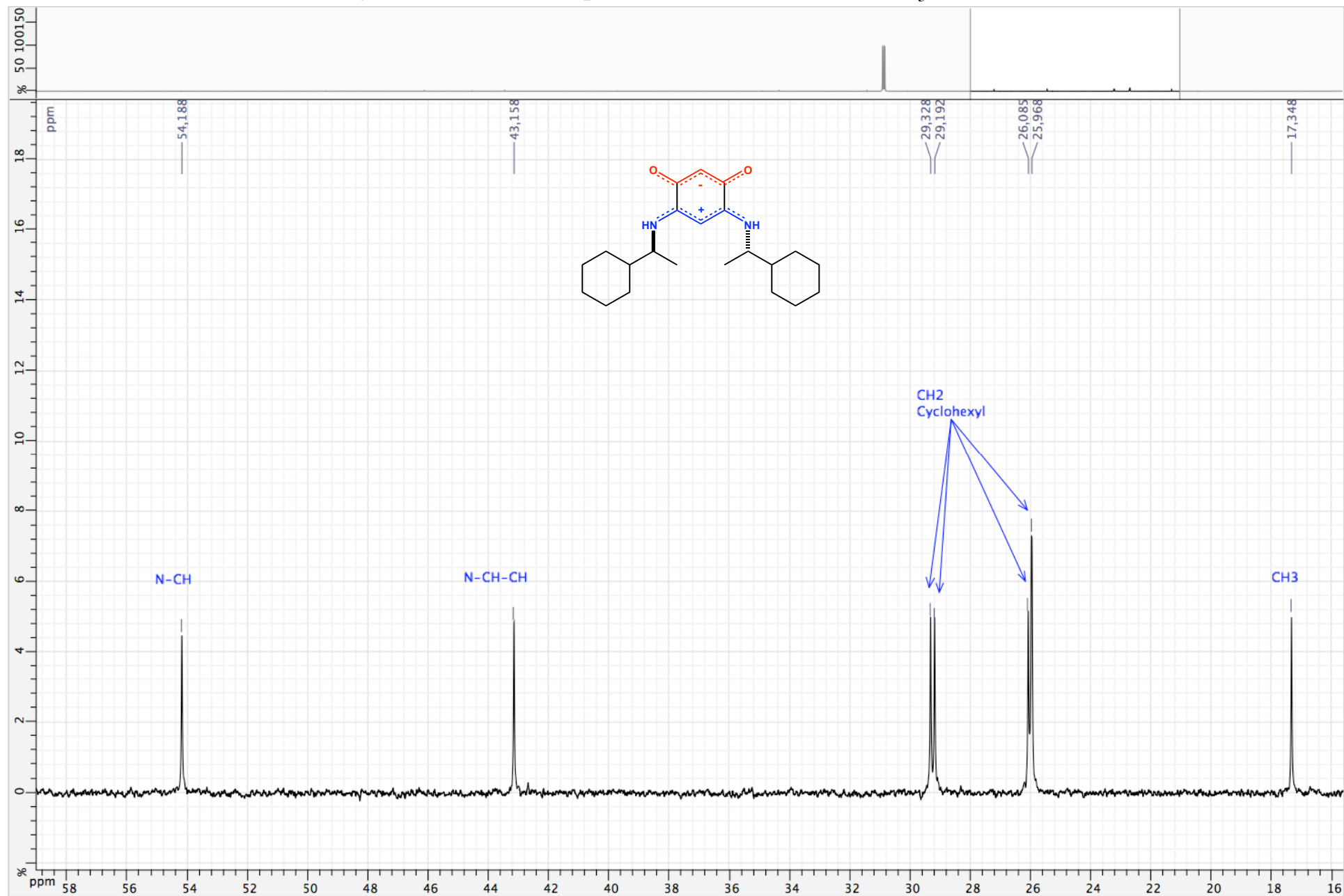


Figure S53. HSQC ($^1\text{H} / ^{13}\text{C}$) spectrum of zwitterion **10** (CDCl_3 ; 500 MHz)

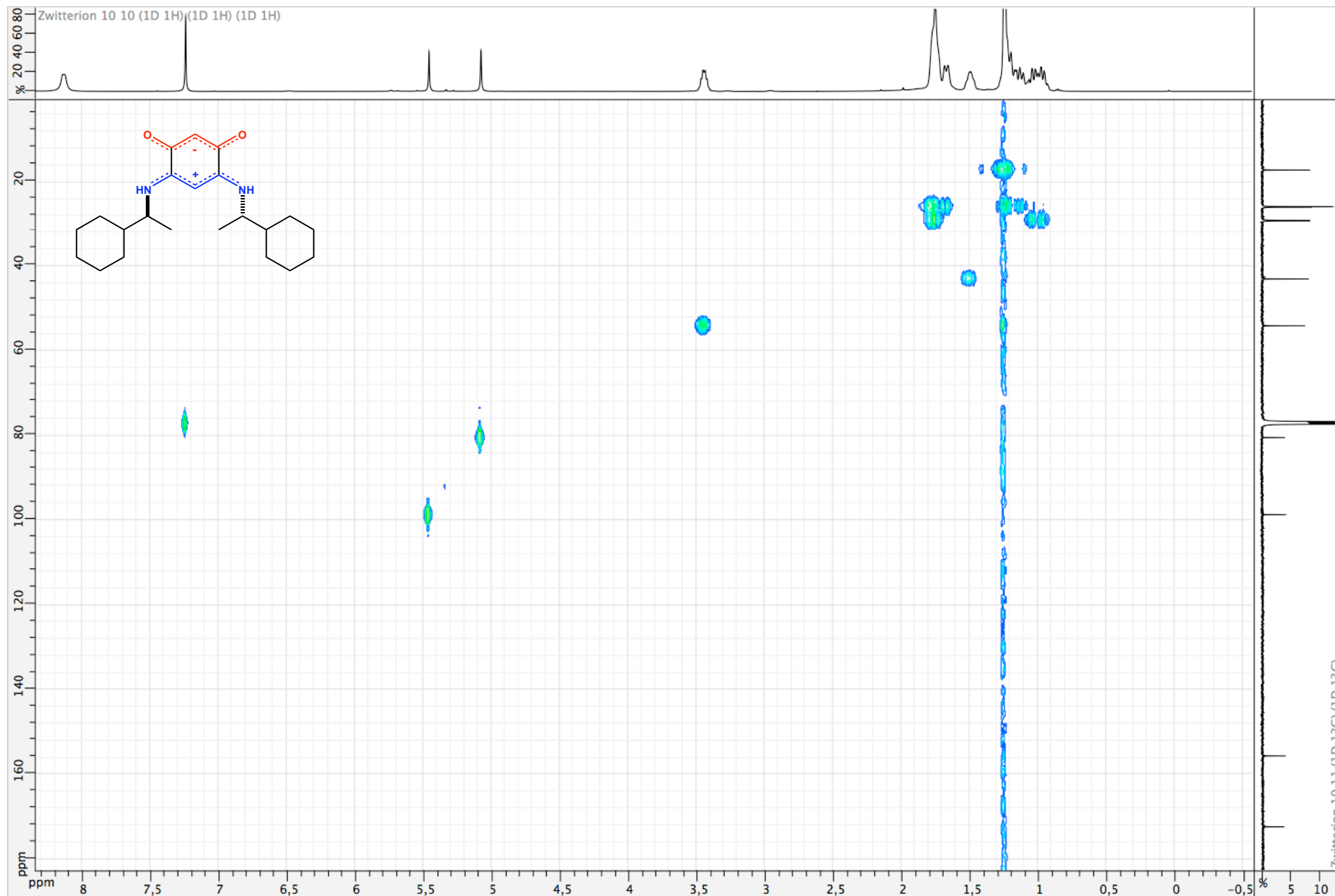


Figure S54. HSQC (^1H / ^{13}C) spectrum of zwitterion **10** (CDCl_3 ; 500 MHz)

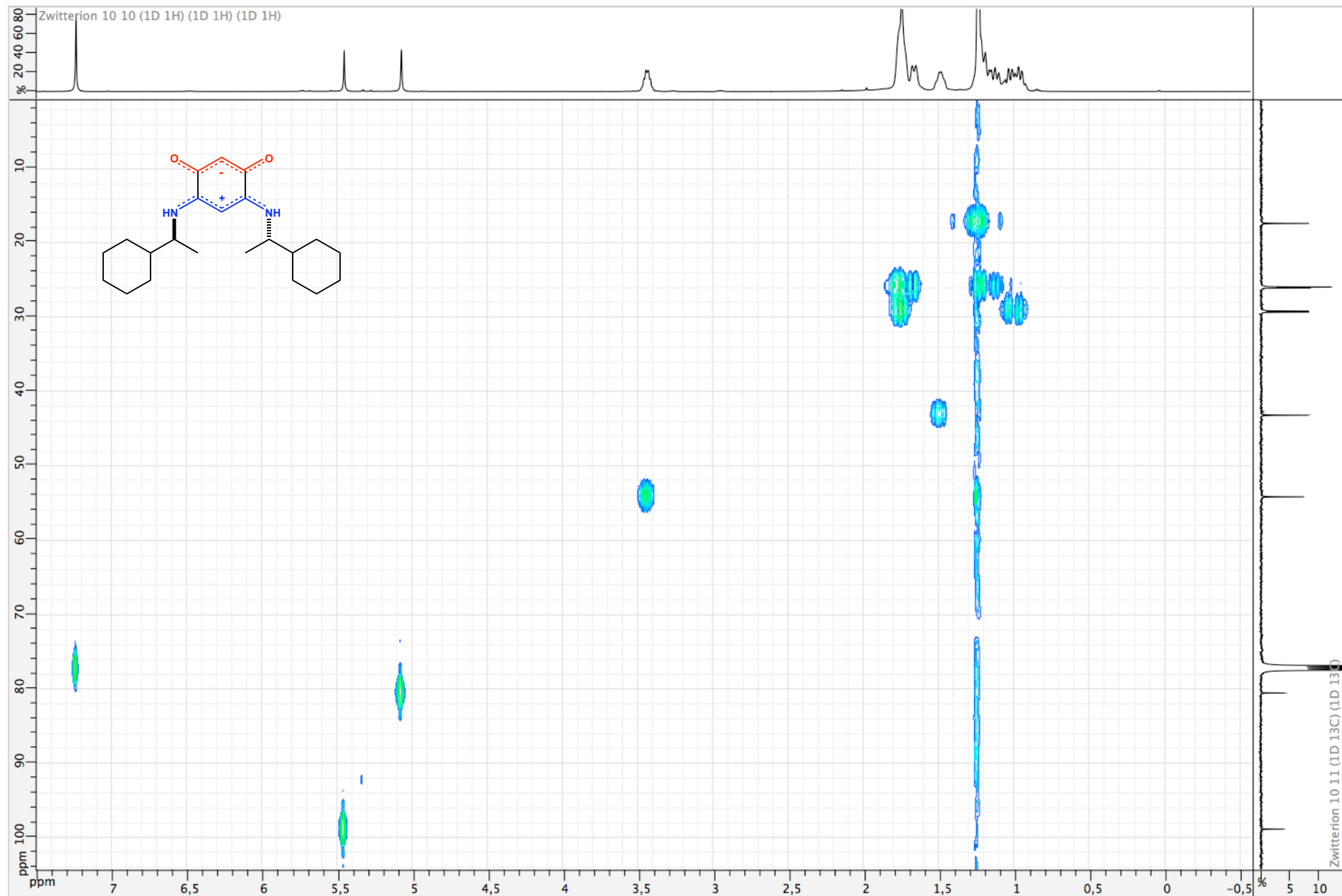


Figure S55. ¹H NMR spectrum of zwitterion **11** (CDCl₃ ; 500 MHz)

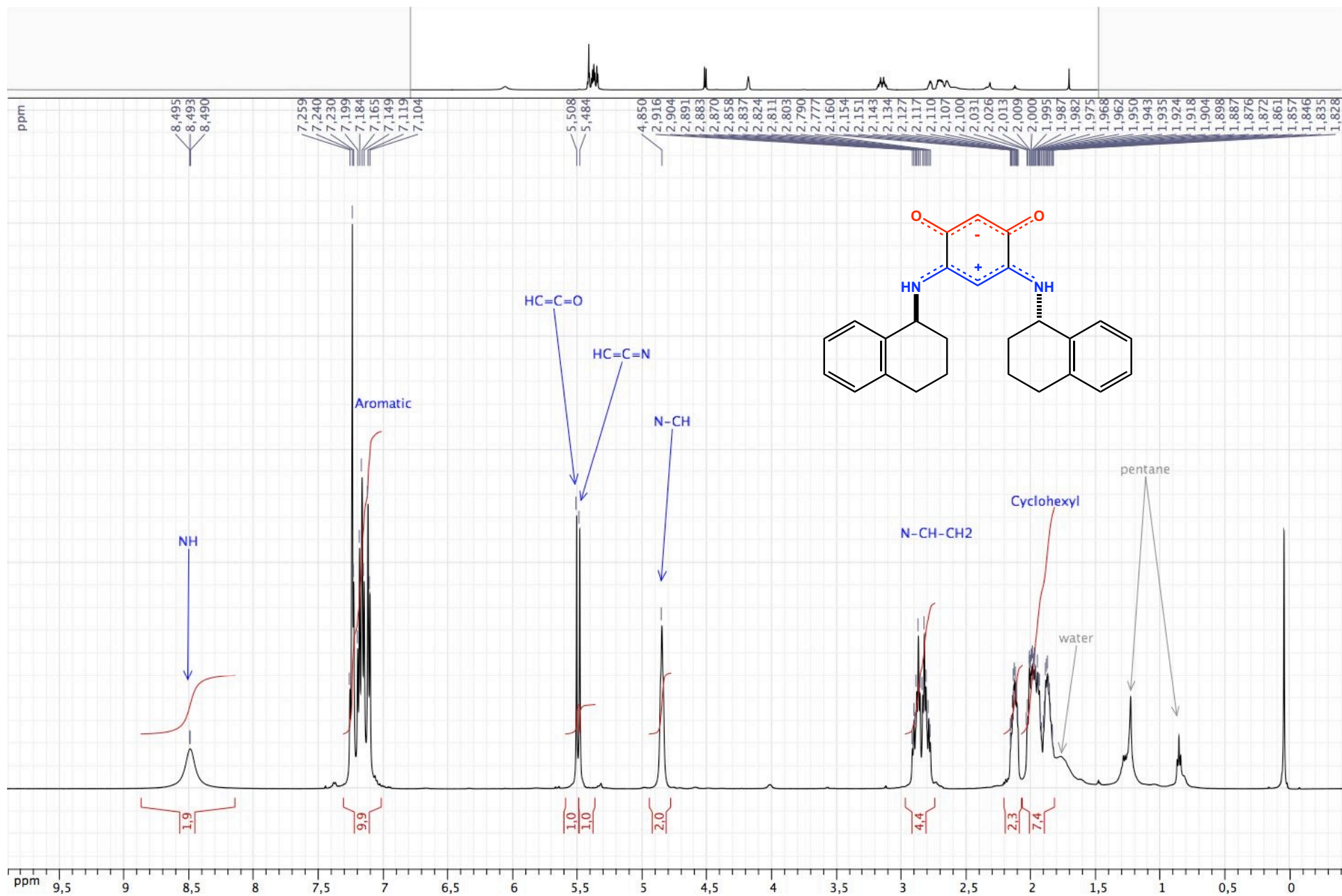


Figure S56. ¹H NMR spectrum of zwitterion **11** (CDCl₃ ; 500 MHz)

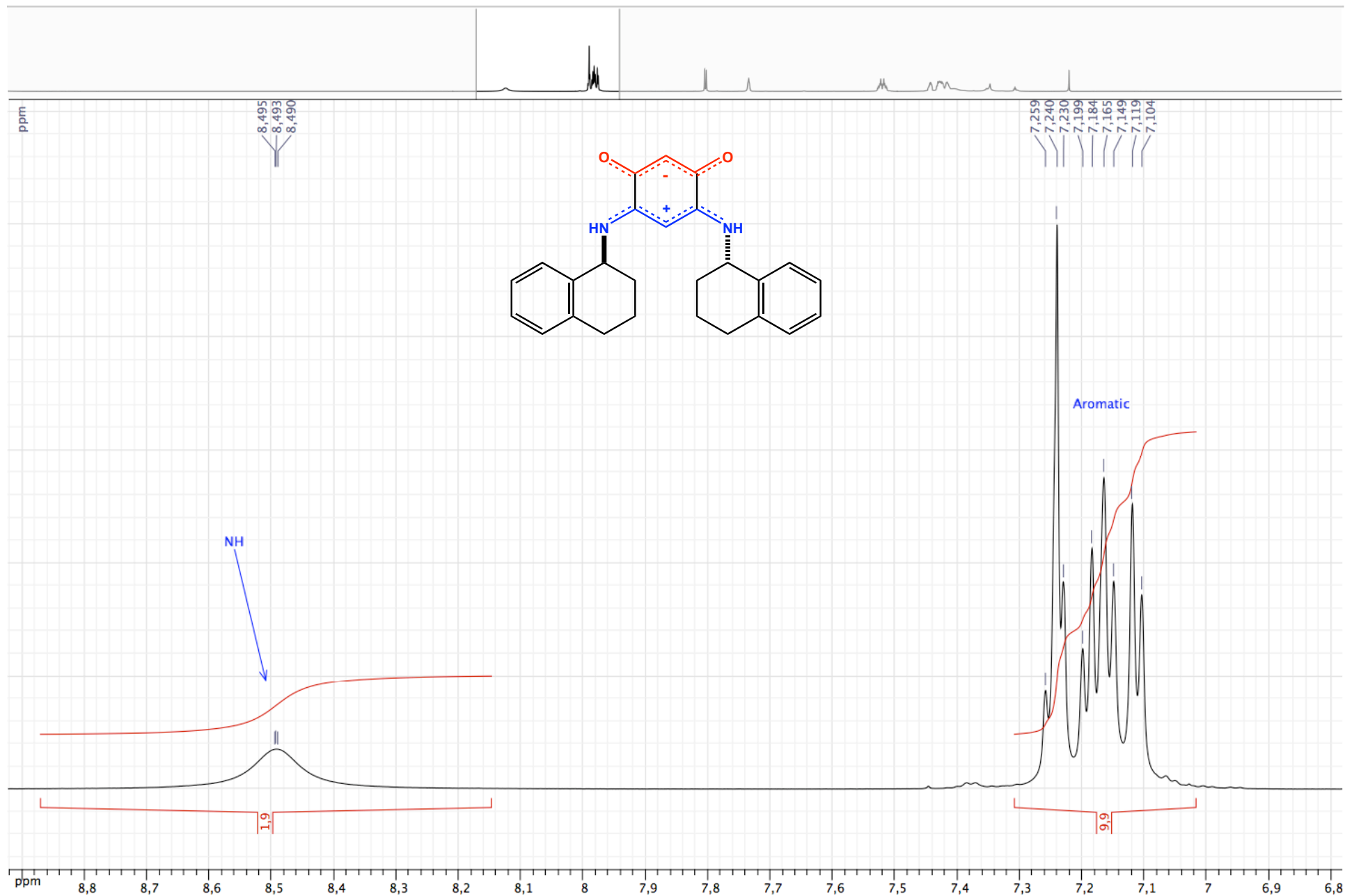


Figure S57. ^1H NMR spectrum of zwitterion **11** (CDCl_3 ; 500 MHz)

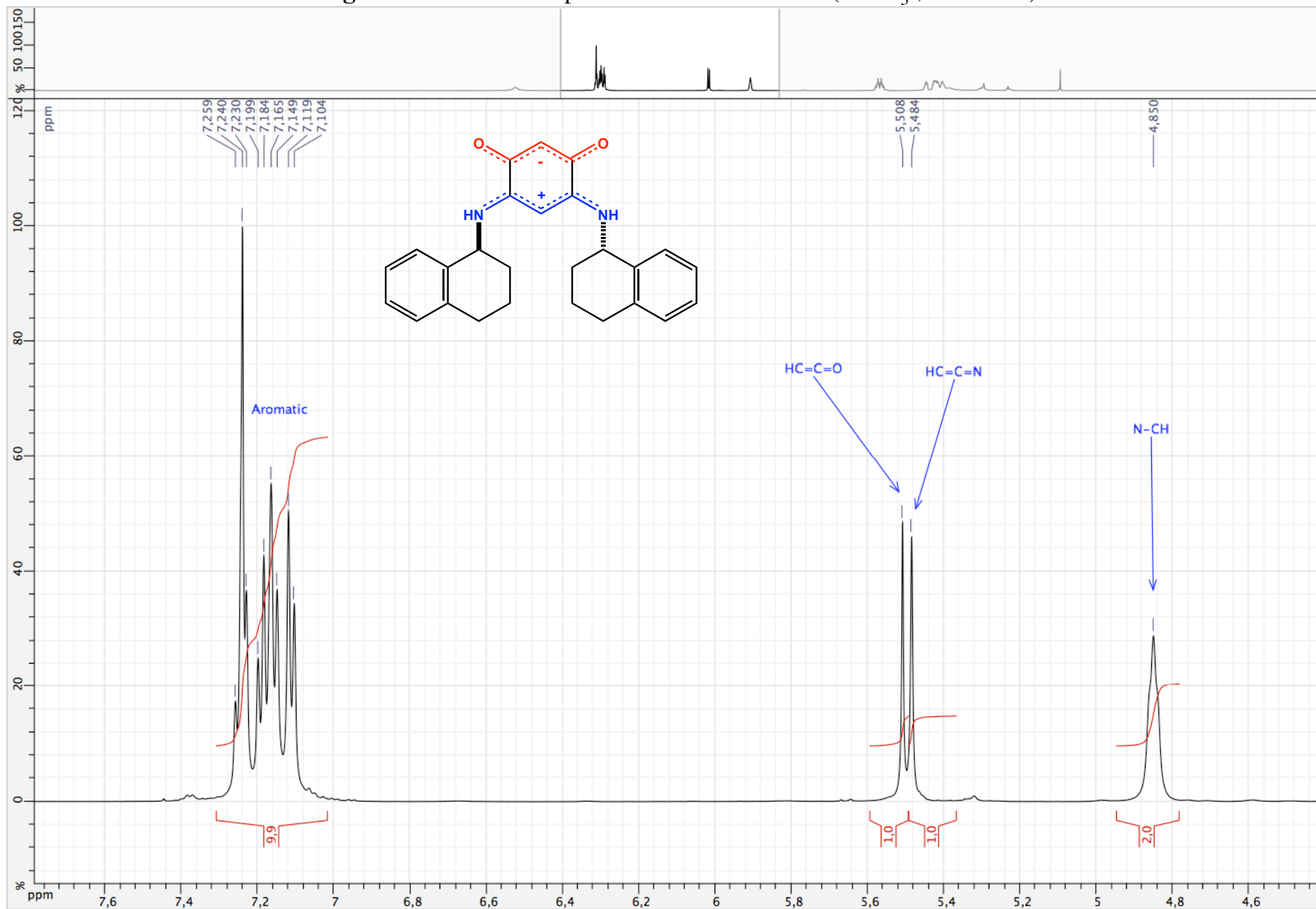


Figure S58. ^1H NMR spectrum of zwitterion **11** (CDCl_3 ; 500 MHz)

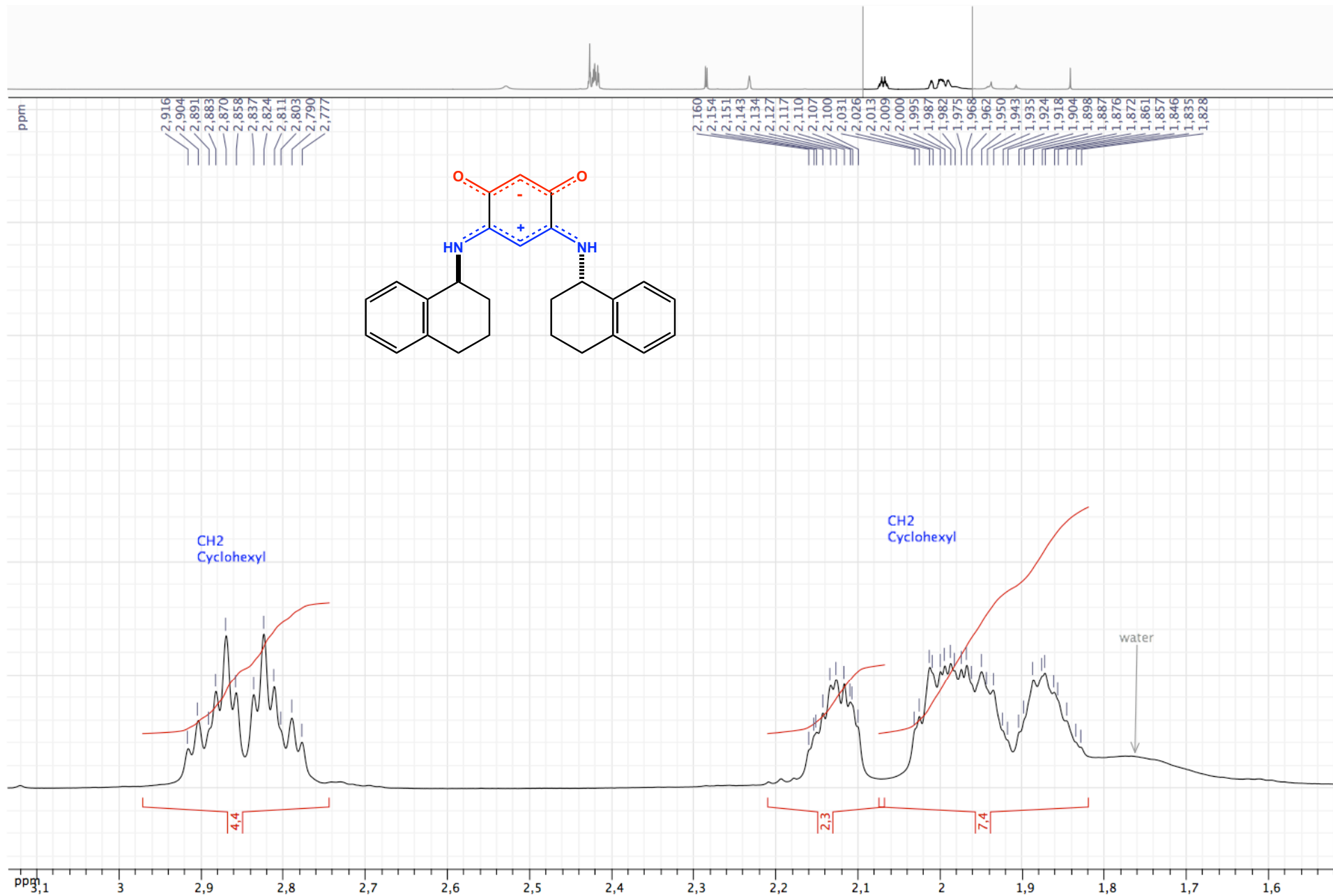


Figure S59. ^{13}C NMR spectrum of zwitterion **11** (CDCl_3 ; 500 MHz)

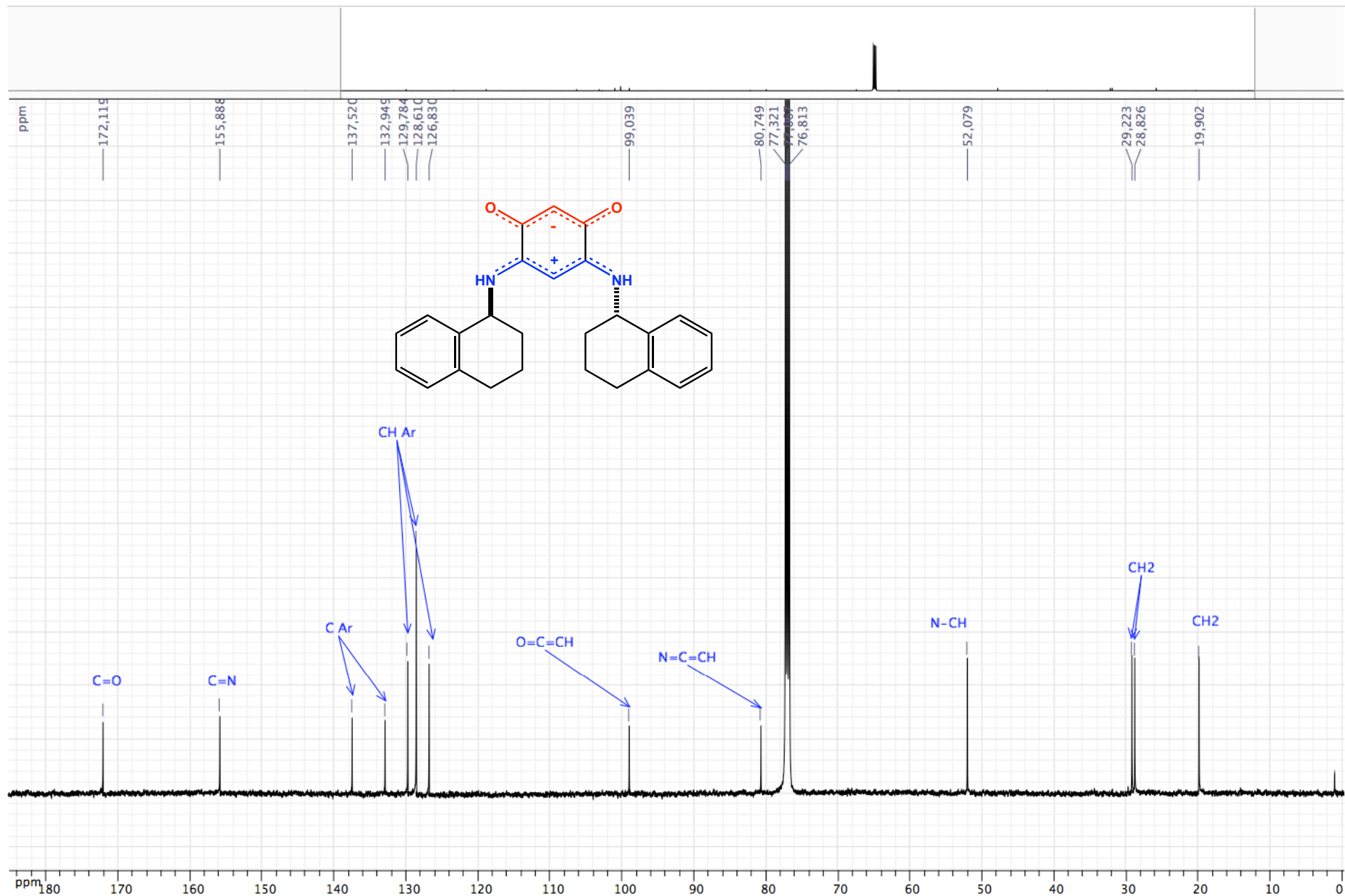


Figure S60. ^{13}C NMR spectrum of zwitterion **11** (CDCl_3 ; 500 MHz)

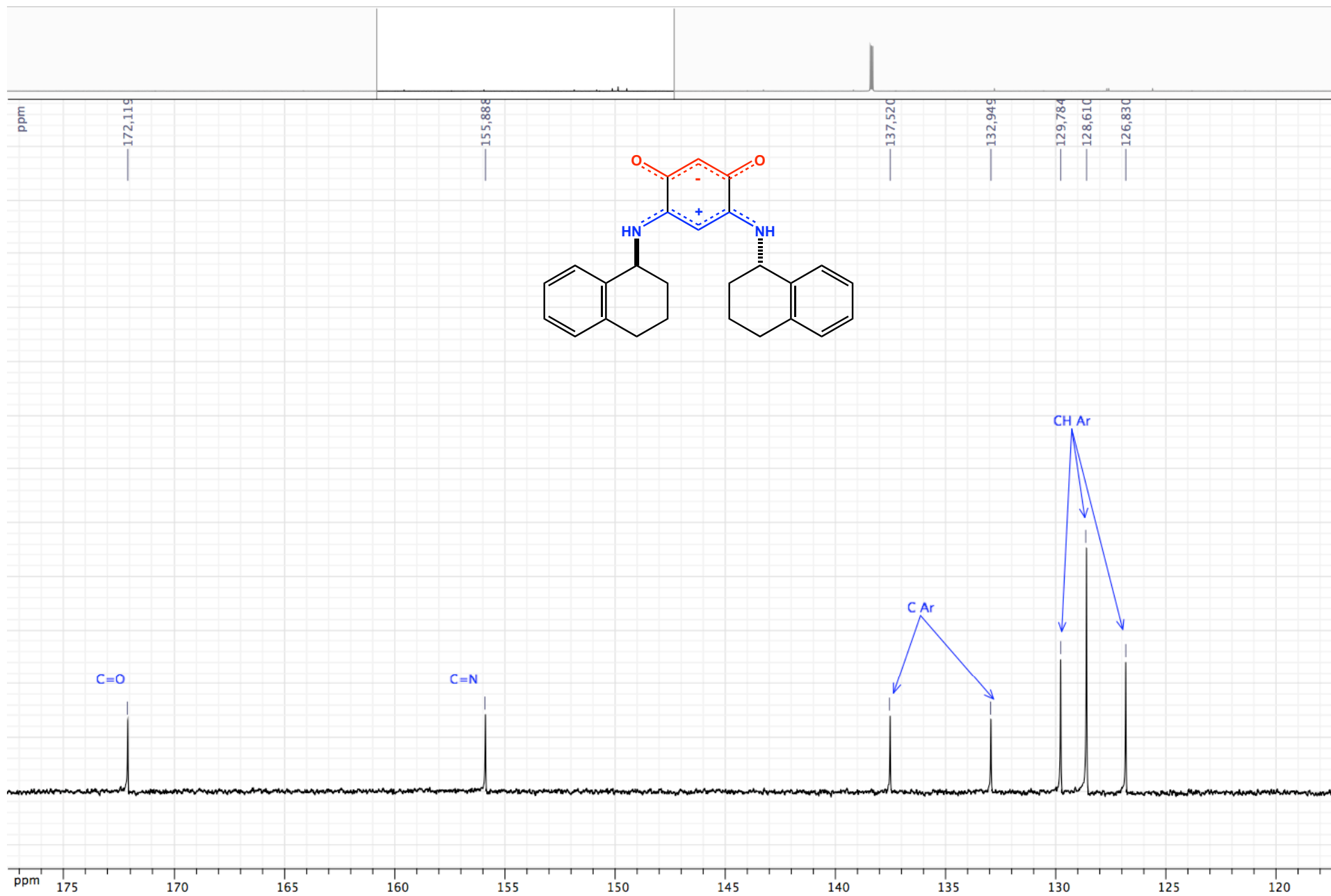


Figure S61. ^{13}C NMR spectrum of zwitterion **11** (CDCl_3 ; 500 MHz)

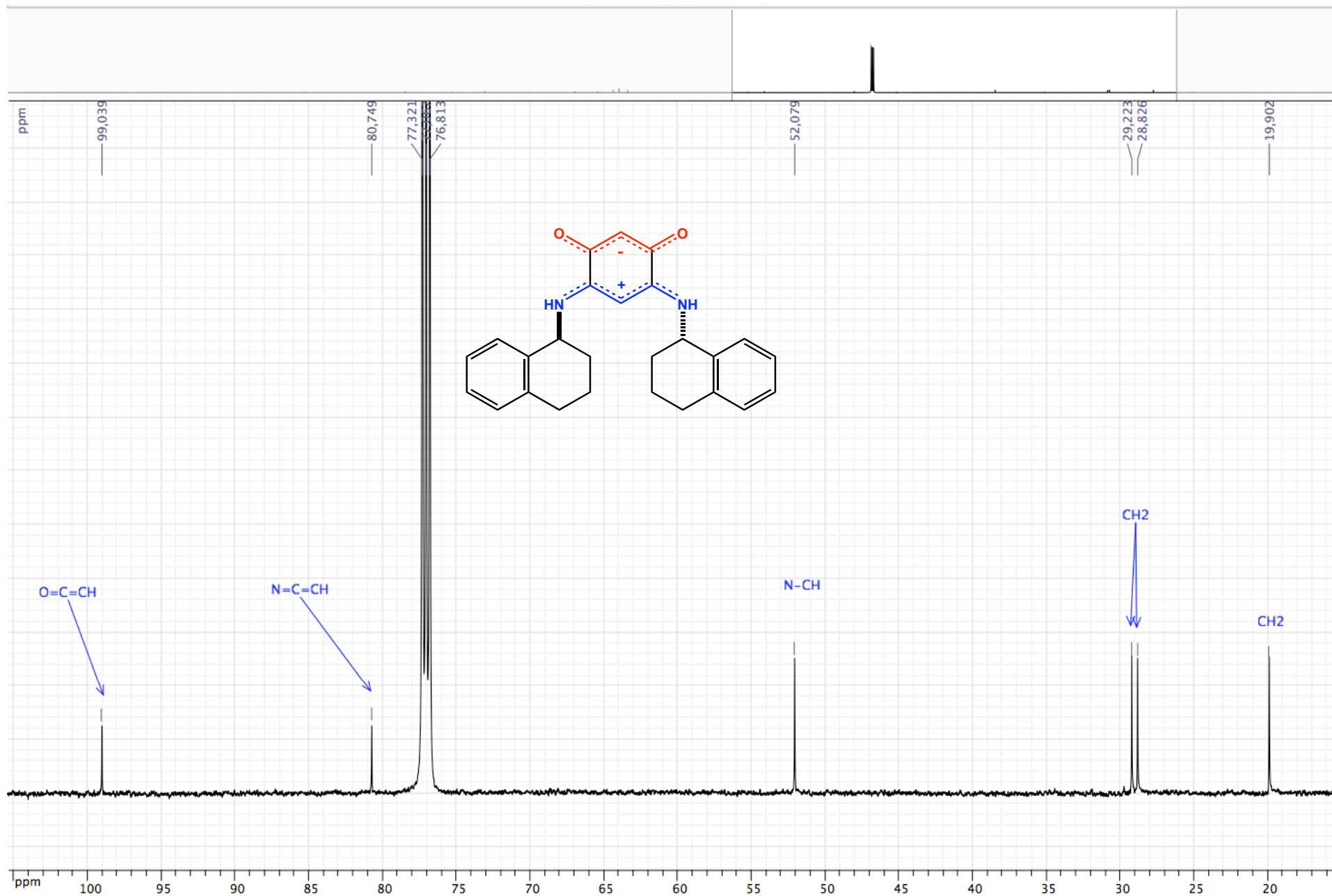


Figure S62. COSY ($^1\text{H} / ^1\text{H}$) spectrum of zwitterion **11** (CDCl_3 ; 500 MHz)

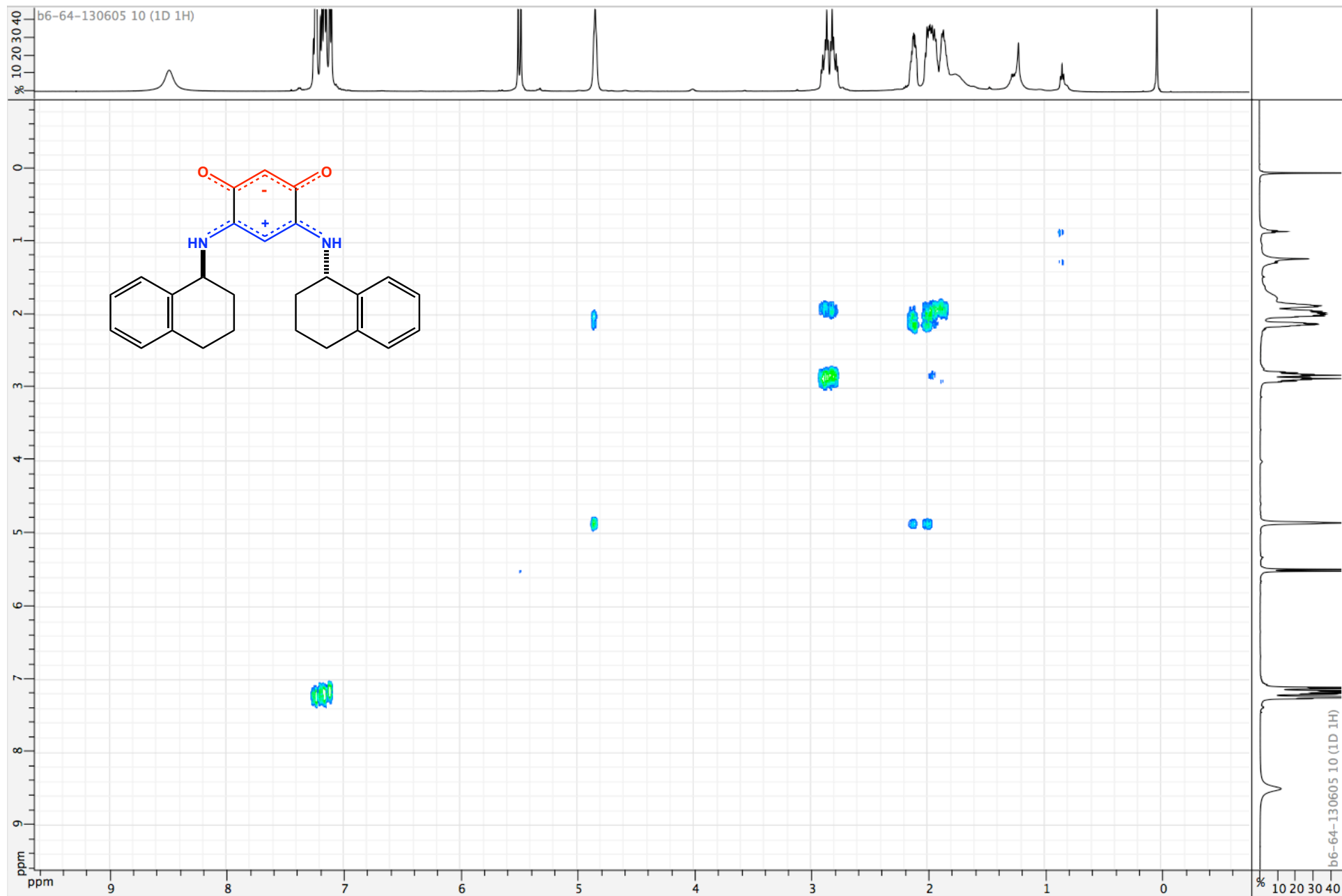


Figure S63. HSQC (^1H / ^{13}C) spectrum of zwitterion **11** (CDCl_3 ; 500 MHz)

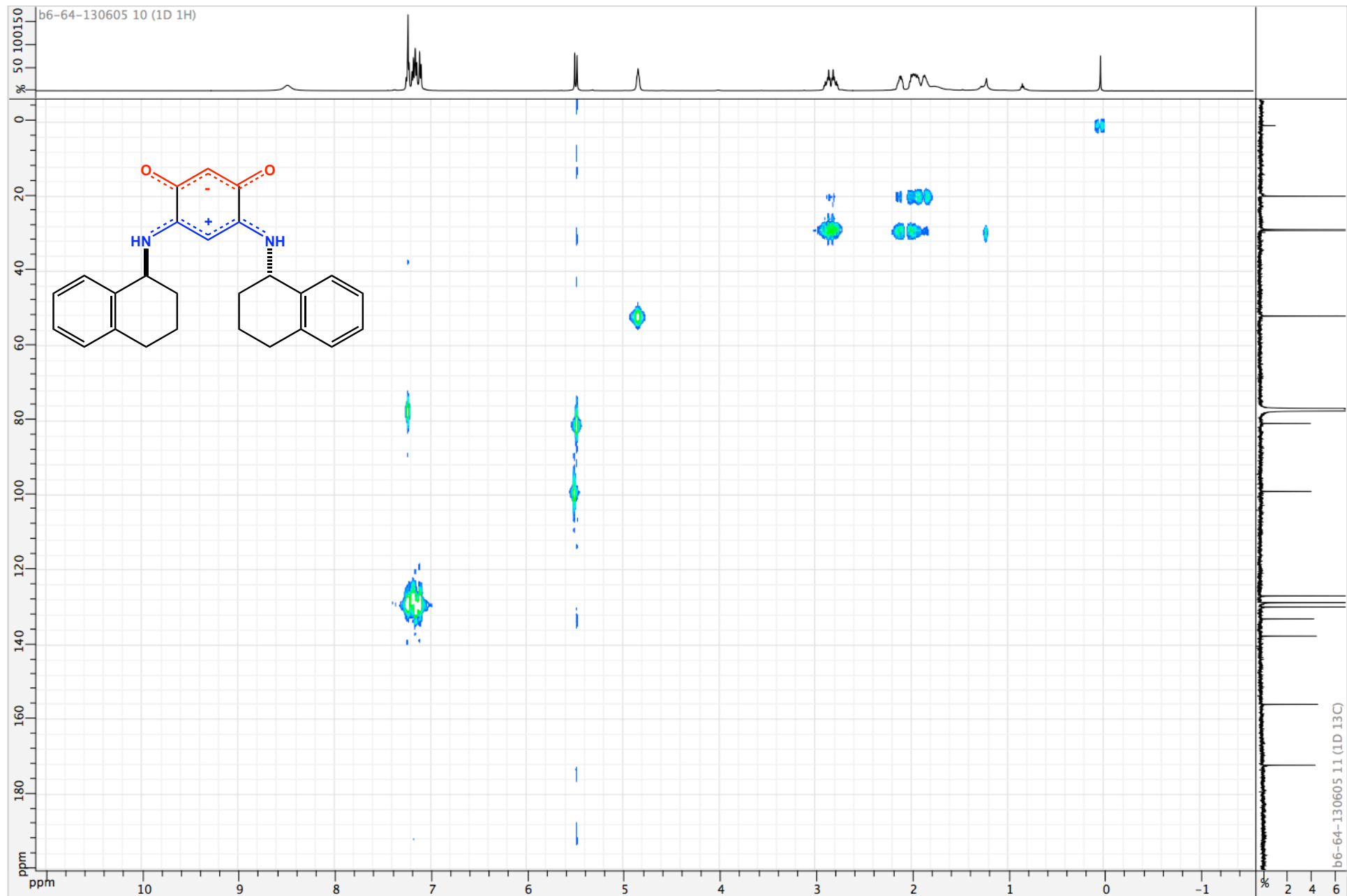


Figure S64. HSQC (^1H / ^{13}C) spectrum of zwitterion **11** (CDCl_3 ; 500 MHz)

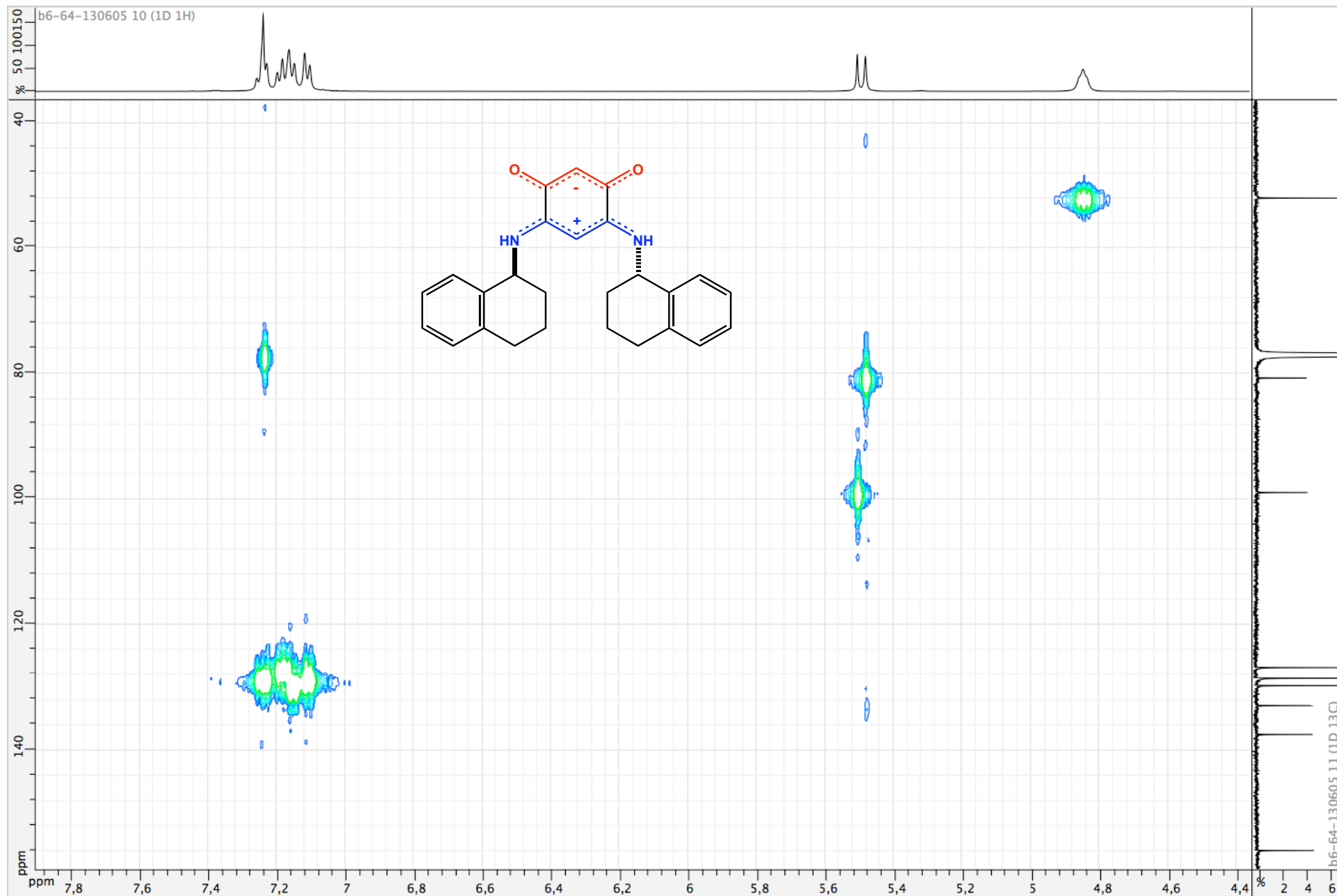


Figure S65. ¹H NMR spectrum of zwitterion **12** (CDCl₃ ; 500 MHz)

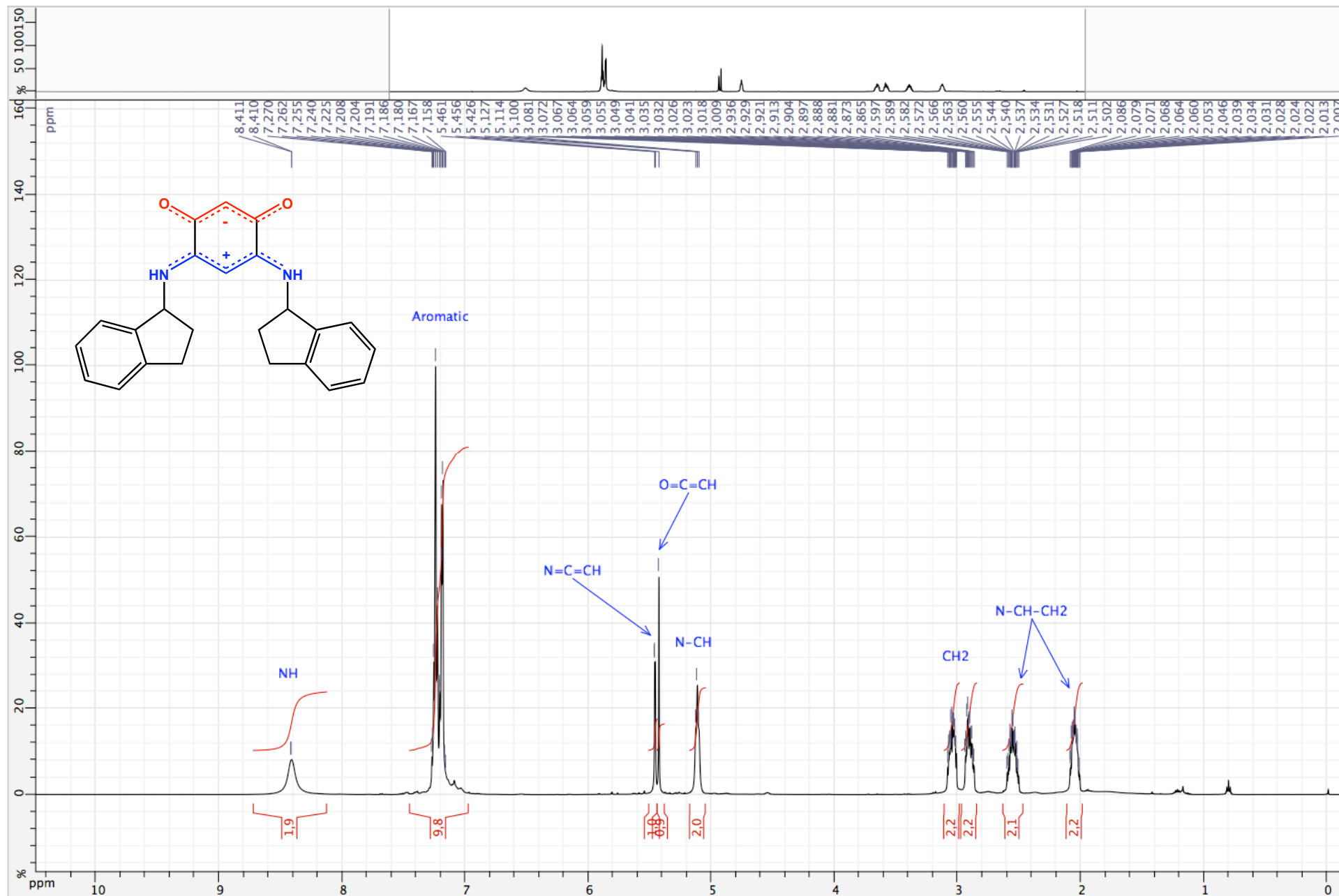


Figure S66. ^1H NMR spectrum of zwitterion **12** (CDCl_3 ; 500 MHz)

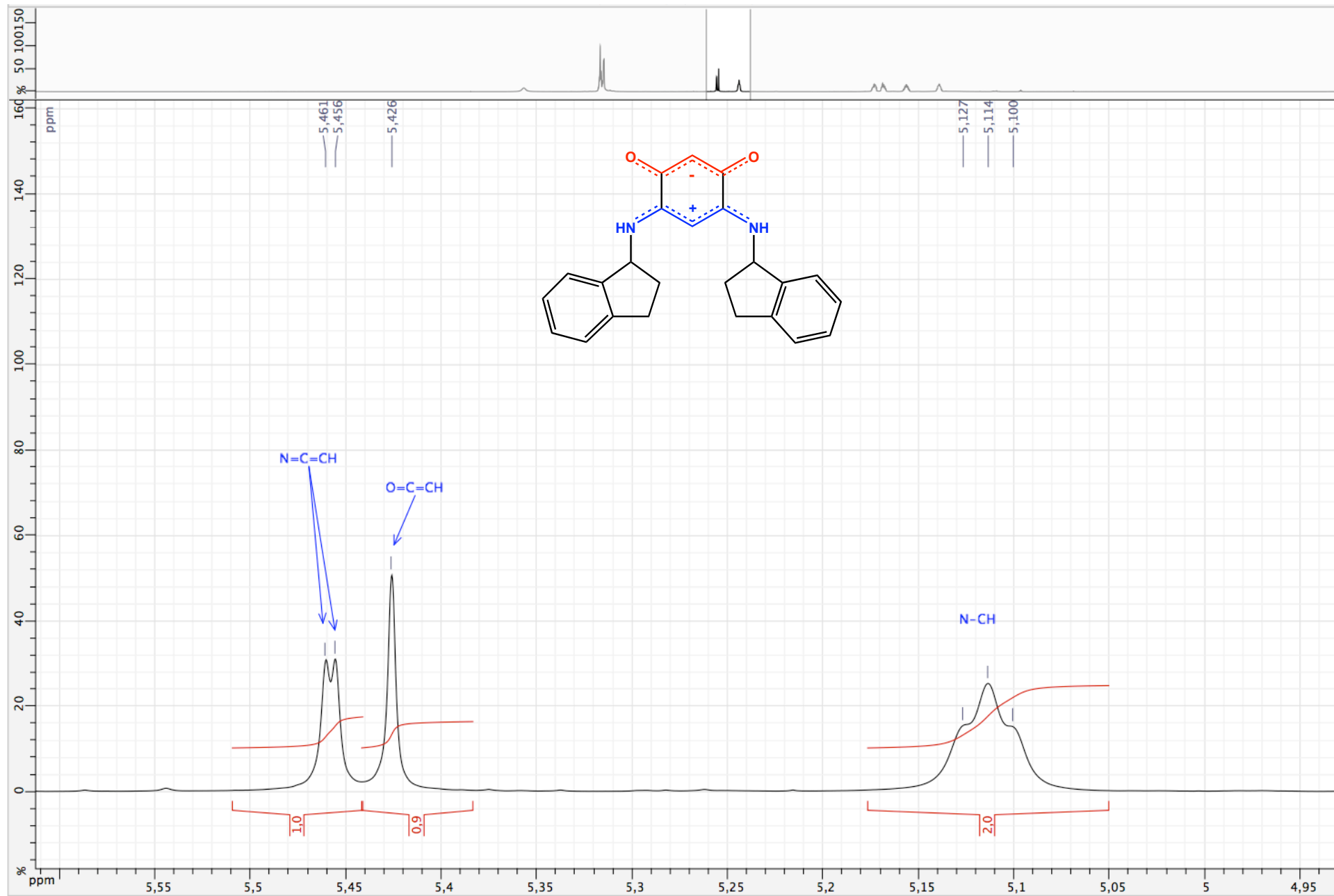


Figure S67. ^1H NMR spectrum of zwitterion **12** (CDCl_3 ; 500 MHz)

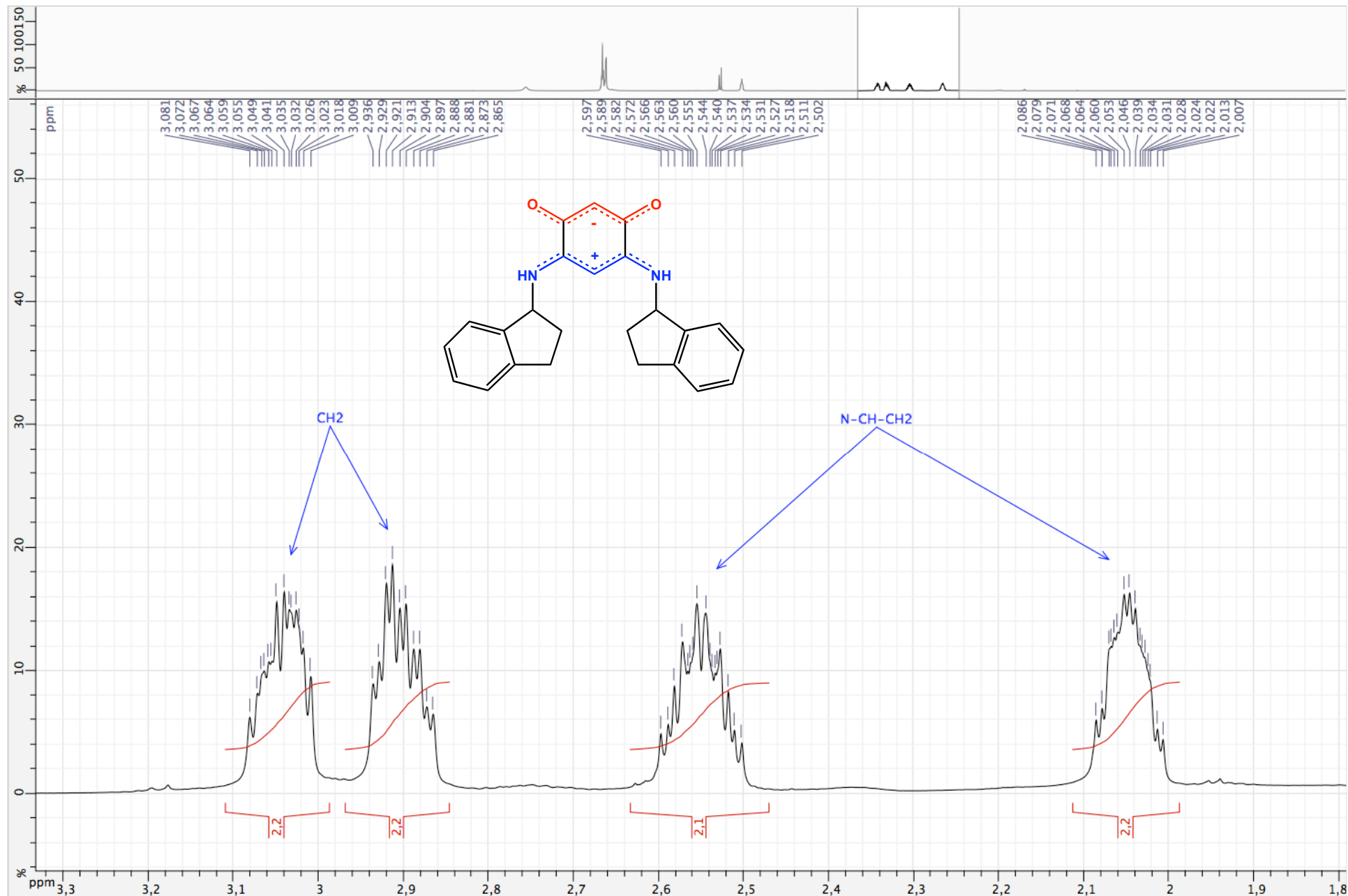


Figure S68. ^{13}C NMR spectrum of zwitterion **12** (CDCl_3 ; 500 MHz)

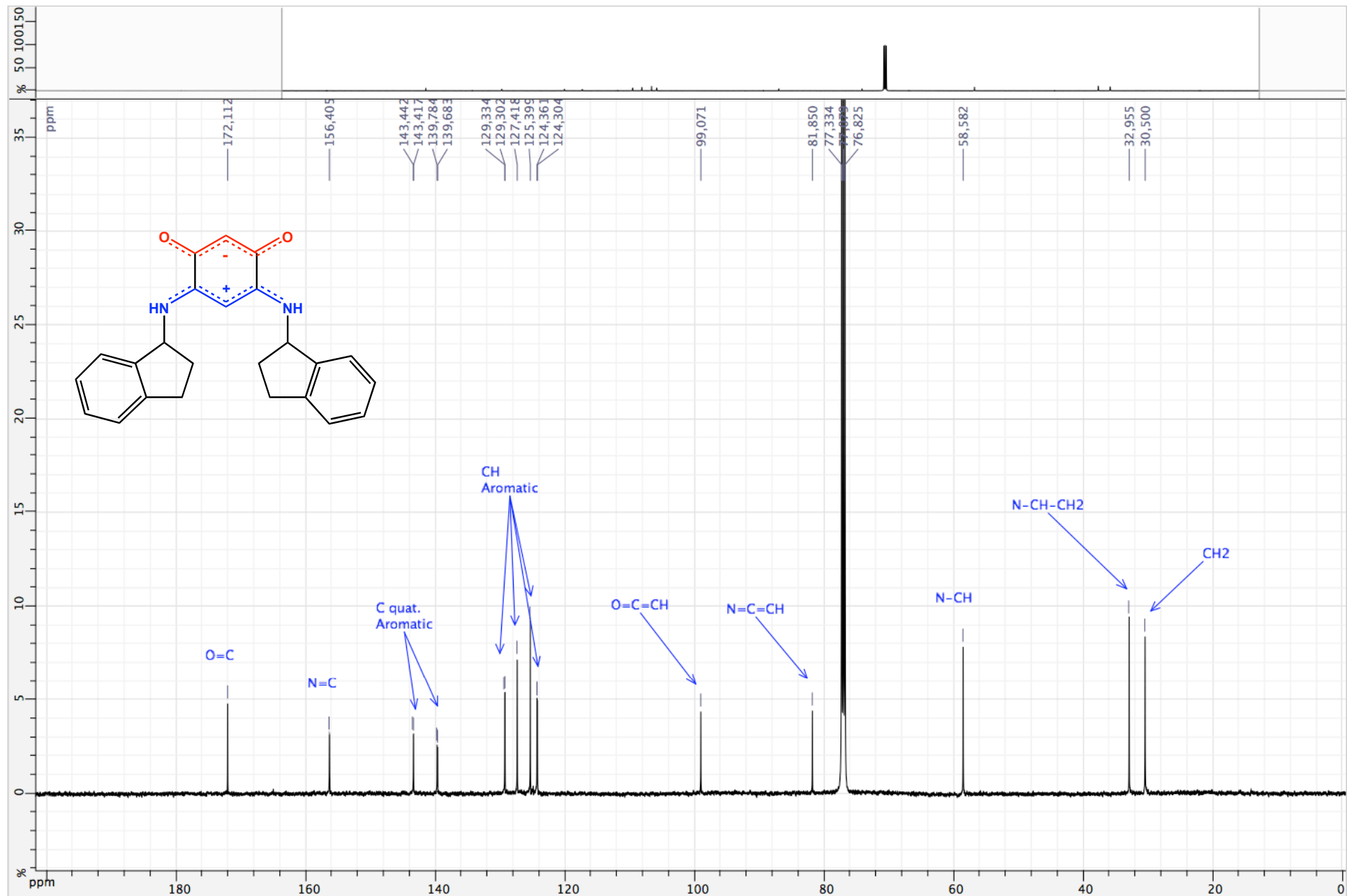


Figure S69. ^{13}C NMR spectrum of zwitterion **12** (CDCl_3 ; 500 MHz)

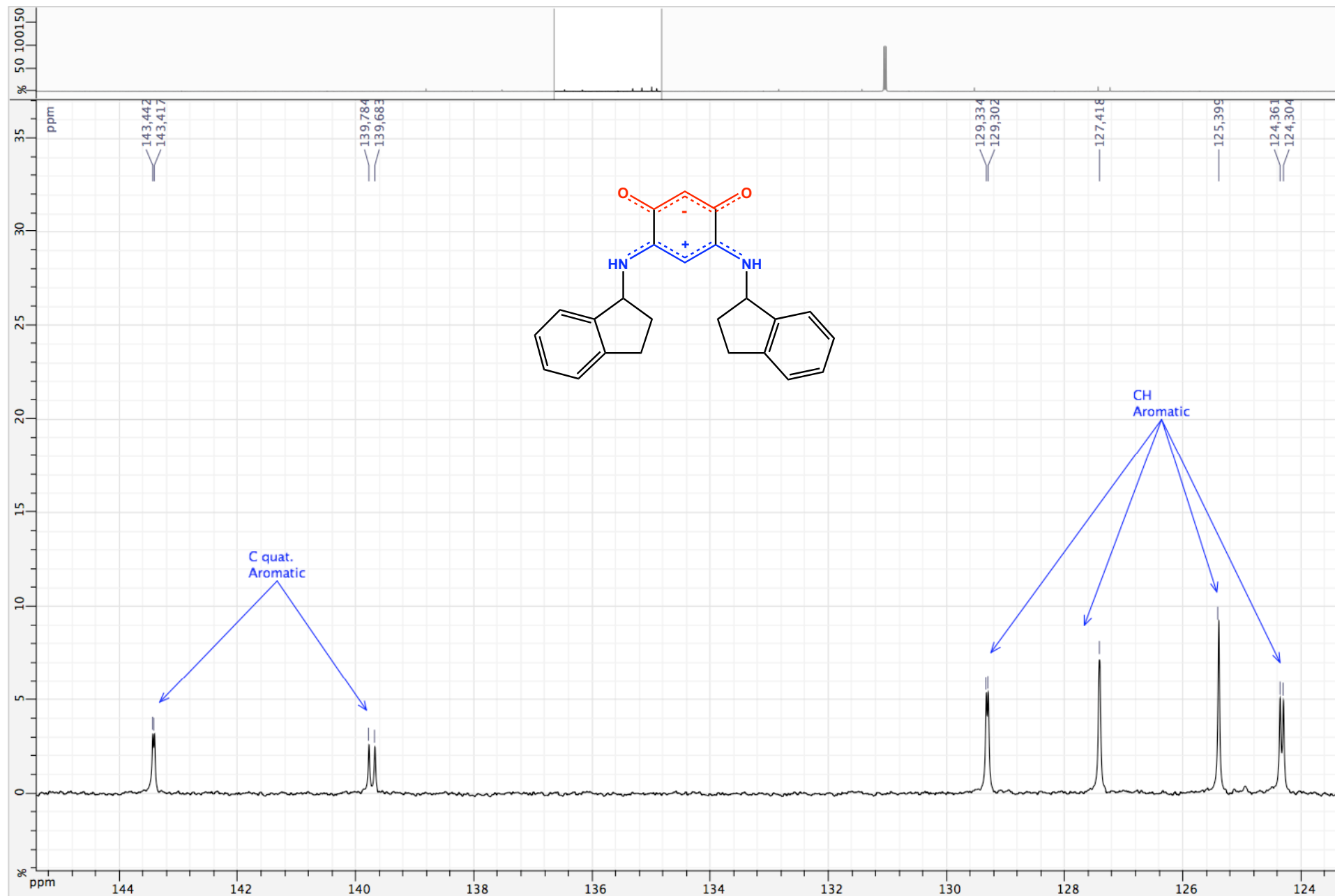


Figure S70. ^{13}C NMR spectrum of zwitterion **12** (CDCl_3 ; 500 MHz)

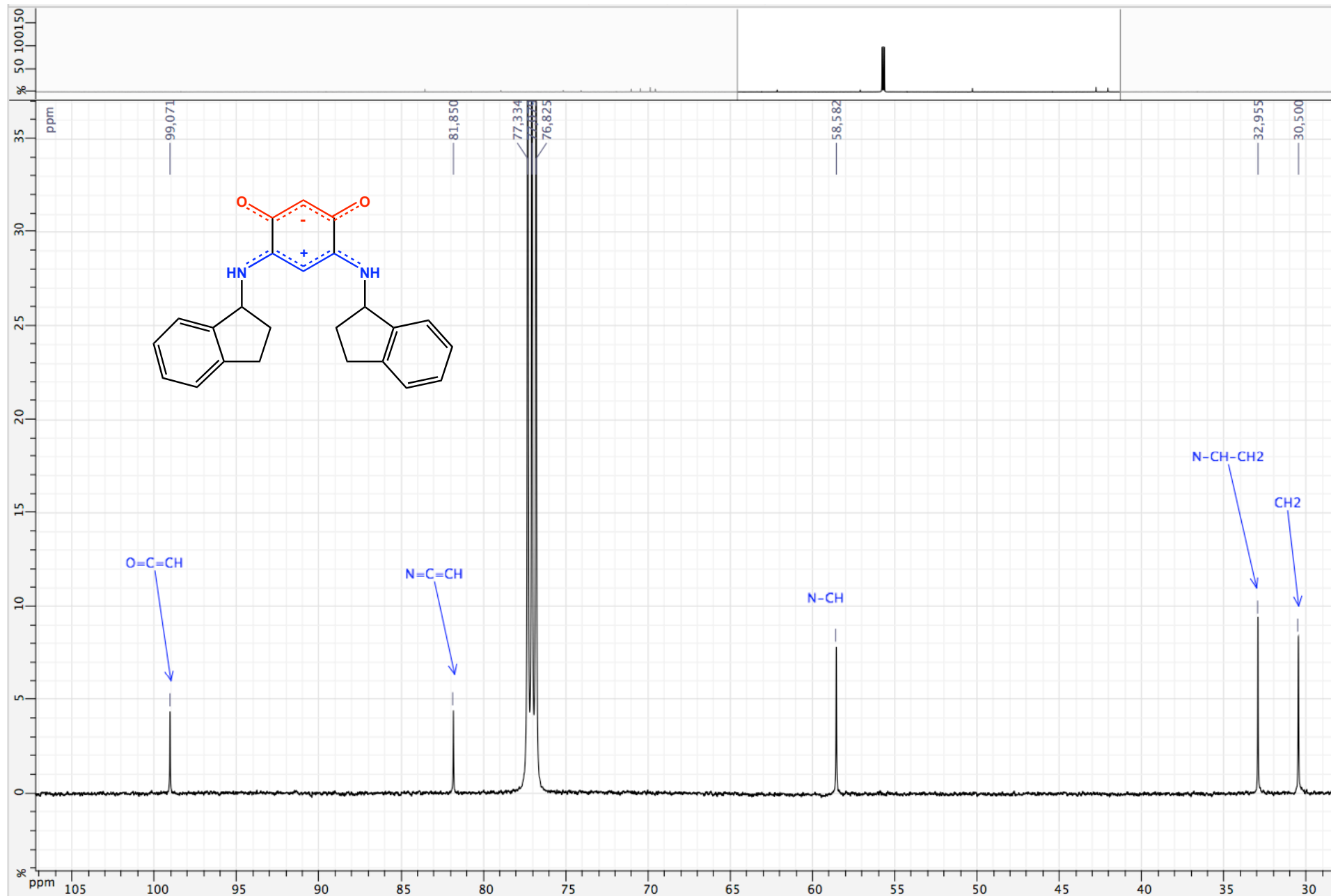


Figure S71. COSY ($^1\text{H} / ^1\text{H}$) spectrum of zwitterion **12** (CDCl_3 ; 500 MHz)

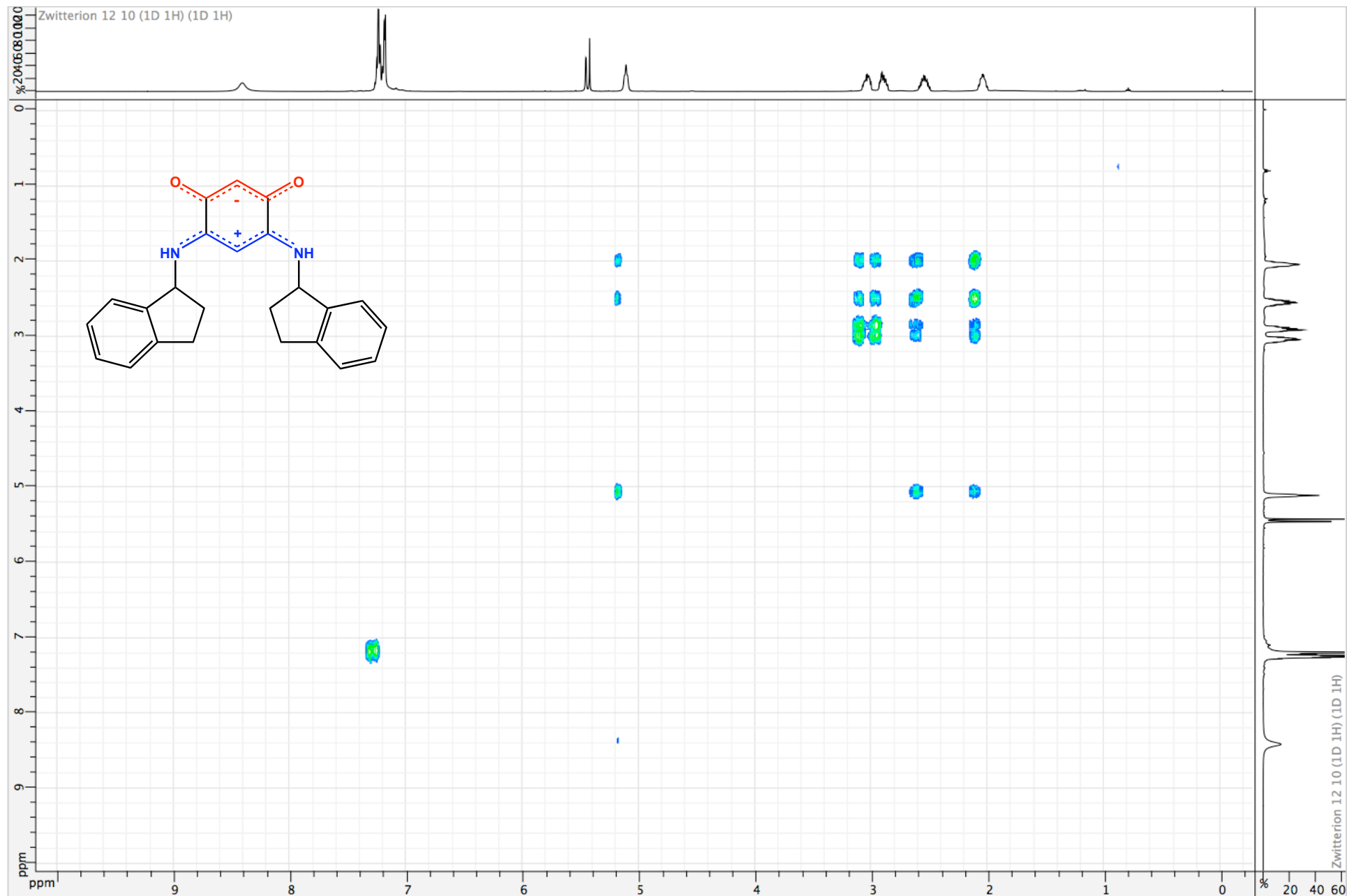


Figure S72. HSQC (^1H / ^{13}C) spectrum of zwitterion **12** (CDCl_3 ; 500 MHz)

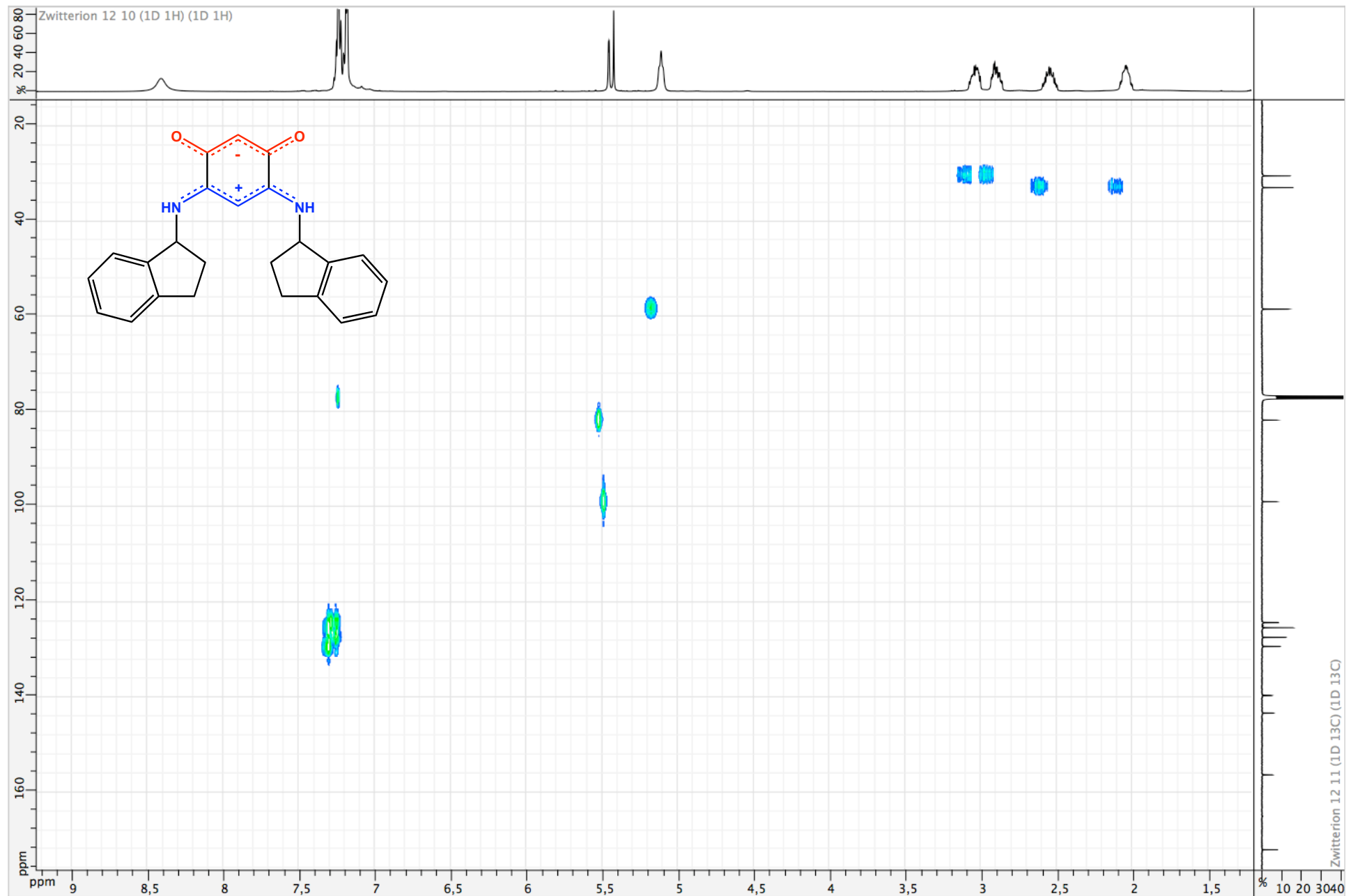


Figure S73. ¹H NMR spectrum of zwitterion **13** (CDCl₃ ; 500 MHz)

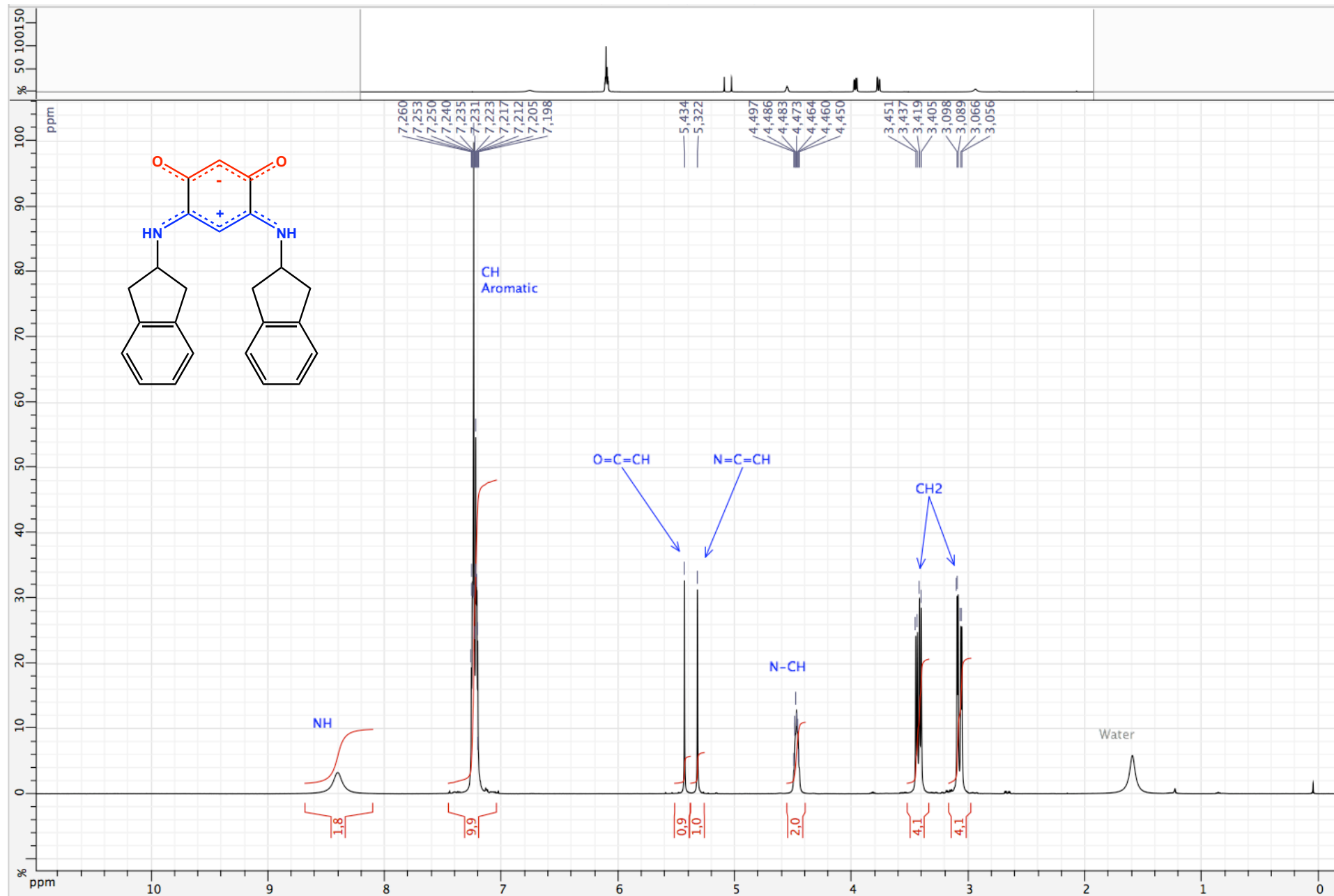


Figure S74. ¹H NMR spectrum of zwitterion **13** (CDCl₃ ; 500 MHz)

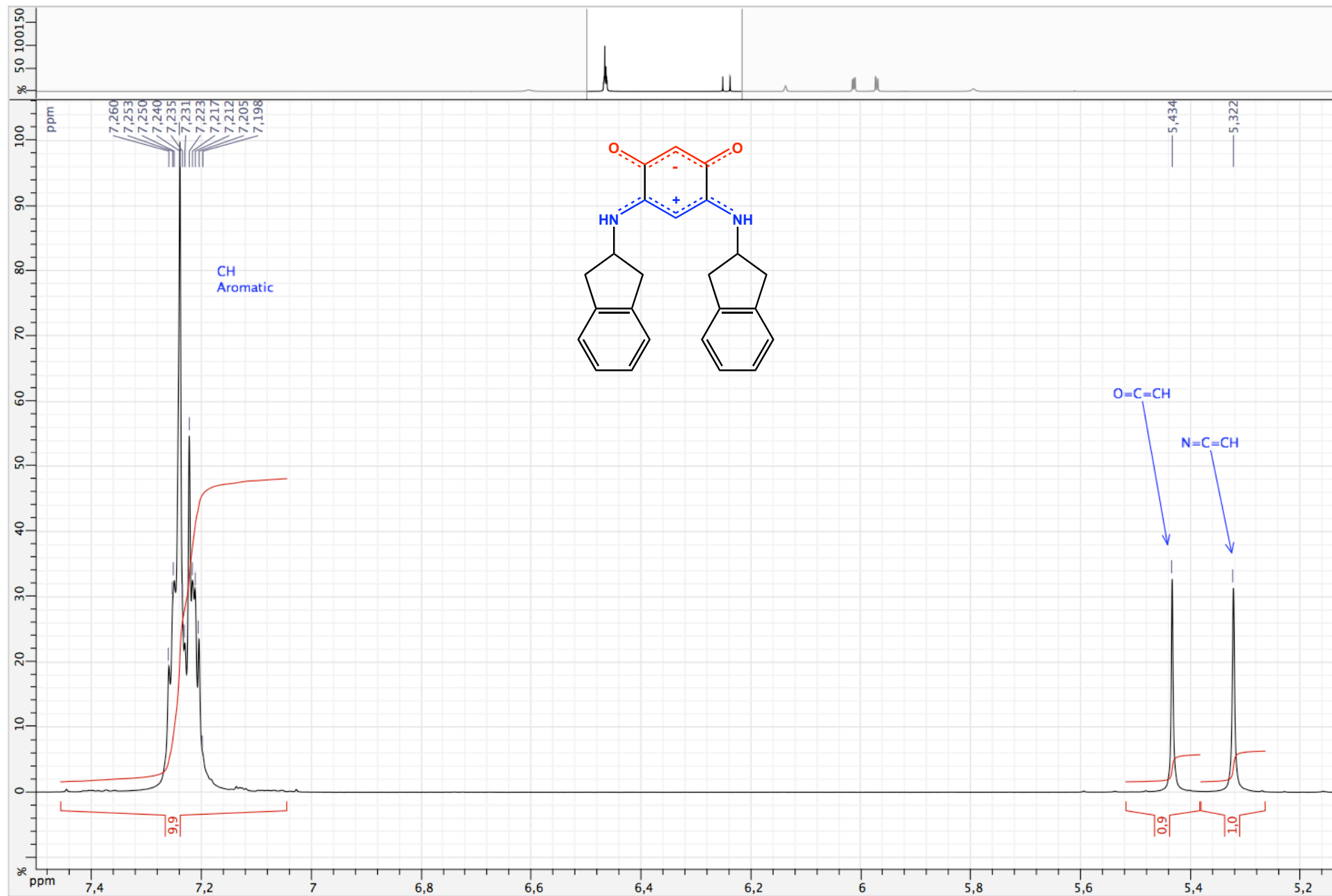


Figure S75. ^1H NMR spectrum of zwitterion **13** (CDCl_3 ; 500 MHz)

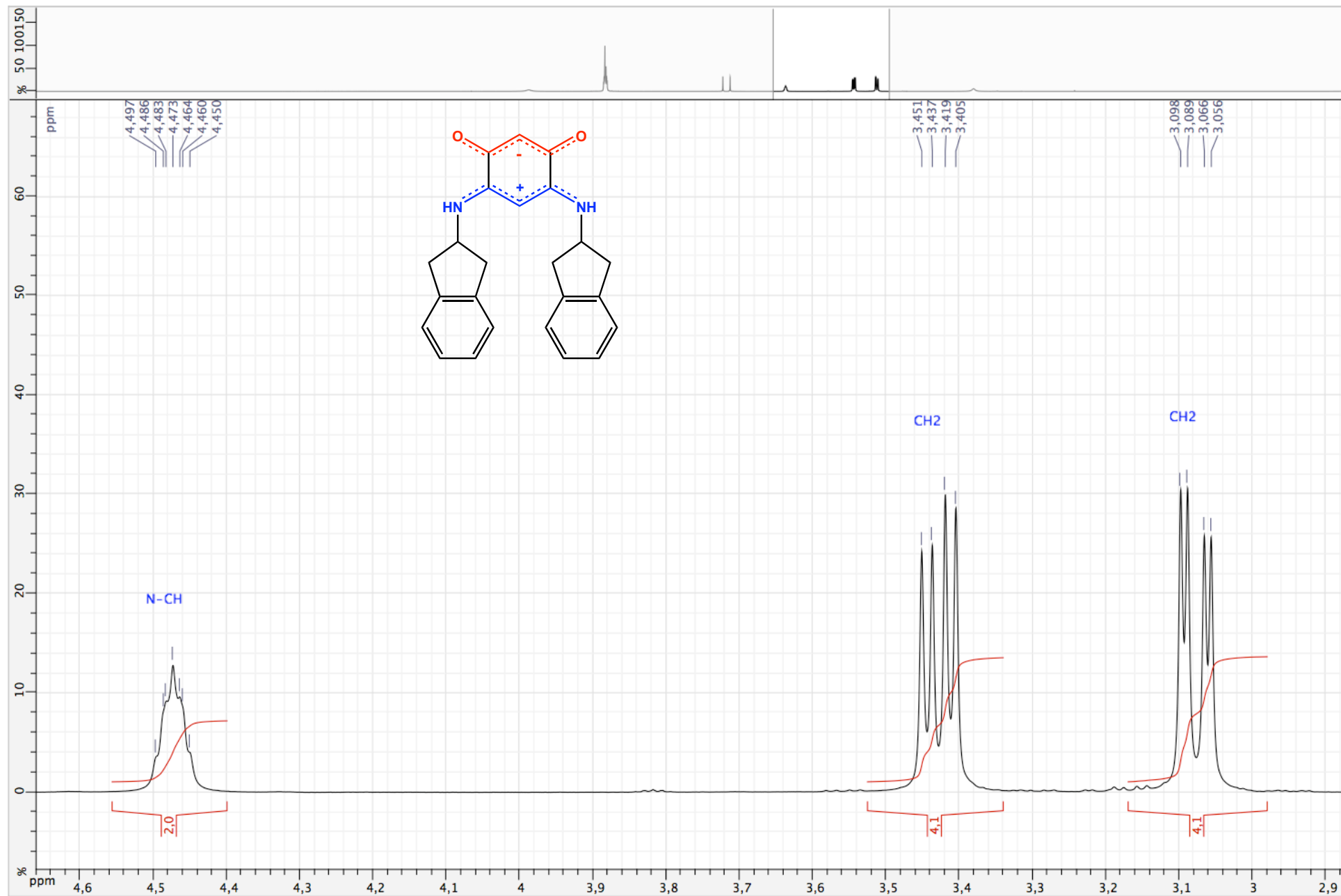


Figure S76. ¹H NMR spectrum of zwitterion **13** (CDCl₃ ; 500 MHz)

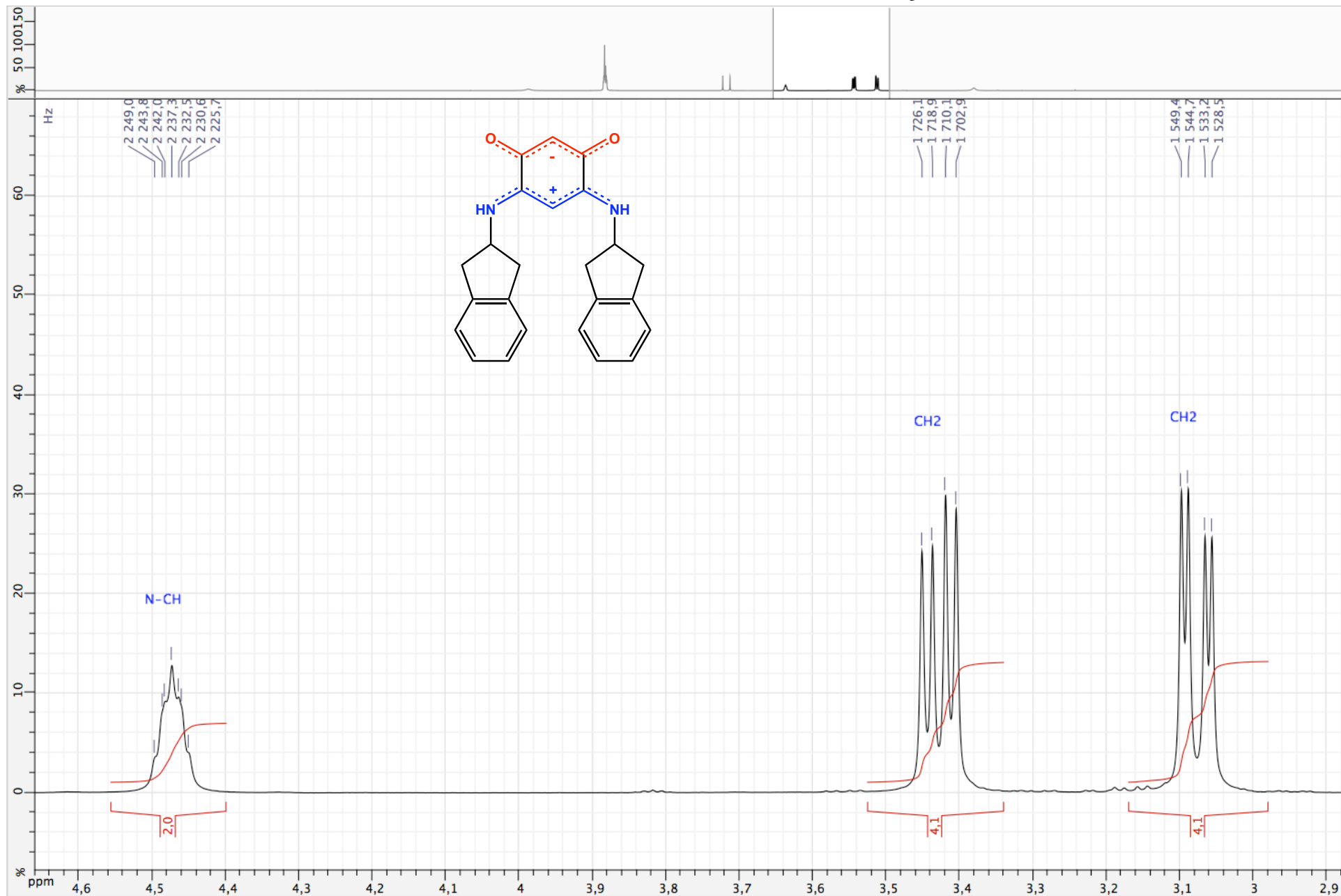


Figure S77. ^{13}C NMR spectrum of zwitterion **13** (CDCl_3 ; 500 MHz)

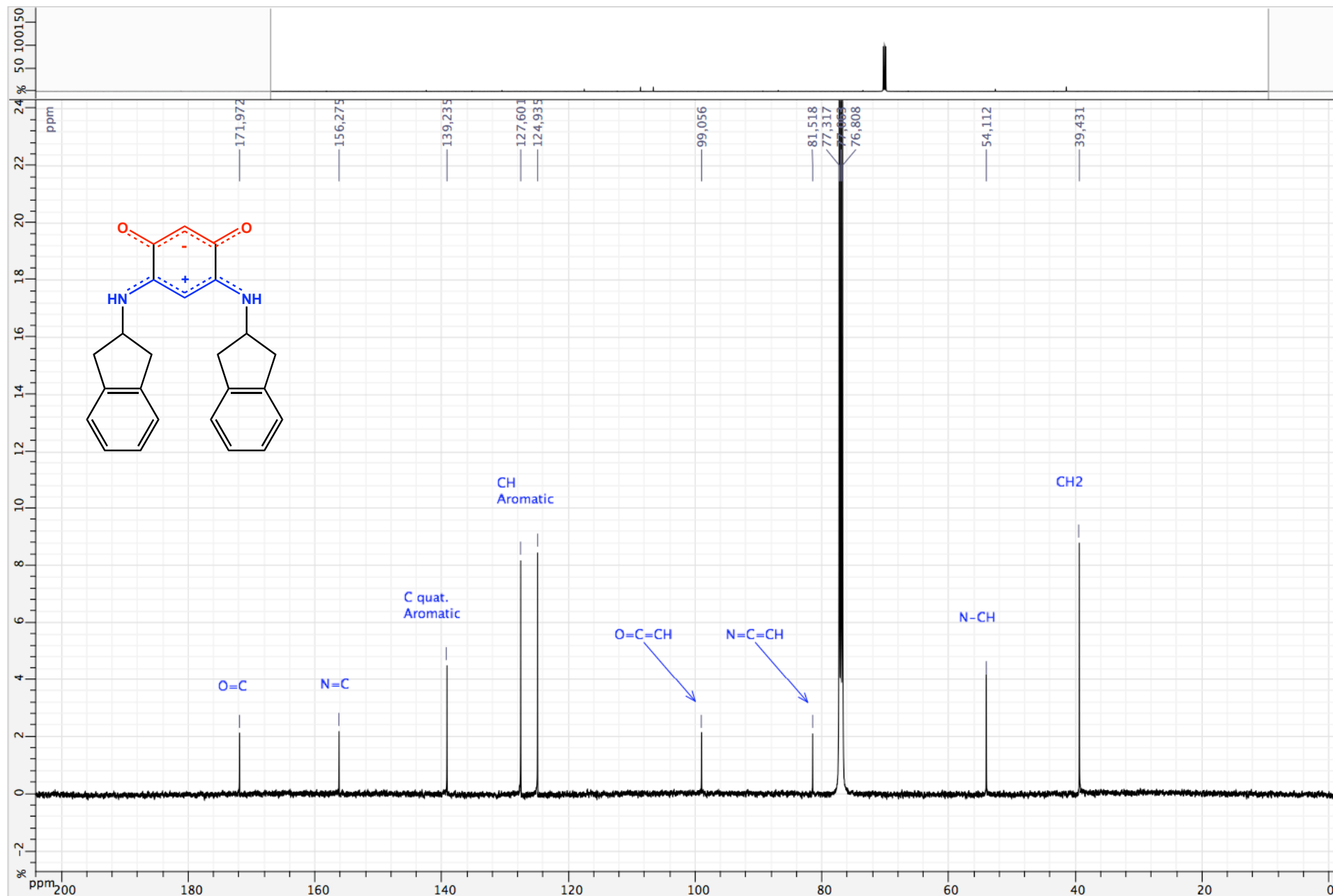


Figure S78. COSY ($^1\text{H} / ^1\text{H}$) spectrum of zwitterion **13** (CDCl_3 ; 500 MHz)

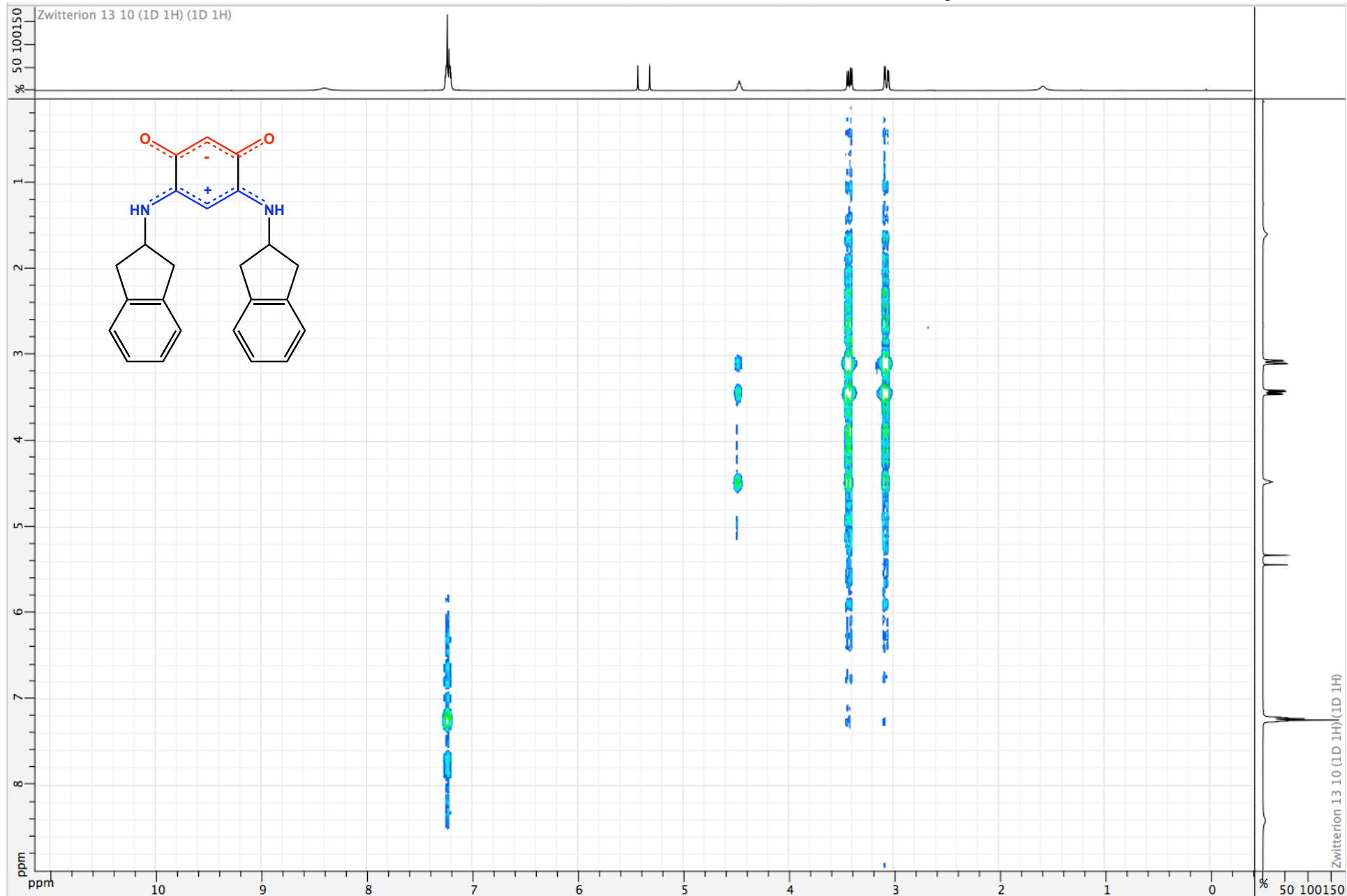


Figure S79. HSQC (^1H / ^{13}C) spectrum of zwitterion **13** (CDCl_3 ; 500 MHz)

